

**Final Report**

**submitted to**

**NATIONAL AERONAUTICS AND SPACE ADMINISTRATION  
GEORGE C. MARSHALL SPACE FLIGHT CENTER, ALABAMA 35812**

**November 1, 1992**

**for Contract NAS8 - 38609**

**Delivery Order 18**

**entitled**

**Materials Surface Contamination Analysis**

**by**

**Gary L. Workman Ph.D.**

**Principal Investigator**

**and**

**William F. Arendale, Ph.D.**

**Consultant**

**In-line Process Control Laboratory  
Center for Automation & Robotics  
University of Alabama in Huntsville  
Huntsville, Alabama 35899**

*(NASA-CR-198-488)* MATERIALS SURFACE  
CONTAMINATION ANALYSIS Final Report  
(Alabama Univ.) 85 p

N93-17000

Unclass

G3/25 0139622

## Table of Contents

	Page
1.0 Introduction .....	1
2.0 Research Objectives .....	2
3.0 Optical Fiber Spectrometry Concepts .....	3
4.0 Brief Description of Chemometric Principles .....	9
5.0 Experimental Approaches .....	12
6.0 Results .....	12
6.1 Spectral Determinations of Contaminants .....	13
6.1.1 Matrix of Contaminants .....	13
6.1.2 Choosing the Reference Spectra .....	19
6.2 Chemometric Determination .....	20
6.3 Discussions Related to Two Models .....	23
6.4 Observations Related to HD2 on D6AC Panels .....	27
6.5 Observations related to the reflected energy from the surfaces .....	55
7.0 Conclusions .....	58
8.0 Optimization of the use of NIR for quality assurance .....	58
9.0 Acknowledgments .....	59
APPENDIX .....	61

## Table of Figures

	Page
Figure 1. Spectral Domain of Interest .....	3
Figure 2. Water and carbon dioxide absorption bands .....	5
Figure 3. Near-infrared spectra of water and deuterium oxide. (Weyer) .....	6
Figure 4. Spectrum of Water in 1mm Cell (UAH) .....	7
Figure 5. Spectrum of acetone in 1mm cell (UAH) .....	7
Figure 6. Example of Reflection/Absorption Process .....	8
Figure 7a. UV Spectra of Contaminants .....	16
Figure 7b. PCA Analysis of Y matrix .....	16
Figure 7c. PLSR of Y and X (UV data) .....	16
Figure 7d. Regression Analysis for HD2 .....	17
Figure 7e. Regression Analysis for WD40 .....	17
Figure 7f. Regression Analysis for Lubriseal .....	17
Figure 7g. Regression Analysis for Apiezon .....	18
Figure 7h. Regression Analysis for TapMagic .....	18
Figure 7i. Regression Analysis for Sebum .....	18
Figure 8. Spectrum 65 Smooth vs Noisy .....	22
Figure 9. Coupon E8A 7 Days at 100°F/60% RH (Front Side) .....	24
Figure 10a. Observed vs Predicted times for samples in HIT series .....	25
Figure 10b. Observed OSEE values vs predicted values in HIT series .....	25
Figure 11. Using Laboratory Data Model SO C to predict HIT and E4 sets .....	26
Figure 12a. Model NAR Loadings Plot for Factor 1 .....	32
Figure 12b. Model NAR Scores Plot for Factor 1 .....	32
Figure 12c. Model NAR Loadings Plot for Factor 2 .....	33
Figure 12d. Model NAR Scores Plot for Factor 2 .....	33
Figure 12e. Model NAR Loadings Plot for Factor 3 .....	34
Figure 12f. Model NAR Scores Plot for Factor 3 .....	34
Figure 12g. Model NAR Loadings Plot for Factor 4 .....	35
Figure 12h. Model NAR Scores Plot for Factor 4 .....	35
Figure 12i. Model NAR Loadings Plot for Factor 5 .....	36
Figure 12j. Model NAR Scores Plot for Factor 5 .....	36
Figure 13a. Loadings Plot for Factor 1 .....	37
Figure 13b. Scores Plot for Factor 1 .....	37
Figure 13c. Predicted with 1 Factor .....	37
Figure 13d. Loadings Plot for Factor 2 .....	38
Figure 13e. Scores Plot for Factor 2 .....	38
Figure 13f. Predicted with 2 Factors .....	38
Figure 13g. Loadings Plot for Factor 3 .....	39
Figure 13h. Scores Plot for Factor 3 .....	39
Figure 13i. Predicted with 3 Factors .....	39
Figure 13j. Loadings Plot for Factor 4 .....	40
Figure 13k. Scores Plot for Factor 4 .....	40

Figure 13l. Predicted with 4 Factor .....	40
Figure 13m. Loadings Plot for Factor 5 .....	41
Figure 13n. Scores Plot for Factor 5 .....	41
Figure 13o. Predicted with 5 Factors .....	41
Figure 13p. Loadings Plot for Factor 6 .....	42
Figure 13q. Scores Plot for Factor 6 .....	42
Figure 13r. Predicted with 6 Factors .....	42
Figure 13s. Loadings Plot for Factor 7 .....	43
Figure 13t. Scores Plot for Factor 7 .....	43
Figure 13u. Predicted with 7 Factors .....	43
Figure 13v. Loadings Plot for Factor 8 .....	44
Figure 13w. Scores Plot for Factor 8 .....	44
Figure 13x. Predicted with 8 Factors .....	44
Figure 14. HD2 ATR Spectrum WA9136 .....	47
Figure 15. HD2 Spread on Aluminum .....	48
Figure 16a. Model ONH Predicted with 10 Factors .....	49
Figure 16b. Model AL2 Predicted with 10 Factors .....	49
Figure 17a. Model ONH Loadings Plot for Factor 1 .....	50
Figure 17b. Model ONH Scores Plot for Factor 1 .....	50
Figure 17c. Model ONH Loadings Plot for Factor 2 .....	51
Figure 17d. Model ONH Scores Plot for Factor 2 .....	51
Figure 17e. Model ONH Loadings Plot for Factor 3 .....	52
Figure 17f. Model ONH Scores Plot for Factor 3 .....	52
Figure 17g. Model ONH Loadings Plot for Factor 4 .....	53
Figure 17h. Model ONH Scores Plot for Factor 4 .....	53
Figure 17i. Model ONH Loadings Plot for Factor 5 .....	54
Figure 17j. Model ONH Scores Plot for Factor 5 .....	54
Figure 18a. Mirror Surface 45° .....	56
Figure 18b. Packed Barium sulfate at 45° .....	56
Figure 18c. D6AC steel plate at 12° .....	56
Figure 18d. D6AC steel plate at 45° .....	57
Figure 18e. D6AC steel plate at 60° .....	57
Figure 18f. D6AC steel plate at 70° .....	57
Figure 19a. Raw data of SOL01 .....	63
Figure 19b. Raw data for SOL02 .....	63
Figure 19c. Raw data of SOL03 .....	63
Figure 19d. Raw data of SOL04 .....	64
Figure 19e. Raw data for SOL05 .....	64
Figure 19f. Raw data of SOL06 .....	64
Figure 19g. Raw data of SOL07 .....	64
Figure 19h. Raw data for SOL08 .....	64
Figure 19i. Raw data of SOL09 .....	64
Figure 19j. Raw data of SOL10 .....	65
Figure 19k. Raw data for SOL11 .....	65
Figure 19l. Raw data of SOL12 .....	65

Figure 20a. Predicted vs. known compositions of Methanol using 1 factor .....	67
Figure 20b. Predicted vs. known compositions of Methanol using 2 factors .....	67
Figure 20c. Predicted vs. known compositions of Methanol using 3 factors .....	67
Figure 20d. Predicted vs. known compositions of Methanol using 4 factors .....	68
Figure 20e. Predicted vs. known compositions of Methanol using 5 factors .....	68
Figure 20f. Predicted vs. known compositions of Methanol using 6 factors .....	68
Figure 20g. Predicted vs. known compositions of Methanol using 7 factors .....	69
Figure 20h. Predicted vs. known compositions of Methanol using 8 factors .....	69
Figure 20i. Predicted vs. known compositions of Ethanol using 8 factors .....	70
Figure 20j. Predicted vs. known compositions of Propanol using 8 factors .....	70
Figure 20k. Predicted vs. known compositions of Glycerol using 8 factors .....	70
Figure 21a. Methanol spectrum compared to Factor 1 .....	71
Figure 21b. Methanol spectrum compared to Factor 2 .....	71
Figure 21c. Glycerol spectrum compared to Factor 1 .....	72
Figure 21d. Glycerol spectrum compared to Factor 2 .....	72
Figure 22. Percent Variance Explained .....	73
Figure 23a. Factor 1 of Hydroxyl Mixture Set .....	74
Figure 23b. Factor 2 of Hydroxyl Mixture Set .....	74
Figure 23c. Factor 3 of Hydroxyl Mixture Set .....	74
Figure 23d. Factor 4 of Hydroxyl Mixture Set .....	75
Figure 23e. Factor 5 of Hydroxyl Mixture Set .....	75
Figure 23f. Factor 6 of Hydroxyl Mixture Set .....	75
Figure 23g. Factor 7 of Hydroxyl Mixture Set .....	76
Figure 23h. Factor 8 of Hydroxyl Mixture Set .....	76
Figure 24a. Scores for Factor 1 of Hydroxyl Mixture Set .....	77
Figure 24b. Scores for Factor 2 of Hydroxyl Mixture Set .....	77
Figure 24c. Scores for Factor 3 of Hydroxyl Mixture Set .....	77
Figure 24d. Scores for Factor 4 of Hydroxyl Mixture Set .....	78
Figure 24e. Scores for Factor 5 of Hydroxyl Mixture Set .....	78
Figure 24f. Scores for Factor 6 of Hydroxyl Mixture Set .....	78
Figure 24g. Scores for Factor 7 of Hydroxyl Mixture Set .....	79
Figure 24h. Scores for Factor 8 of Hydroxyl Mixture Set .....	79

## Tables

Table I.	Vibrational assignments for water vapors .....	4
Table II.	Samples used for UV study .....	15
Table III.	Witness Panels Data Sets .....	29
Table IV.	Environmental Chamber Test .....	31
Table V.	HD2 Grease Samples .....	45
Table VI.	Mole Percentage of Respective Alcohol .....	62
Table VII.	Some Groups and their Wavelengths .....	62

## 1.0 Introduction

The aerospace manufacturing industries are currently in a state of flux with respect to environmental restrictions. Old (and proven) methods of manufacturing are under scrutiny, particularly, if there are any negative connotations associated with a process or its wastes. To understand processes developed many years ago, many innovations in process development are required in order to transition between the old, known methods and new, unproven methods which are more environmentally sound. For this reason, new and innovative methods of surface characterization are being used to assist in the determination of contaminants which cause weaker bonds or debonds in solid rocket motor cases.

Technological advances in spectroscopic instrumentation have provided several new and more potent tools for solving some of the above problems. Technologies that are applicable to spectroscopy include higher sensitivity detectors, high speed analog-to-digital converters with improved signal/noise ratios that allows 16, 18, and higher bits of reliable data, holographic optical elements, optical fibers, and stronger sources of illumination. Improved computing power at the personal computer level allows collection and processing of spectroscopic data in near real time. Since large amounts of data can be collected in rather short periods of time, processing the data into meaningful information and archiving data and summaries has led to the evolution of a specialty called 'chemometrics'.

Chemometrics is a discipline which uses mathematical and statistical methods for handling, interpreting, and predicting chemical data. Examples of chemometric methods are factor analysis and multivariate analysis. Factor analysis is a multivariate technique for reducing complex data sets to their lowest dimensionality to yield recognizable features and/or predictions. Since there is a strong statistical component in chemometrics, hypothesis testing followed by new postulates and further testing can lead to information that is normally not available by direct observation.

Multivariate calibration is an approach to combining many different instrument channels in order to reduce selectivity problems. The foremost application of multivariate calibration today is in Near Infra-red Spectroscopy (NIR) [1]. NIR relies upon multichannel calibrations to provide the selectivity enhancement needed for quantitative spectroscopy in less than perfect conditions. Examples include intact biological samples or turbid process mixtures. General benefits include less sample preparation, higher reliability, and wider range of instrument application.

Optical fiber spectrometry has been around several years and has penetrated many applications in the food and chemical process industries. With optical fibers as transmissions lines for spectrometers, spectral information can be obtained in very difficult and sometimes remote locations due to the flexibility of the optical fiber transmission link. Several companies currently market such systems. The concept is expanding into areas once not available for optical spectrometry.

## 2.0 Research Objectives

The original concept at the beginning of the project was to demonstrate the ability of optical fiber spectrometry to determine contamination levels on solid rocket motor cases in order to identify surface conditions which may result in poor bonds during production. The capability of using the spectral features to identify contaminants with other sensors which might only indicate a potential contamination level provides a real enhancement to current inspection systems such as Optical Stimulated Electron Emission (OSEE). The optical fiber probe can easily fit into the same scanning fixtures as the OSEE.

The initial data obtained using the Guided Wave Model 260 spectrophotometer was primarily focused on determining spectra of potential contaminants such as HD2 grease, silicones, etc.. However, once we began taking data and applying multivariate analysis techniques, using a program that can handle very large data sets, i.e. Unscrambler II, it became apparent that the techniques also might provide a nice scientific tool for determining oxidation and chemisorption rates under controlled conditions. As the ultimate power of the technique became recognized, considering that the chemical system which has most frequently been studied in this work has been water + D6AC steel, we became very interested in trying the spectroscopic techniques to solve a broad range of problems. The complexity of the observed spectra for the D6AC + water system is due to overlaps between the water peaks, the resulting chemisorbed species, and products of reaction which also contain OH stretching bands. Unscrambling these spectral features, without knowledge of the specific species involved, has proven to be a formidable task.

## 3.0 Optical Fiber Spectrometry Concepts

The use of silica optical fibers allows a very broad spectral region to be interrogated since the optical transmission of silica extends from around 190 nm in the UV to around 2.5 microns in the IR. Figure 1 shows how several spectral regions are related to wavelength, wavenumbers, and photon energies. These relationships are significant for this work, because of the interplay with the optical stimulation phenomena occurring in OSEE. There is no single light source or detector which covers such a broad range. Several light sources detectors, and gratings are available, easily interchangeable, which allows full spectral coverage with fairly limited change-out periods for the optics.

During the course of this research we have recorded spectra throughout the range 190 nm to 2500 nm. We have used two different gratings; one with 300 lines/mm for the NIR and another with 1200 lines/mm for the UV. Due to the specific application being researched, that of implementing an optical fiber spectrometer in conjunction with OSEE scanning operations, we did not record any spectra in the visible region. Consequently we were able in general to record spectra under ambient conditions with minimum interference from external lighting.

Due to the nature of the environment being investigated a large proportion of the spectra were recorded under very moist or humid conditions. It is well known that water has several absorption bands in the NIR region. The water and carbon dioxide absorption bands make

# SPECTRAL DOMAIN OF INTEREST

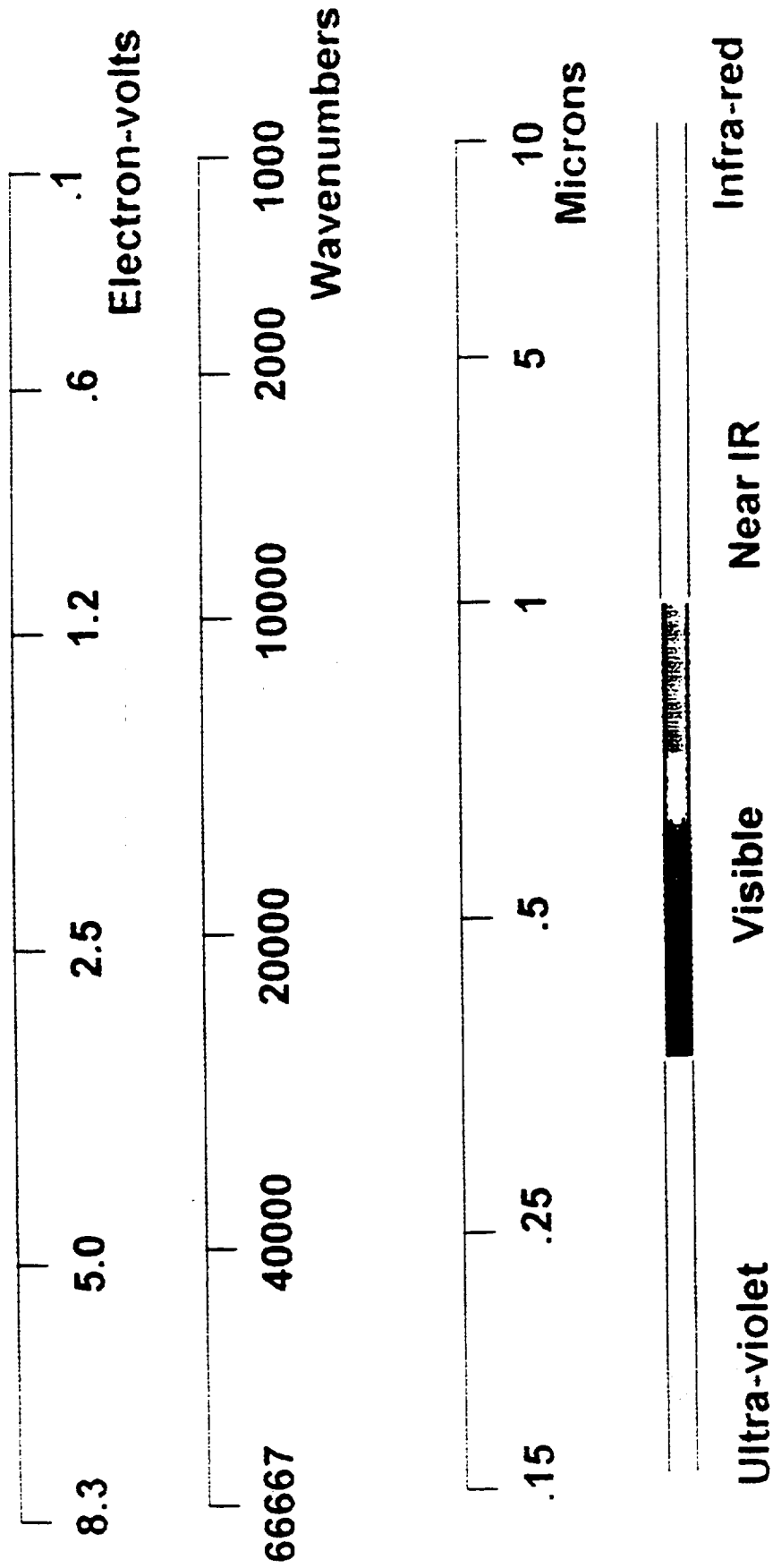


Figure 1

conventional and Fourier transform spectroscopy almost impossible in the presence of water. Fiber optic spectroscopy raises silica fibers to transport the light beam. This eliminates the long paths through the atmosphere. Two separate published spectra for water are given in Figures 2 and 3. Figure 2 shows the spectra published in the Handbook of Military Infra-red technology (2), which is a compilation of atmospheric absorption features of water and carbon dioxide vapor. We originally looked for correspondence with these absorption features in our data due to the similarity of the chemical species involved. In addition, there was an NIR spectrum of water reported by Weyer(3) that shows the per cent transmission of bulk water. Note that the absorption are significantly different. Table I shows the spectral absorption's attributed to water and the corresponding harmonics which would be observed in the NIR.

Table I. Vibrational assignments for water vapors

Vibration(s)	Assignment	Wavenumbers ( $\text{cm}^{-1}$ )	Wavelengths (microns)
$\nu_1$	Sym-stretch mode	3657	2.73
$\nu_2$	Bending mode	1595	6.27
$\nu_1 + \nu_2$	Combination band	5252	1.9
$\nu_1 + 2\nu_2$	Combination band	6847	1.46
$2\nu_2$	Second Harmonic	7314	1.37
$\nu_1 + 2\nu_2$	Combination band	8442	1.19

The wavelengths for the combination and overtone bands shown in Table I fall into the spectral region in the NIR where most of the work has been performed in this research. Since there is some discrepancy between the spectra published by Weyer and the IR Handbook, we took our own observations to determine what the spectra looked like with the optical fiber spectrometer. This data is shown in Figures 4. A spectrum of acetone is shown as figure 5 to illustrate the large number of carbon hydrogen bands in the near infrared. Sharp carbon hydrogen bonds are also observed for silicones.

Specular reflections, angle of incidence equals angle of reflection, produce spectra when chemical species on the surface absorb light. Diffuse spectra are observed when the surface is rough or contains small particles that result in multiple reflections from surfaces that contain absorbing species. Absorption/reflection refers to the condition where a dielectric is covered by an absorbing film. Light can be specularly reflected at the surface of the film or pass through the film, with absorption, be reflected at the surface and pass a second time through the film. Since the index of refraction of a material goes from a finite values to  $+\infty$ , to  $-\infty$ , and again to finite values at the center of an absorption band, the band shapes appear similar to those obtained by differentiation.

A significant aspect of the work performed deals with the absorption/reflection phenomena associated with spectral observations from D6AC surfaces. The problem to be

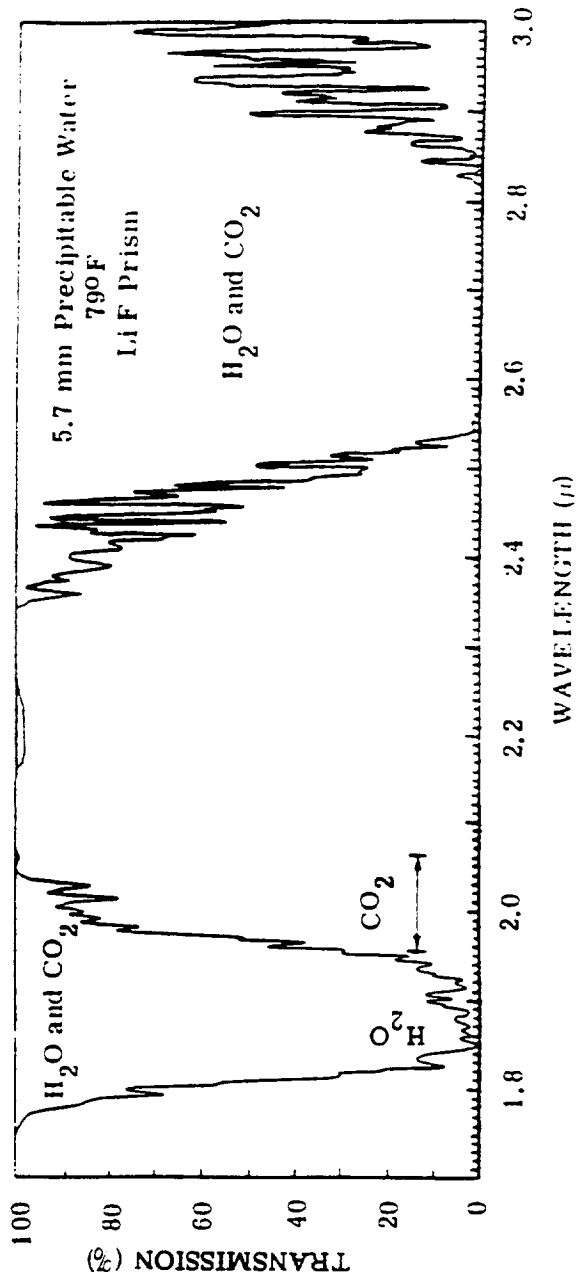
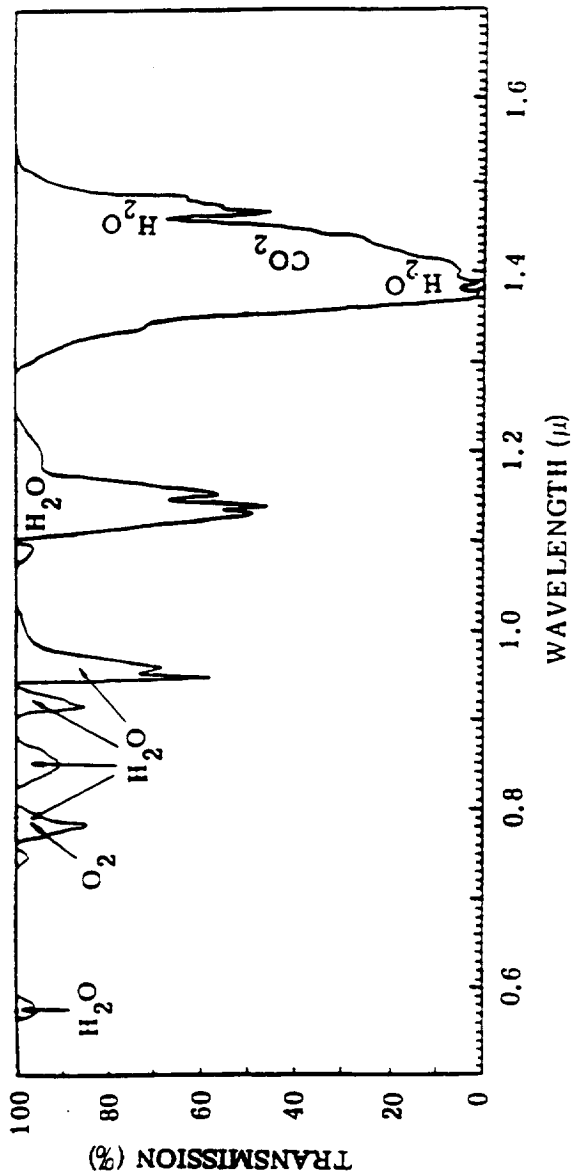


Figure 2. Water and carbon dioxide absorption bands

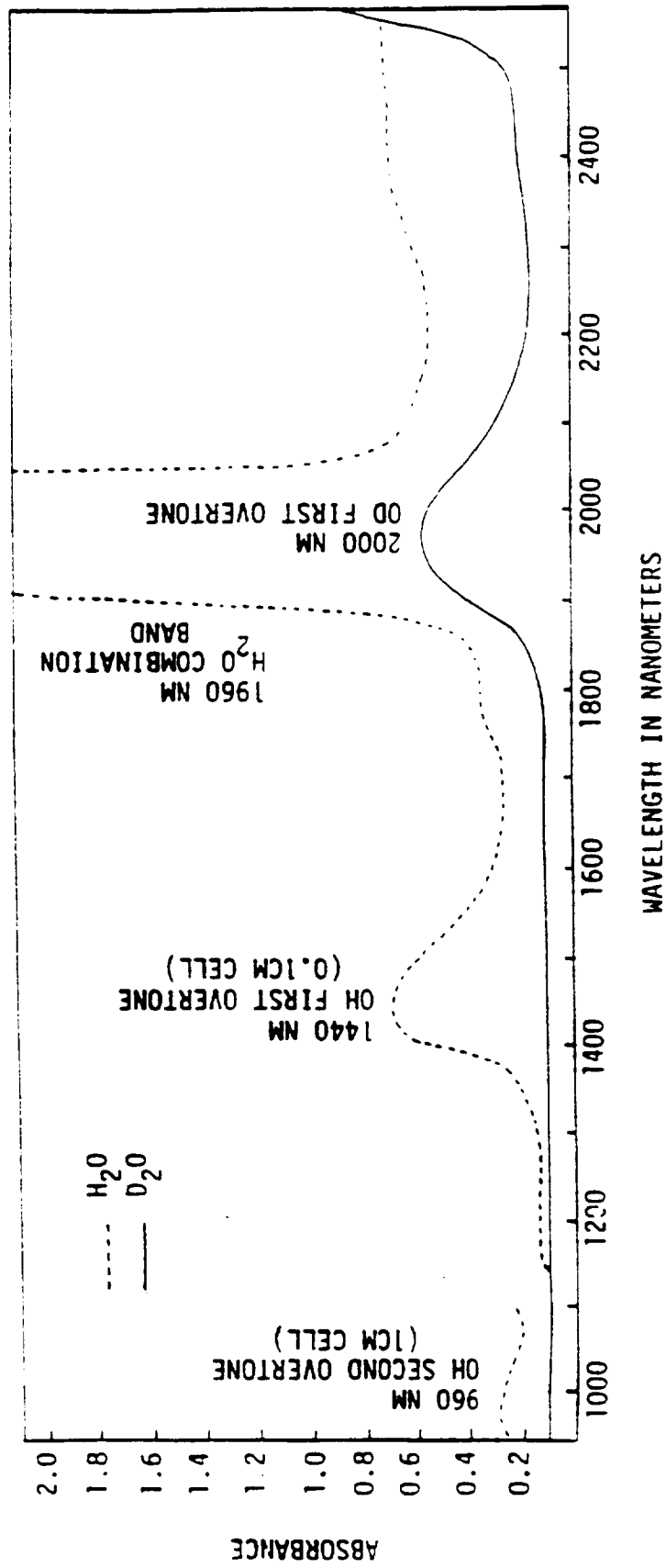


Figure 3. Near-infrared spectra of water and deuterium oxide. (Weyer)

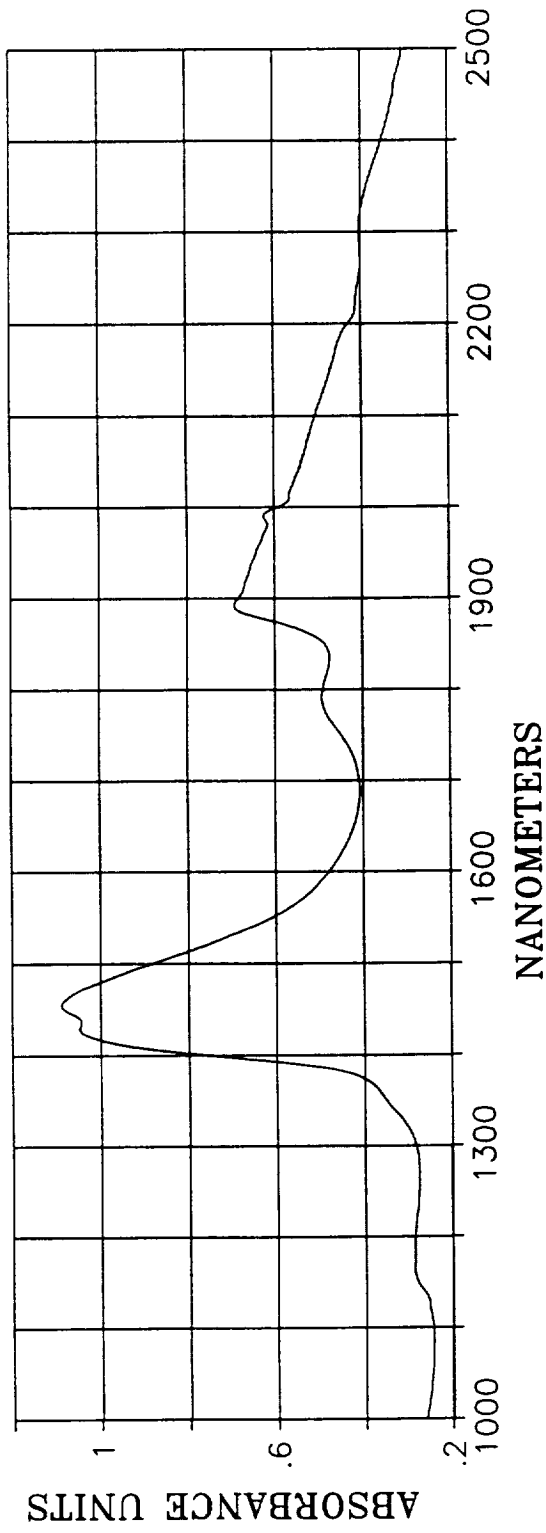


Figure 4. Spectrum of Water in 1mm Cell (UAH)  
ESMOOTH 30

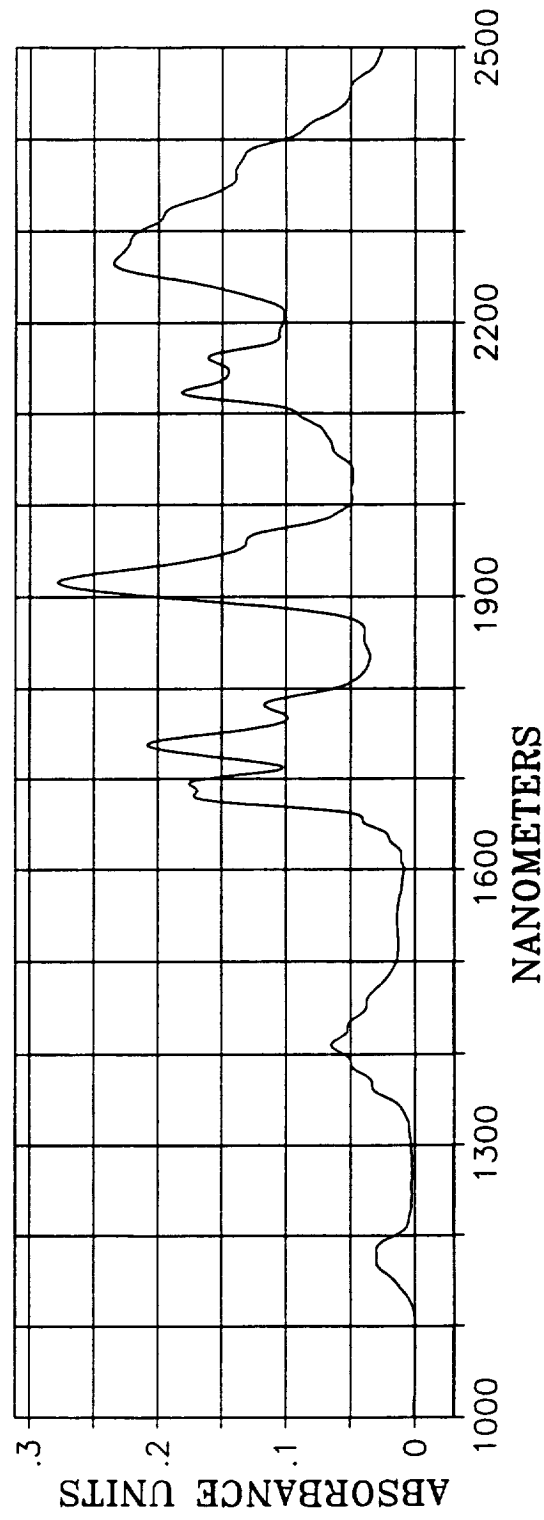


Figure 5. Spectrum of acetone in 1mm cell (UAH)  
ESMOOTH 30

# EXAMPLE OF REFLECTION/ABSORPTION PROCESS

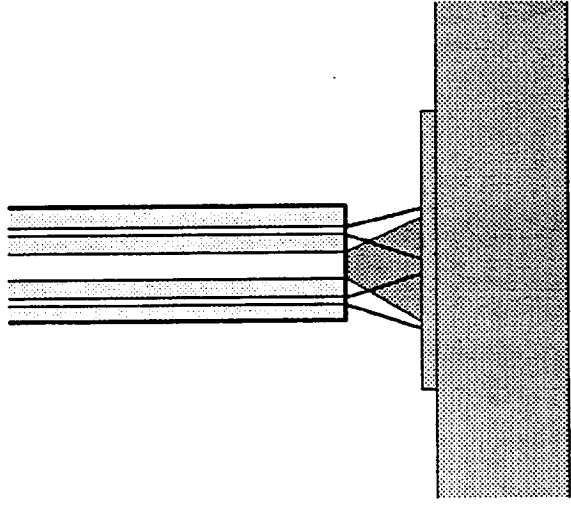
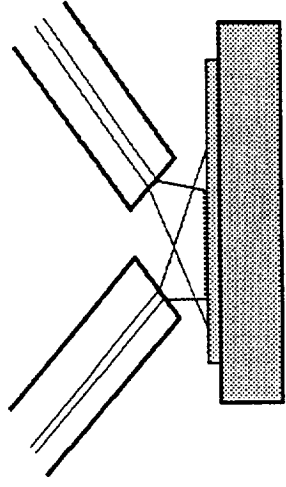


Figure 6

overcome, particularly if an automated procedure is developed, lies in the difference observed in spectra if the process occurs through reflection (specular or diffuse) or absorption/reflection.

Each case requires a different procedure to extract the molecular absorption features imbedded in the signals. Figure 6 shows a cross-sectional view of the optical fiber transmission and receiver characteristics and the optical phenomena affecting whether reflection or absorption/reflection processes account for the observed spectra. There will more discussion of these concepts throughout the results and conclusions sections.

#### 4.0 Brief Description of Chemometric Principles

The chemometric concepts used most frequently in this work are basic approaches to improving the signal-to-noise of the acquired spectra and principal component (or factor analysis) to pick out the significant features of the spectra [1, 4-5]. The procedures performed for the spectra presented here were procedures embedded in commercial software packages. They will be identified during the discussion on the experimental approaches.

For improving the signal-to-noise ratio we made use of several smoothing routines. The Savitsky-Golay method is a moving average type filter that is based on asymmetric convolution function around the data point to be smoothed. Each data point is then averaged according to:

$$y_{s,i} = \sum_{j=-m}^{+m} c_j y_{j+i} / NORM$$

With Gaussian peaks, the signal-to-noise is improved according to the square root of the window size. For example, a 25 point smoothing routine provides a factor of 5 improvement in S/N. Other routines used in this work, part of the software package SpectraCalc marketed by Galactic Inc., include the ESmooth routine which is a Maximum Likelihood filter that takes an *a priori* peakshape, such as Gaussian or Poisson, and then computes the most likely set of peaks which are buried in the spectra. ESmooth is also a maximum entropy filter which allows it to maximize upon the possible probability states.

Multivariate data reduction techniques are required for the following reasons[1]:

1. Lack of selectivity - No single x variable is sufficient to predict y.
2. Collinearity - Redundancy and intercorrelations between the x variables.
3. *A priori* information about the nature of the data is not known.

There are several methods for reducing a data matrix into a smaller number of factors. The algorithm ultimately used depends upon the particular software package or characteristics of the data set being analyzed. The first step is to combine a group of measurements into one data matrix. The measurements may include any set of chemical or physical observations and may include several instrumental techniques. For example, in the data matrix a row may concern a molecular species and a column may concern a particular measurement. Factor analysis yields a score matrix that depends on the characteristics of the molecular species and a loading matrix

which depends solely on the nature of the matrix.[5] Such a separation provides the analyst with improved insight into the number of phenomena being observed.

A data matrix  $D$  consists of  $r$  rows and  $c$  columns:

$$d_{ik} = r_{ij} \quad c_{jk}$$

or in matrix terms:

$$D = R_{\text{rows}} \quad C_{\text{columns}}$$

Mathematical algorithms decompose  $DD^T$  to give  $R_{\text{abs}}$  and  $C_{\text{abs}}$  that contain abstract row and column vectors related to variance. Although these factors can be used to quantitate the information contained in  $D$ , it is usually desirable to find a transformation matrix  $T$  such that  $R_{\text{abs}}T$  gives a matrix,  $R_{\text{real}}$ , related to the chemical or physical content and  $T^1C_{\text{abs}}$  gives a matrix,  $C_{\text{real}}$ , related to the instrumental observations of real components. Since  $TT^1$  is the identity matrix, the following relation is obtained:

$$D = R_{\text{abs}}TT^1C_{\text{abs}}$$

Using the same notation as above, spectra that obey Beer's law can be expressed by the equation

$$AU_1 = e_{11} C_1 + e_{21} C_2$$

When the spectra of all components are available, it is possible to find  $T$  such that  $T^1C_{\text{abs}}$  gives the absorptivities of each component and  $R_{\text{abs}}T$  gives the concentrations of each component. When the condition exists where we have error free data, minimum noise and the spectrum of each component is known, we can calculate  $T$  and hence the concentration of each component. If the concentrations are known by an independent method of analysis, then we can calculate  $T^1$  and find the unknown spectra. This method is frequently called the A matrix method. As noise increases due to unknown interferences or poor signal-to-noise ratio, only approximate solutions are available. One approach to reducing the number of unidentified factors is to analyze samples for the analytes of interest by an independent method and to use these samples as a training set. A Principal Component Regression or a Partial Least Square Algorithms can be used to select the spectral features that are used to quantitate real data sets for the analytes of interest. This method works only when the training set contains all the variables that will be encountered in future data sets. Materials other than the chosen analytes remain unknown.  $R_{\text{abs}}$  and  $C_{\text{abs}}$  are used to quantitate the analytes of interest without calculating  $T$ . If a species is present that was not in the training set, a warning of the presence of an outlier is given.

When very little is known about the components of  $D$ , all is not lost. One can use all of the chemistry that is known and make hypothesis to be evaluated using multivariate methods. The postulates are reformed and the procedures repeated iteratively. A number of examples illustrating the power of this approach occur in the literature.

The discussion found in the text by Martens and Naes[1] is probably the one most relevant to this work. The software package Unscrambler II has been developed along the concepts derived in that text. Defining factor analysis in the data compression sense, we can write

$$\mathbf{T} = \mathbf{X} \mathbf{V}$$

where  $\mathbf{X}$  represents the observed spectra and  $\mathbf{V}$  is the transformation matrix which produces  $\mathbf{T}$ , the matrix of regression factors or *scores*.

Spectra free from noise are not obtained in most spectral observations; therefore,

$$\mathbf{X} = \mathbf{T} \mathbf{P}' + \mathbf{E}$$

for the data set of spectra where  $\mathbf{X}$  represents the set of observed spectra.  $\mathbf{P}'$  is the *loading* matrix which contains the regression coefficients of  $\mathbf{X}$  on  $\mathbf{T}$ . It is the loadings and the *scores* which are presented most often in the analysis results section.  $\mathbf{E}$  is the error or residuals matrix.

When spectral data can be related to some other experimental parameter corresponding to the observed spectra, principal component regression analysis can be performed on this matrix. The defining relation is now:

$$\mathbf{Y} = \mathbf{T} \mathbf{Q}' + \mathbf{F}$$

where  $\mathbf{Q}'$  now represents the loading matrix or regression coefficients of  $\mathbf{Y}$  on  $\mathbf{T}$ .  $\mathbf{F}$  represents the residuals or unique variation in  $\mathbf{Y}$  that is not explained by the bilinear structure of the analysis. Partial Least Squares Regression (PLSR) forces a common  $\mathbf{T}$  for both the  $\mathbf{X}$  and  $\mathbf{Y}$  matrix.

Principal component regression (PCR) is a method that once a calibration model has been established, predictions of future spectral observations can be performed.

Partial Least Squares Regression (PLSR) can reduce the impact of large, but irrelevant  $\mathbf{X}$ -variations in the calibration modeling by balancing the  $\mathbf{X}$  and  $\mathbf{Y}$  information. PLSR differs from PCR because it uses the  $\mathbf{Y}$  variable actively during the decomposition. However, the simultaneous use of  $\mathbf{X}$  and  $\mathbf{Y}$  does provide some disadvantages relative to PCR. For instance, the PLSR needs to utilize two sets of loading vectors, hence it may be more complex than PCR. Also PLSR has a stronger tendency to overfit noisy  $\mathbf{Y}$ -data than PCR. Neither of these conditions have been found in the work described in this report.

## 5.0 Experimental Approaches

The major software packages used to support this work included SpectraCalc and Unscrambler II. Typically spectra were recorded in units of log watts and transformed into absorbance using the relationship:

$$A = -\log \frac{I}{I_{\text{ref}}} = \log I_{\text{ref}} - \log I$$

Much work was spent at the beginning of the research effort in determining what reference surface to use for  $I_{\text{ref}}$ . A major problem arises when a spectral feature goes negative; i.e.  $I < I_{\text{ref}}$ , then most of the matrix multiplication techniques are not applicable. Practically, a negative absorbance is undefined and means the reference is not valid. Several reference surfaces used in this work include a mirror, total or specular reflecting; barium sulfate, diffuse reflecting; and metal surfaces such as D6AC steel or aluminum. We continue to search for a reference source that could be used for all samples. An improved reference will be required for real-time monitoring.

## 6.0 Results

The activities performed for this research effort provided a broad scope of experiments to build a knowledge base upon which one could improve bonding processes in SRM's. In response to the research objectives defined earlier, a number of spectra were recorded in both the UV and NIR regions. The spectra were typically D6AC witness panels which had been exposed to various temperatures and humidity environments for selected periods of time. In general the environmental exposure conditions were developed by AC Inc and SAIC as a Taguchi devised plan to determine the effect of temperature, humidity, and time on bonding for the SRM. UAH participated in this study using the Guided Wave 260 optical fiber spectrophotometer to record spectra as needed.

In addition to the UV and NIR spectra presented here, UAH personnel also assembled an OSEE scanning system at UAH and was able to get most of it going during the early part of the contract. More emphasis was placed on spectroscopy later on in the contract; and very little was done to produce OSEE measurements at the University. Part of the problem was that version 1 of the OSEE detectors were received with the scanning apparatus and the overall sensitivity was mediocre. The OSEE scanning systems at MSFC were much better in most functional specifications and since that data was constantly being acquired by AC and SAIC, there was no point to our taking the same data over.

Using multivariate analysis to better understand the spectral results was very beneficial to building up an interpretation of the spectra obtained in view of the very difficult chemical system interrogated. Water from the humidity of the environments and a proposed FeOOH chemi-sorbed oxidation species form a complex difficult to unravel. Adding to the situation was the observation of absorption/reflection phenomena in the observed spectra. With this complexity in interpretation, it is very difficult to understand what chemistry is occurring without such techniques as PCA, PCR, and PLSR.

## 6.1 Spectral Determinations of Contaminants

A number of different spectral observations were recorded in this work. At the very beginning of the activity, identification of contaminants on SRM surfaces was the primary thrust. Hence, the first sets of data were various contaminants on specular and diffuse surfaces. Examples of contaminants used were Tap Magic, HD2 grease, Masking Tape Adhesive, Human Sebum, Machine Cutting Fluid, WD-40 spray lubricant, and Lubriseal vacuum grease. The test matrix is shown as Table II, in section 6.1.1 spectra were recorded in the UV region from 200 to 350 nm.

Brian Benson, then set up a calibration using PLSplus in SpectraCalc that indicated that sensitivity was probably around  $8 \mu\text{g}/\text{in}^2$ . There was a problem, however, in obtaining consistency in the spectral observations on D6AC steel. The spectra from D6AC steel change with time and from location to location on the plate.

In conjunction with this activity, Morgan Wang, a graduate student in ECE at UAH worked on developing an eddy current proximity sensor to measure the stand-off of the optical fiber and the OSEE, very much like the arrangement of the CONSCAN at MSFC. This work was pre-empted by the need to concentrate on making measurements of D6AC steel exposed at various humidities and temperatures in the environmental chamber at Building 4712 at MSFC.

### 6.1.1 Matrix of Contaminants

UV spectra were obtained for the composition shown in Table II. The contaminants were dissolved in  $\text{CHCl}_3$ . Appropriate quantities of the solutions were placed on a solvent cleaned D6AC plate using a micropipette. The additions were controlled so that each spot remained approximately the same size as the solvent evaporated. Shown in Figure 7A is the spectrum of the pure component. Shown in Figure 7B is the Principal Component Analysis, PCA, of the sample matrix. As expected there are 6 factors, one for each component. This is the number of factors that are expected in the X data if there are no interactions between component or between any of the components and the substrate. When the components are mixed interactions, for example, hydrogen bonding, require an additional factor for each type of interaction. When a PLS2 analysis was done using the X and Y matrix at the same time, 16 factors are required. Figure 7C shows the variance found for each factor. Sixteen factors were more than anticipated. However, we have learned as this program has progressed, several factors are required to describe the D6AC substrate. The contribution of each factor to a description of the steel changes with time and from spot to spot on the plate. If this analysis were to be repeated, this should be done on a freshly prepared grit cleaned surface and the time between the cleaning and the use carefully recorded. These interactions are described in the next section.

Figures 7D - 7I show the predictions from the model versus the compositions shown in Table II. Note that very good correlation is obtained for HD2, WD-40, Lubriseal, and Apiezon. The poorest predictions were for Sebum. It should be noted that this contaminant was used in the smallest quantities; therefore, shows the greatest error due to poor signal/noise ratio. The greatest surprise at the time the study was made was the poor fits at 0 concentration. There is no

signal from the component: therefore, the worst signal/noise condition. Also recall that these plates were only solvent cleaned and there is a strong gradient related to humidity on the steel surface.

We conclude that a UV method to detect contaminants as represented by these contaminants is feasible. The NIR should also be considered.

TABLE II. Samples used for UV study

Component	HD2	Tap Magic	WD-40	Lubriseal	Apiezon	Sebum
3 19 2	0	0	0	0	0	0
3 19 3	0	0	0	0	0	0
3 19 4	0	0	0	0	0	0
3 19 5	0	0	0	0	0	0
3 19 6	0	0	0	0	0	0
3 19 7	0	0	0	0	0	0
3 19 8	25	0	0	0	0	0
3 19 9	0	12.5	0	0	0	0
3 19 10	0	0	40	0	0	0
3 19 11	0	0	0	20	0	0
3 19 12	0	0	0	0	25	0
3 19 13	0	0	0	0	0	2.5
3 19 14	50	0	0	0	0	0
3 19 15	0	25	0	0	0	0
3 19 16	0	0	80	0	0	0
3 19 17	0	0	0	40	0	0
3 19 18	0	0	0	0	50	0
3 19 19	0	0	0	0	0	5
3 19 20	12.5	0	0	0	0	0
3 19 21	0	6.25	0	0	0	0
3 19 22	0	0	20	0	0	0
3 19 23	0	0	0	10	0	0
3 19 24	0	0	0	0	12.5	0
3 19 25	0	0	0	0	0	1.25
3 19 26	25	0	20	0	0	0
3 19 27	0	12.5	0	0	0	2.5
3 19 28	0	0	0	20	12.5	0
3 19 29	12.5	0	0	0	0	2.5
3 19 30	0	0	20	20	12.5	0
3 19 31	0	6.25	40	0	25	0
3 19 32	0	0	0	10	0	2.5
3 19 33	0	0	40	0	0	2.5
3 19 34	25	12.5	0	0	0	0
3 19 35	12.5	0	0	0	25	2.5
3 19 36	0	0	20	20	0	0
3 19 37	0	0	0	0	0	0

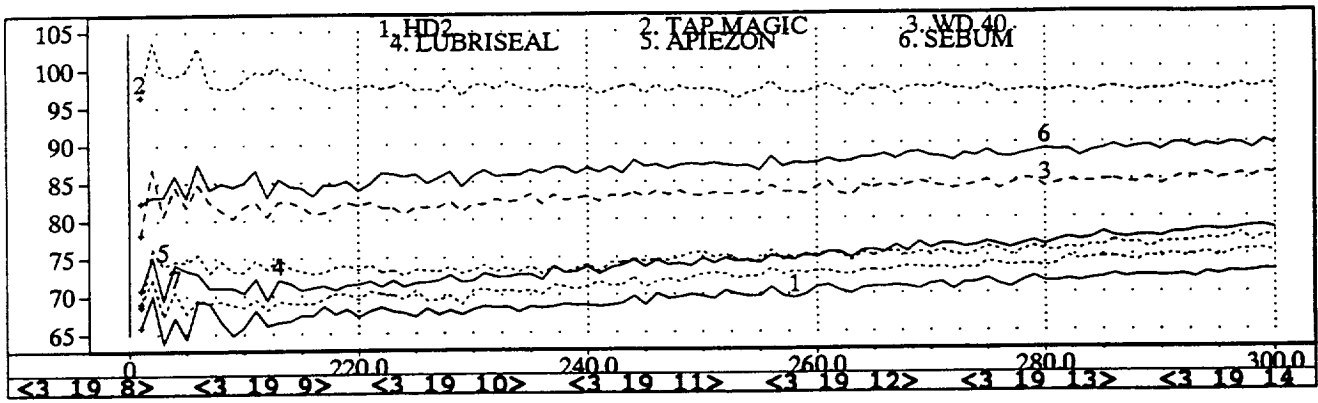


Figure 7a. UV Spectra of Contaminants

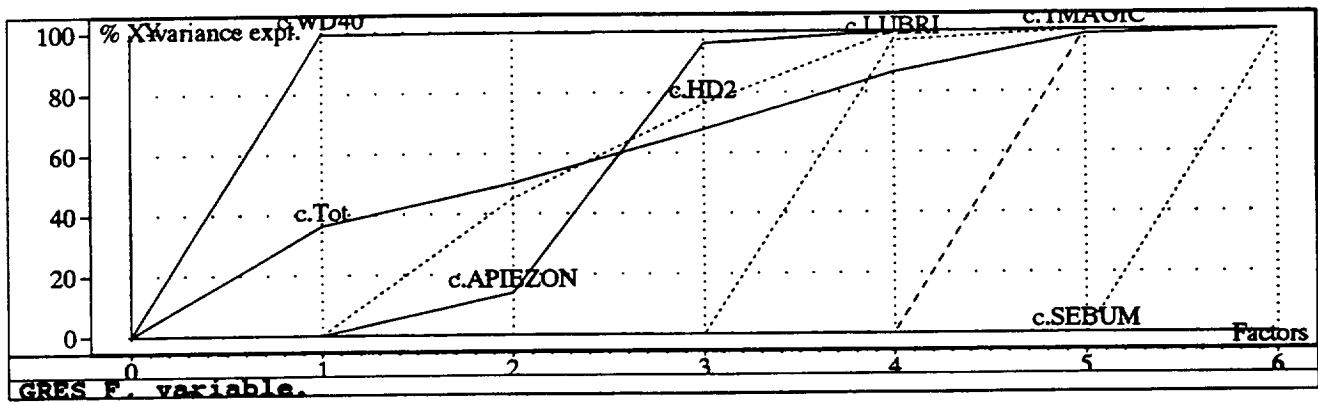


Figure 7b. PCA Analysis of Y matrix

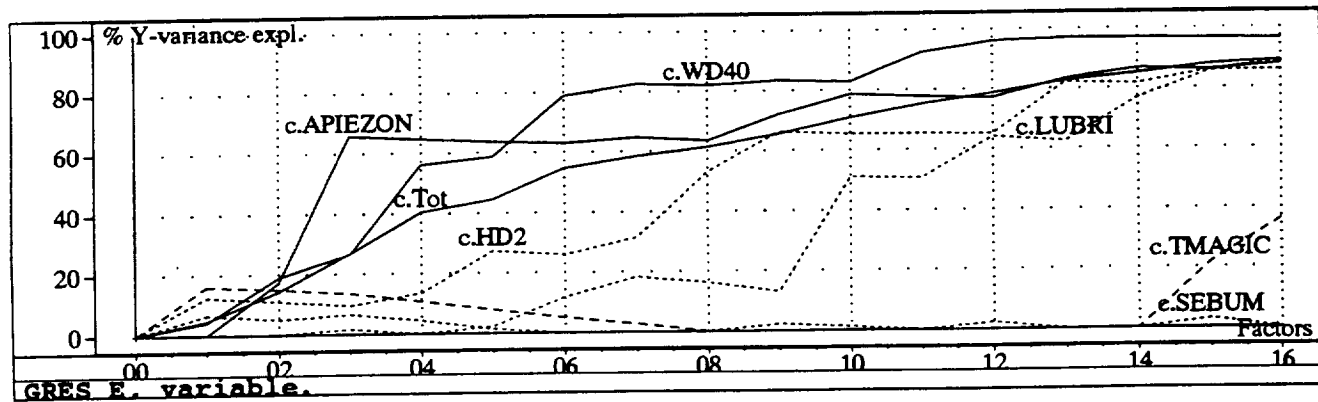


Figure 7c. PLSR of Y and X (UV data)

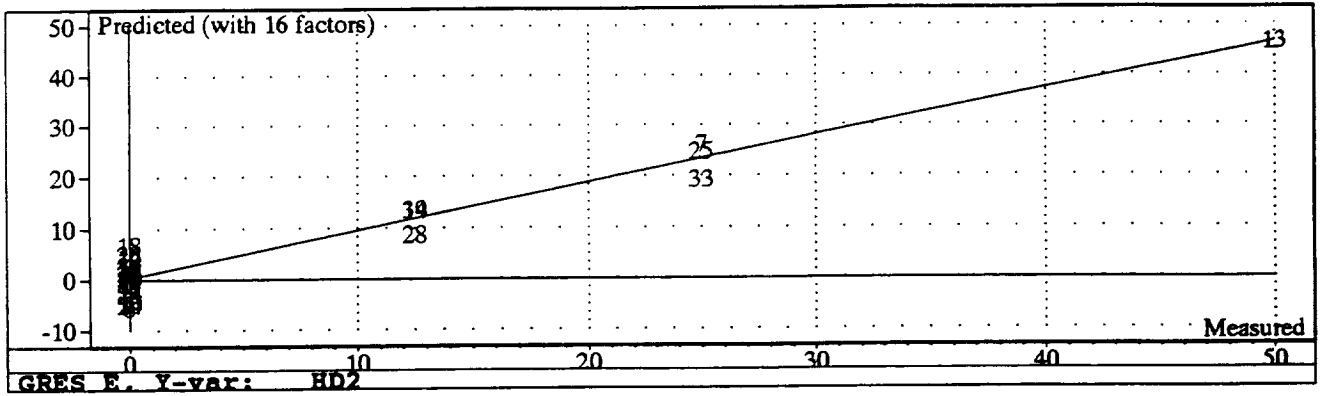


Figure 7d. Regression Analysis for HD2

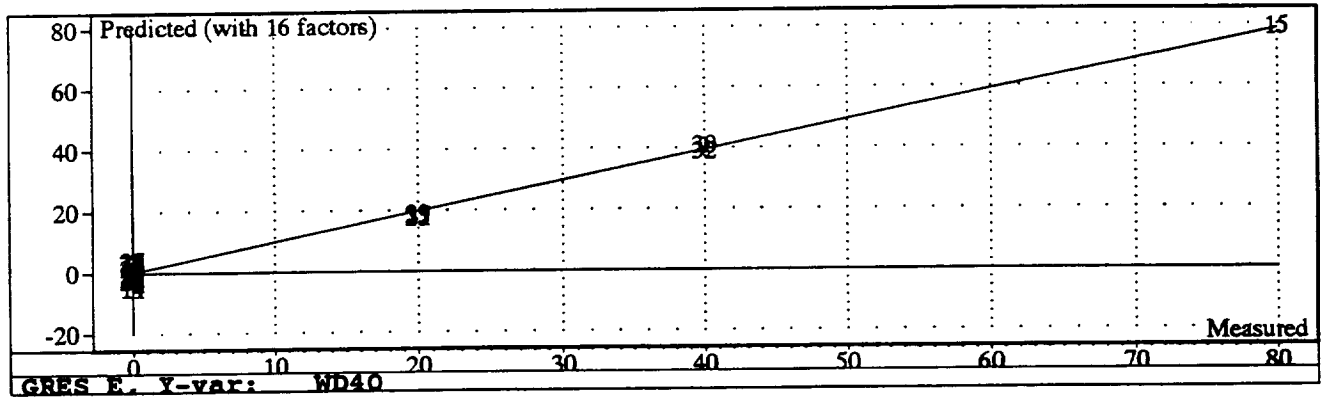


Figure 7e. Regression Analysis for WD40

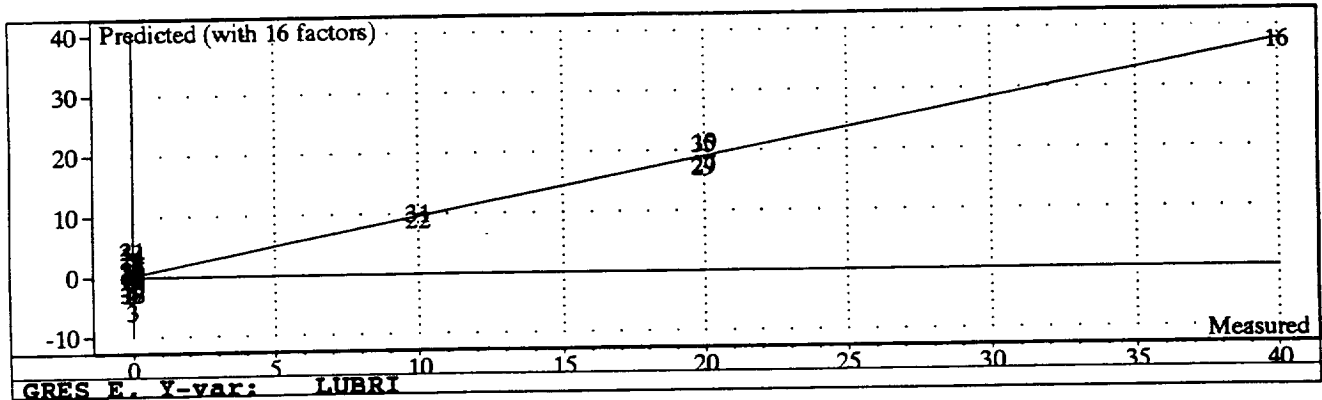


Figure 7f. Regression Analysis for LubriSeal

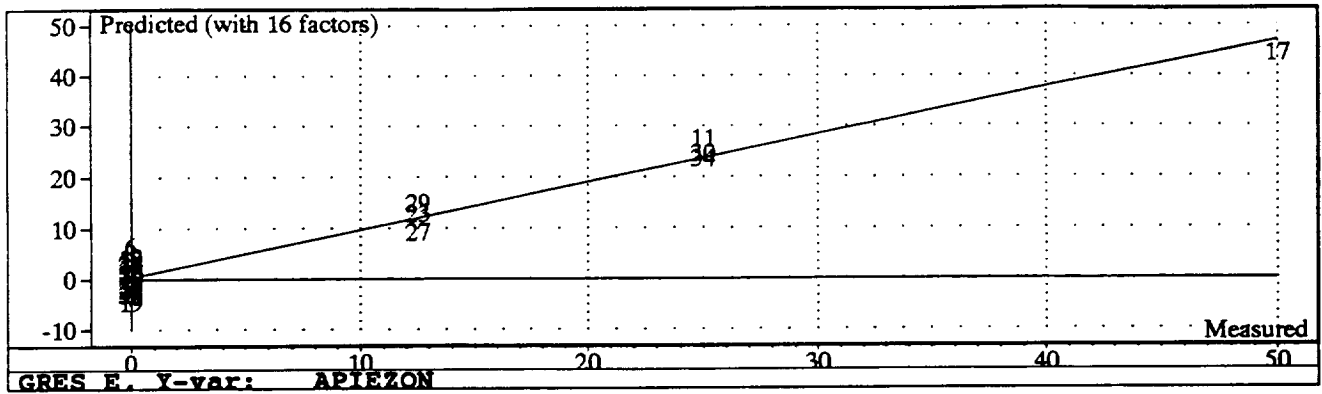


Figure 7g. Regression Analysis for Apiezon

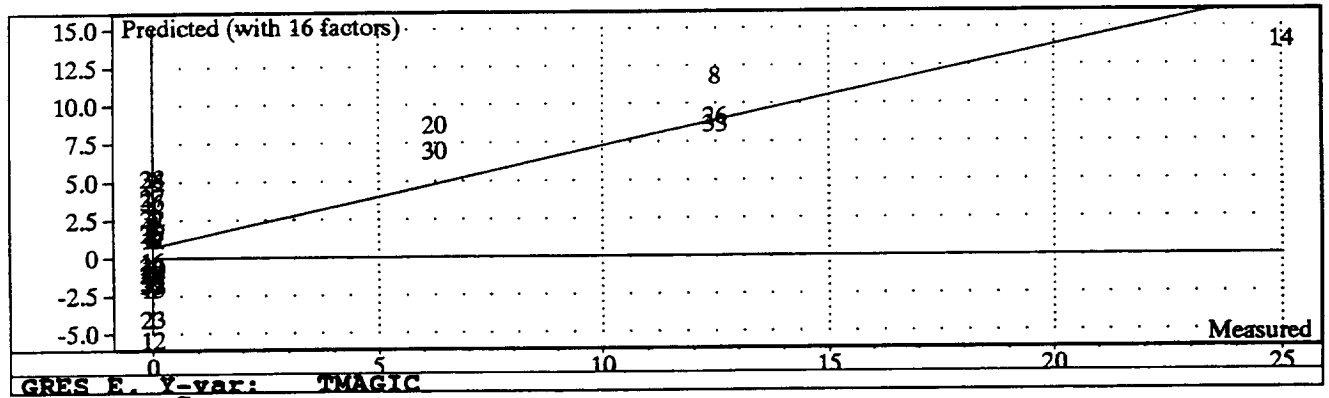


Figure 7h. Regression Analysis for TapMagic

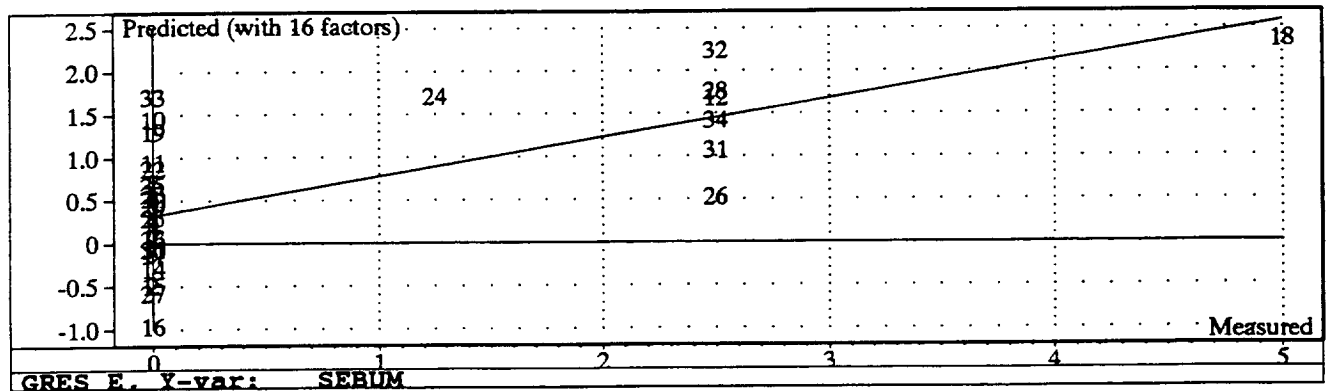


Figure 7i. Regression Analysis for Sebum

## 6.1.2 Choosing the Reference Spectra

When working with spectrophotometric data Absorption Units are preferred.

$$AU = - I/I_{ref} = \text{Log}(I_{ref}) - \text{Log}(I)$$

The Guided Wave Model 260 is a single beam spectrophotometer. Therefore it is necessary to record the spectrum of a reference and store it in the memory to be used when the sample data is taken. Choice of the reference sample is very important. For many purposes a reference is recorded, the spectrum of the sample taken, and then the reference again checked. For the experiment described in Section 6.1.1, a spot on the blank plate was chosen for the reference and the sample data referenced to this spectrum and the data recorded as Percent Reflectance (%R). When the laboratory initially received the D6AC panels there was not a comparable procedure. The entire panel had been treated. A search was made for an appropriate reference. Front surface mirrors, pressed BaSO<sub>4</sub>, thin layer chromatographic plates, and Kodak Color References were tried. None of these were satisfactory for this project. The Guided Wave Model 260 can write to disk a log(watts) file. Therefore, the data has been archived as log(Watts). These files can be used to try various data reduction methods as other reference samples become available.

The spectral differences, when the same spot is observed as a function of time, are usually small (0.000 to 0.03 AU). If the reference is not a perfect match and we subtract the sample spectrum from the reference spectrum, negative values are obtained. A negative state for AU is undefined. The condition can only be defined as the sample reflecting more light than the reference. If a specular reference is used AU values greater than 4 are obtained. If a true value, then 99.999 percent of the light is being absorbed.

For the D6AC data which was recorded as a function of time and included in this report the first spectrum obtained was used as the reference and the later values subtracted from it. This gives a consistent set of data for a given condition. Comparison between tests where conditions differ are less reliable.

As indicated above many of the values were buried in a noisy signal. Therefore after the subtraction was made the noise was smoothed using a maximum likely hood- maximum entropy routine (6). For these studies a Gaussian shape peak and normally distributed noise was assumed. The effect of the smoothing is shown as Figure 8.

The search for a standard that can be used for all types of samples continues. We are also investigating other approaches to data reduction. Any time a mathematical operation is performed there is a chance of adding noise (data that is a function of the method rather than the sample). For many purposes watts would be better than log(watts). The values for reflected energy from steel and aluminum for the Guided Wave Model 260 is 10<sup>-10</sup> to 10<sup>-11</sup>. The antilog is a smaller number than the PC can store in a buffer. An approach that we are currently trying is to add 9 or 10 to the data to multiply the data by 10<sup>9</sup> or 10<sup>10</sup> and then take the antilog. The new spectra are suitable for spectral subtraction and similar procedures. Multivariate analysis

procedures can be used on the data without further processing. This procedure may be applicable as we move toward automated inspection with automatic data reduction and display.

## 6.2 Chemometric Determinations

Several types of information can be derived from accumulated spectroscopic observations on the sets of witness panels that have been processed by a standard procedure. The initial observations were related to possible correlations between spectral data and OSEE data on witness panels that were placed in an environmental chamber at MFSC and maintained at different temperatures and relative humidities for various times up to 28 days. The conditions were meant to simulate potential working environments for SRM manufacturing to determine whether some of these conditions would affect bonding parameters for the chemical system used in the SRM. The test specimens and environmental conditions are given in Table III. PCA analyses were made using 4 to 8 spots distributed uniformly on the test specimens. As we attempted to obtain reproducible results from the analyses we began to realize that the reactions do not terminate when the samples are removed from the environmental chamber and stored in nylon bags containing nitrogen. The time between removal from the environmental chamber and the NIR observations made at UAH varied from a few hours to several weeks. A cluster analysis indicated that there was a difference between the 28 day sample and the samples stored for shorter periods. The reference problem discussed in the last section was discovered. Since log watts records had been archived, several spots on the plates were tried as reference spots. The magnitude of the differences within a panel are shown in Figure 9.

The surfaces were also changing as the samples were exposed to the UAH laboratory environment. We were convinced that the spectra represented absorption bands for water physically and chemisorbed, and the OH bands of reaction products. We also were confident that the Guided Wave Model 260 Spectrophotometer was sensitive enough, using the probe containing 9 fibers to illuminate the surface and 10 fibers to observe the surface, to provide real time data. The Guided Wave Model 260 spectrophotometer was set up on two occasions at the MFSC chamber. These experiments were labeled E4 and HIT. The test conditions are given in Table IV. A third series of data was obtained in a UAH laboratory. A small laboratory was used for the experiment. This laboratory has no outside windows or doors. The environment was found to be reasonably constant over a 2 week period. The test conditions are also given in Table IV.

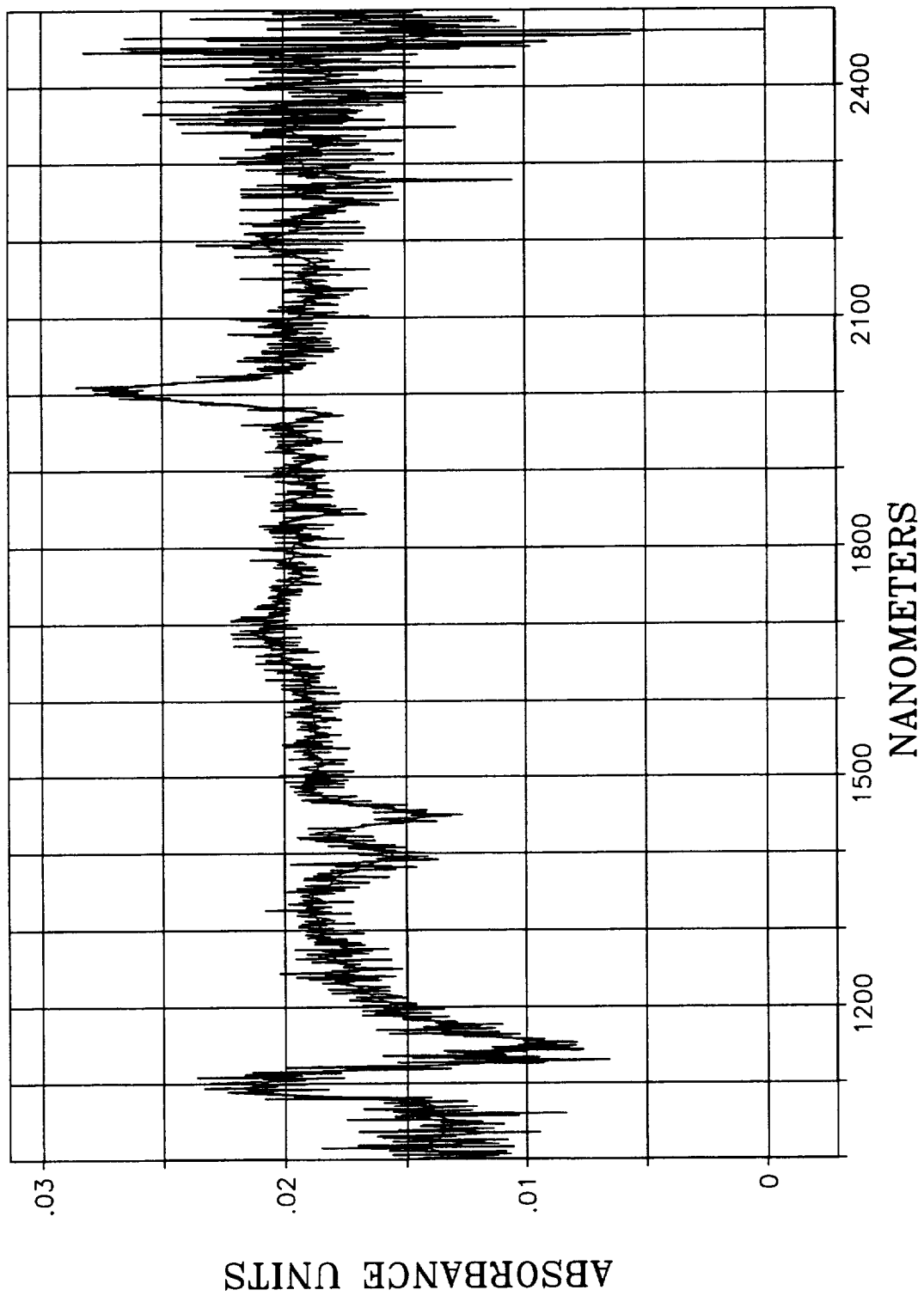
All of the real time data was processed by subtracting the values for a sample from the initial sample to convert to absorbance units, using ESMOOTH and when necessary correcting the base line to 0 (offset). The spectra that are obtained do not have a baseline reference and the peaks appear to overlap. A common method to deal with these conditions is to convert to the second derivative. Many peaks were observed. The software available at the time was not suitable for multivariate analyses on the derivative spectra. Therefore, the absorption spectra were used with the PCA algorithm found in UNSCRAMBLER II. The 78 spectra in the E4 set were considered as one set. Six to eight factors were required to model the data. Considering the large number of possible compounds this is considered a small number. In an attempt to determine the time sequence of the appearing and disappearing spectral lines the data was divided into several sets.

For the first attempt a factor analysis of spectra 1 through 10 was used followed by analysis of spectra 5 - 15 etc. The individual sets were often modeled with one factor and seldom showed more than 3 factors were required. The factors found in these sets were combinations of the factors obtained on the entire set. This procedure was used in an attempt to see if reactions were repeating in a sequence. As we have accumulated data it is now believed that the segments were too small, that is the reactions are slow. The model would be consistent with a long induction period before a reaction begins and a fast reaction following initiation. A significant variant is the absorption and deabsorption of water vapor. A third procedure was tried. Samples 1 - 15 were used, then 1 - 25 etc. The analyses followed the scores and loadings of the total set. However, we did get some indications where reactions started. A companion study that starts from the back and moves forward was not attempted as data from the second series was becoming available. As described above, PLS algorithms use the X matrix with a Y matrix. A Y matrix that used the sample number was used with the 78 spectrum matrix. It was necessary to remove spectrum 67 from the data as an outlier. It was then found that the sequence was predicted correctly. The exposure time in minutes was used to replace the sample number in the Y matrix. The result was smoother curves.

Since we are modeling data related to compounds with unknown identity, data reduction requires iterative attack. Both time and OSEE values were available for the HIT series. Now we have two columns of values for the Y matrix. Therefore, the PLS2 algorithm in UNSRAMBLER II was used. Shown in Figures 10a and b are the predicted values for time and OSEE vs observed values using 10 factors. The predicted values for time are better than the predicted values for OSEE. The largest differences in the OSEE predicted and observed values are at the beginning of the sequence when the OSEE values are changing rapidly and at the observations following power interruptions.

Model SO C constructed using the UAH Lab data was used to predict the values for the E4 and HIT sets. The model predicted the correct sequence; however, the times are different from the observed. The 70° runs predicts high values for the HIT set. This is what would be expected if endothermic reactions are taking place. Less time would be required to reach a given state at the higher temperature. The three rates are composed in Figure (11).

A number of attempts were made to extract kinetic data for oxidation of the D6AC. Unfortunately the data for E4 and HIT data sets showed sufficient oscillatory behavior in the factors over time that we are not confident that the kinetics of the oxidation species are obtainable from the data. We also are wary of environmental control in these tests which might affect the oxidation and hydrolysis of the D6AC steel.



SPECTRUM 65 SMOOTH vs NOISY  
ESMOOTH 30

Figure 8

### 6.3 Discussions Related to Two Models

Two data sets are discussed in this section to illustrate the methods which are used. Shown in Figures 11a through 11j is results of an early model, NAR A. The data is taken from the E4 set. Loadings are plotted at the top of the page and scores at the bottom of the page. Wavelength - 1000 nm is the abscissa for the loadings. The loadings are selected features of the spectra. The scores, representative of amount of a species, are plotted vs sample number. Note that factor 1 is primarily for sample 67. This was a spectrum recorded after a power outage. Factor 1 is so dependent on a single factor that we would repeat the procedures and obtain a new model. This was done. However, further discussion of Model NAR A is profitable.

We must remember that we are working with unknown compounds and their spectra. As we have continued our investigations looking at additional models we are beginning to interpret this early data. The three predominant peaks in Factor 1 the loading appear to be first derivatives. The shape of these three peaks suggest that they result from reflection/absorbance phenomena i.e. the beam passes through a film is reflected at the steel surface and makes a second pass through the film before reaching the spectrophotometer. A current hypothesis is that the composition of the film is some form of water. The peak at 1000 (2000 nm) has the reverse shape to the peak at approximately 1450 and 1100 nm. If these peaks are related to H<sub>2</sub>O the thickness of the peaks near 1450 and 1100 nm are greater than the thickness on the reference (sample 1). The peak at 2000 nm is less than the reference. This is the usual pattern in most of the spectra. Recently we have recorded spectra in the laboratory in which all three of these peaks were increasing. These changes are related to changes in the relative humidity. Looking at Factor 2, we find that this factor looks similar to the first factor but peaks around 2400 nm are important to the last 10 samples. These could represent a hydroxyl containing species. Since it is late in the run these species may be more stable. Note that there is no indication that the beam has passed through a film. Note that the same peaks are involved and that sample 67 is a heavy contributor. Factor 4 loadings show strong bands near 1450 and 1900 nm. The scores indicate that these absorption peaks are important throughout the run. Note that the peaks appear to contain more than one component. We have noticed that the ratio of these peaks can be different from sample to sample. We offer no interpretation for Factor 5. It may be related to the metal surface.

Model SO version C is one of several models made for the run that was done in the UAH laboratory. The Model is described in Figures 13a through 13x. Looking first at the predicted vs observed plot at the bottom of the page, we find that one factor describes a lot of the variance and has a general upward trend. However with only one factor there are a number of peaks and valleys. The spectra represented in the loading all show intensities less than the reference. The peak at 2000 nm is easily observed but does not appear to have sufficient thickness that the peak has the shape of a derivative. Note that the peaks near 1850 nm are almost resolved. Turning to Factor 2 prediction vs observed curve at the bottom of the page we see that some of the valleys have been filled in. The scores plot indicates the quantitative aspects. The scores curve shows that Factor 2 was important for the 35th through the 60th spectra. The peak at 2000 nm now appears to be a derivative indicating a thicker film. In addition to the peaks around 1900 there are feature around 1400 nm. where OH bands would be expected. Turning to Factor 3, we find that the predicted vs observed curve continues to straighten out. The bands at 2000 nm, 1450 nm, and

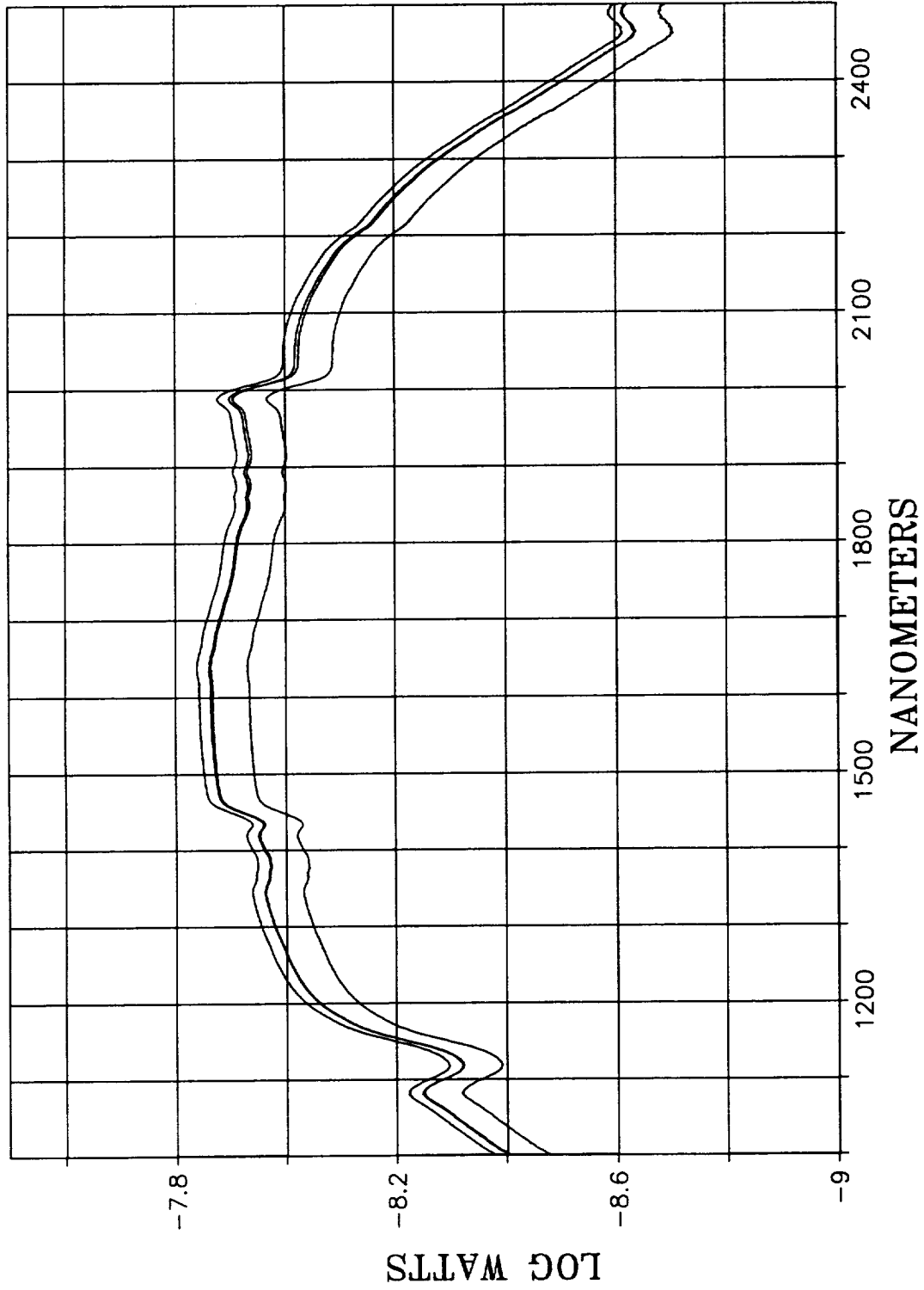


Figure 9. Coupon E8A 7 Days at 100 F/60% RH (Front Side)  
ESMOOTH 30

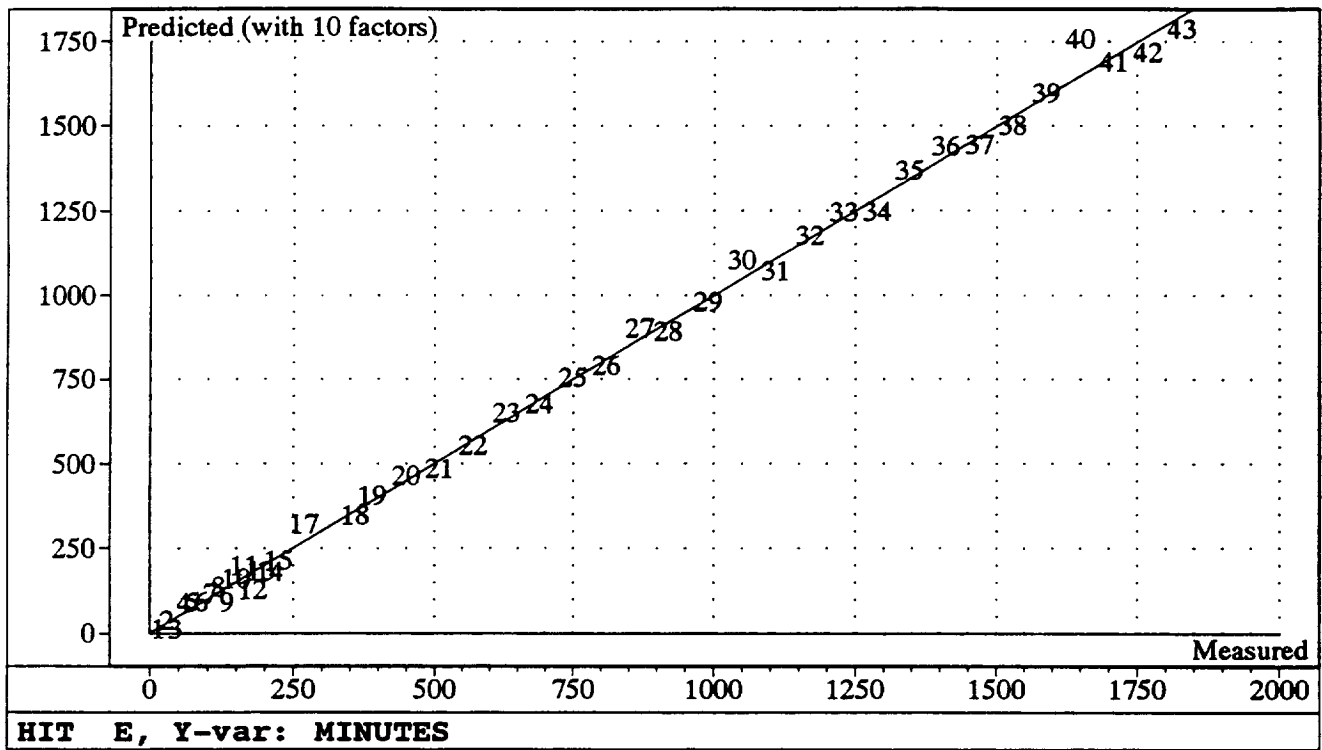


Figure 10a. Observed vs Predicted times for samples in HIT series

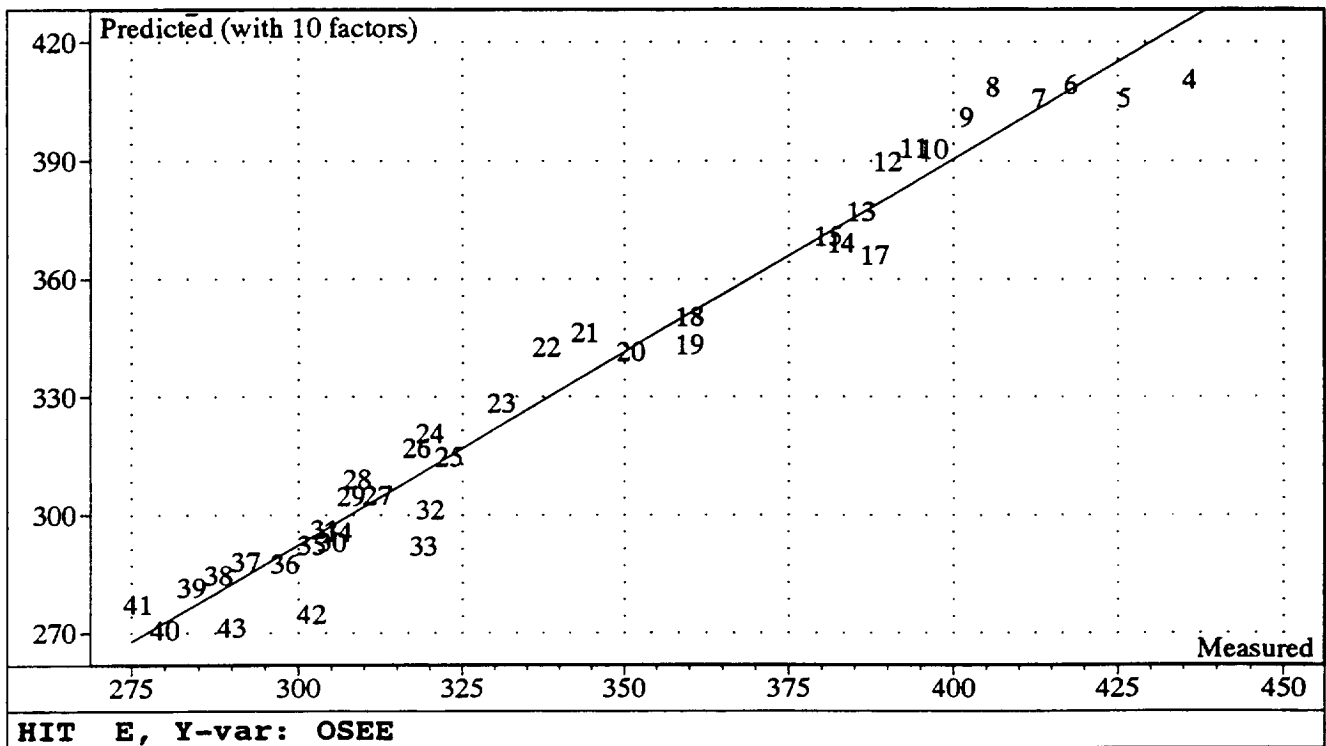


Figure 10b. Observed OSEE values vs Predicted values in HIT series

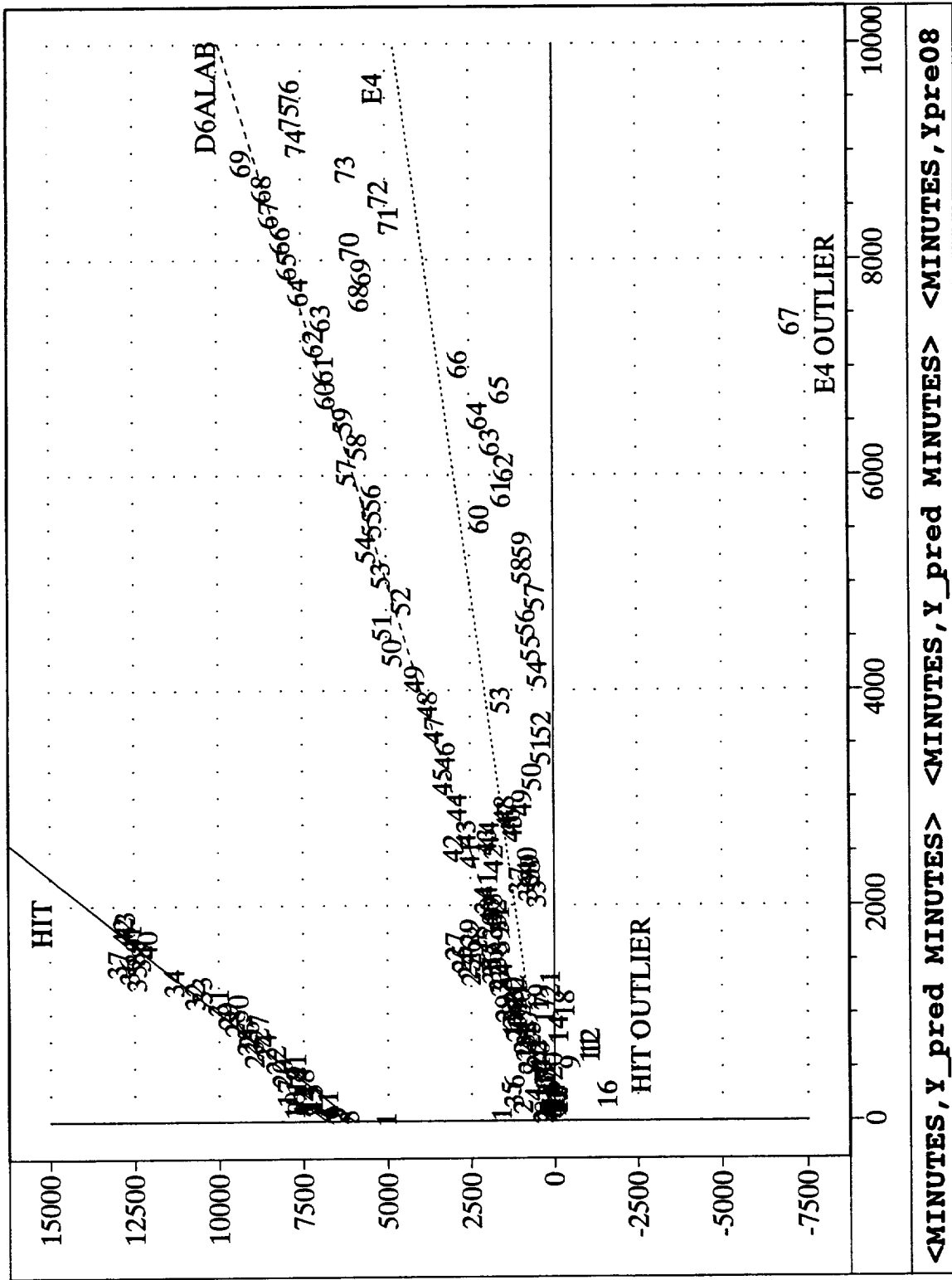


Figure 11. Using Laboratory Data Model SO C to predict HIT and E4 sets.

around 1100 nm appear to represent spectra of thin films. Note that there are two peaks in the 1100 region. As we continue to add factors the predicted vs the observed curve improves. It is difficult to interpret the loadings plot. The magnitudes are decreasing and noise is observed. The observed spectral features are consistent with the NAR A model.

#### 6.4 Observations Related to HD2 on D6AC Panels

An investigation related to methods of covering steel panels uniformly with a known weight of HD2 was running concurrent with the environmental test chamber experiments. While the Guided Wave Model 260 Spectrophotometer was at MSFC, reflectance measurements were recorded in log(watts). Some of the first measurements were made on panels that could be identified as being nonuniform by visual inspection. For the first group of samples, a reference was taken before the panel was coated. For the second group of samples, the panels had been coated before the reflectance measurements were made. A reference was taken of a solvent cleaned spot. Including blanks a total of 48 spectra were taken. If a spectrum of HD2 on the substrate was available this would be a simple calibration. We have worked with this set of spectra as we investigate better methods of gaining the maximum information from a data set

The 48 spectra have all of the features and problems identified in previous discussions. There is some evidence that the panels had the film that has been tentatively identified with water absorption and deabsorption before the coating operation began. Also the coating procedure may be adding water in addition to the trapped water. The first attempts to visually identify peaks that were increasing as the thickness increased was unsuccessful. An ATR spectrum was recorded. This spectrum is shown in Figure 14. More recently, we have obtained a reflection spectrum of HD2. This film was sufficiently thick that only reflections from the surface were obtained. This spectrum is shown as Figure 15. A series of models were made systematically reducing the number of spectra in the calibration set until a consistent set was obtained. There is significant scatter in the data. Some of the variance is probably related to non uniformity resulting from separation of the chemical components.

Rather than report the data related to the models discussed above, some recent work related to a different method of handling the data is reported. The reflection curves are recorded in log(watts). The procedure for reducing the data to AU has been described. Since adding or subtracting logarithms is equivalent to multiplication and division the original data cannot be averaged or smoothed prior to conversion. An additional objective is to reduce the number of mathematical operations since each operation can add noise (data not related to the sample). Since the values are approximately  $10^{-10}$ , if the antilog is taken the values are too small for the PC buffers. Spectra appear on the screen with 10 zero's for the absorbance units and values can not be saved to disk files. We add 10 (equivalent to multiplying by  $10^{10}$  and then take the antilog. Using this procedure, we obtain a spectrum in watts. These spectra can be averaged, subtracted from each other, or a ratio obtained. Any of the multivariate analyses can be made directly on the spectra. During this time period Dr. Arendale had a Perstorp SCL spectrophotometer on loan. This instrument has less than 20 microAU noise level. Therefore, more digits must be accommodated. We used the SCL software to process the data. Since there is significant differences in the signal level for the various samples, each sample is normalized to have a value of

1.0. This results in the elimination of the mean as Factor 1. A prediction vs observed graph is shown as Figure 16a. Model ONH B was obtained after removing outliers (spectra 13 - 14, 24, 26 - 28, and 30). Sample numbers and spectrum identifications are given in Table V. The prediction for all samples is shown on Figure 16b. The scores and loadings for Model ONH B are shown in Figures 17a through 17m. Factor 1 shows features that can be identified in Figure 15, The water and OH lines begin to dominate in the other factors. Some of the variance is probably due to specific compounds that are used in the HD2 formulation.

TABLE III. WITNESS PANELS DATA SETS

SAMPLE	TITLE IN UNSC	ORIG. SC NAME	DESCRIPTION
1	E6B1 (TOP LEFT)	OSE6B_1	7 DAYS @ 100°F/20% RH (SMOOTH AND OFFSET)
2	E6B2 (TOP RIGHT)	OSE6B_2	
3	E6B3 (BOTTOM RIGHT)	OSE6B_3	
4	E6B4 (BOTTOM LEFT)	OSE6B_4	
5	E8A1 (TOP LEFT)	OSE8A_1	7 DAYS @ 100°F/60% RH (SMOOTH AND OFFSET)
6	E8A2 (TOP RIGHT)	OSE8A_2	
7	E8A3 (BOTTOM RIGHT)	OSE8A_3	
8	E8A4 (BOTTOM LEFT)	OSE8A_4	
9	E8A5 (TOP LEFT)	OSE8A_5	
10	E8A6 (TOP RIGHT)	OSE8A_6	
11	E8A7 (BOTTOM RIGHT)	OSE8A_7	
12	E8A8 (BOTTOM LEFT)	OSE8A_8	
13	0E830A10 (TOP LEFT)	SE830A10	28 DAYS @ 100°F/60% RH (SMOOTH AND OFFSET)
14	0E830A11 (TOP RIGHT)	SE830A11	
15	0E830A12 (CENTER)	SE830A12	
16	0E830A13 (TOP LEFT)	SE830A13	
17	0E830A14 (BOTTOM LEFT)	SE830A14	
18	0E830A15 (BOTTOM RIGHT)	SE830A15	
19	OS7221 (TOP LEFT)	OS7_22_1	SAMPLE E3A 3 HRS @ 50°F/60% RH (SMOOTH AND OFFSET)
20	OS7222 (TOP RIGHT)	OS7_22_2	
21	OS7223 (BOTTOM RIGHT)	OS7_22_3	
22	OS7224 (BOTTOM LEFT)	OS7_22_4	
23	OS7225 (CENTER)	OS7_22_5	
24	OS7231 (TOP RIGHT)	OS7_23_1	SAMPLE E5A 3 HRS @ 100°F/20% RH (SMOOTH AND OFFSET)
25	OS7232 (TOP LEFT)	OS7_23_2	
26	OS7233 (BOTTOM LEFT)	OS7_23_3	
27	OS7234 (BOTTOM RIGHT)	OS7_23_4	
28	OS7236 (CENTER)	OS7_23_6	SAMPLE E7A 3 HRS @ 100°F/60% RH (SMOOTH AND OFFSET)
29	OS7237 (BOTTOM LEFT)	OS7_23_7	
30	OS7238 (BOTTOM RIGHT)	OS7_23_8	
31	OS7239 (TOP RIGHT)	OS7_23_9	
32	OS72310 (TOP LEFT)	OS7_23_10	

33	OS7246 (CENTER)	OS7_24_6	SAMPLE E1A 3 HRS @ 50°F/20% RH (SMOOTH AND OFFSET)
34	OS7247 (BOTTOM LEFT)	OS7_24_7	
35	OS7248 (BOTTOM RIGHT)	OS7_24_8	
36	OS7249 (TOP RIGHT)	OS7_24_9	
37	OS72410 (TOP LEFT)	O7_24_10	

TABLE IV. ENVIRONMENTAL CHAMBER TEST

**E4 Data Set  
(50°F/60% RH)**

Spectra Number	Date Spectra was taken	Time Span Between each Spectra
E4_ 1 - 50	August 6, 1992	One Hour
E4_ 51 - 78	August 6 - 12, 1992	Four Hours

**High Temperatuare (HIT) Data Set  
(100°F/60% RH)**

Spectra Number	Date Spectra was taken	Time Span Between each Spectra
HIT 1 - 17	September 16, 1992	15 Minutes
HIT 18 - 44	September 16 - 17, 1992	One Hour

**D6AC Data Set  
Average Temp. 73.5  
Average Humidity 36.7**

Spectra Number	Date Spectra was taken	Time Span Between each Spectra
D6AC 1 - 17	September 28, 1992	15 Minutes
D6AC 18 - 40	September 28 - 29, 1992	One Hour
D6AC 41 - 115	September 29 - August 12, 1992	Four Hours

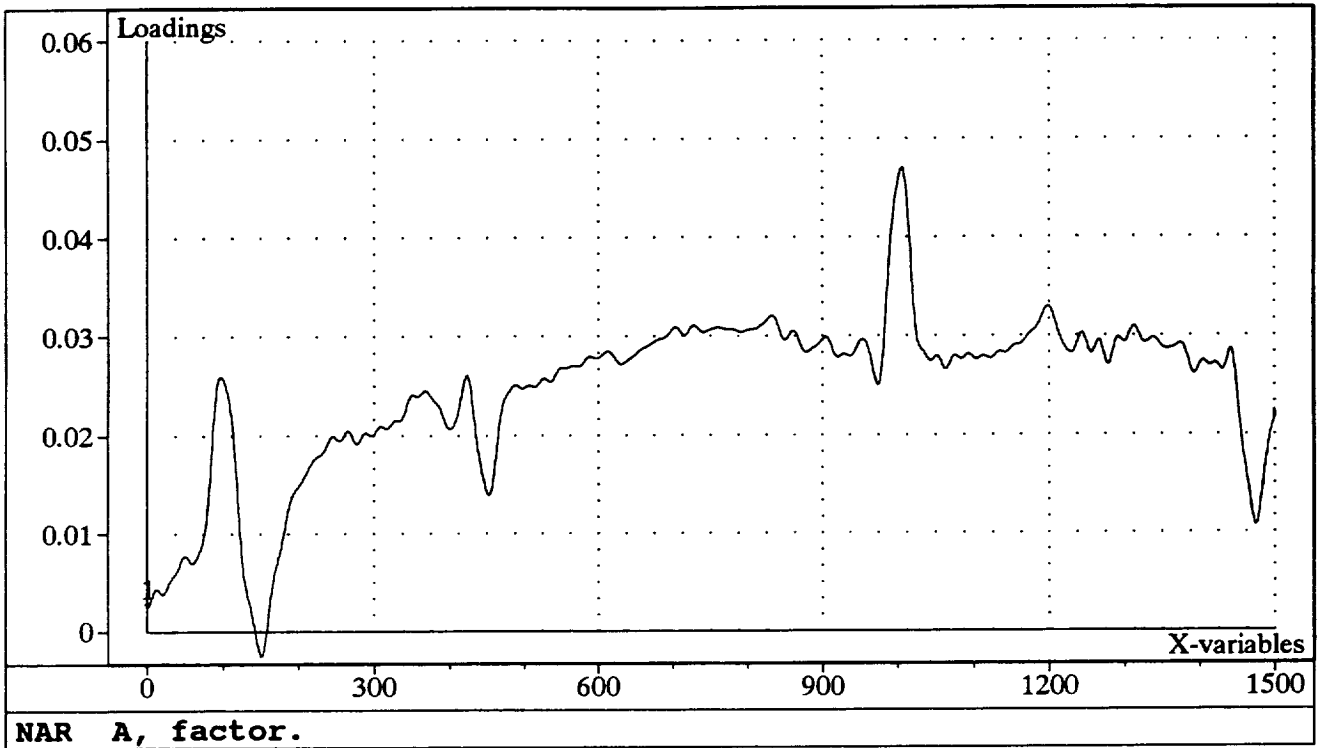


Figure 12a. Model NAR Loadings Plot for Factor 1

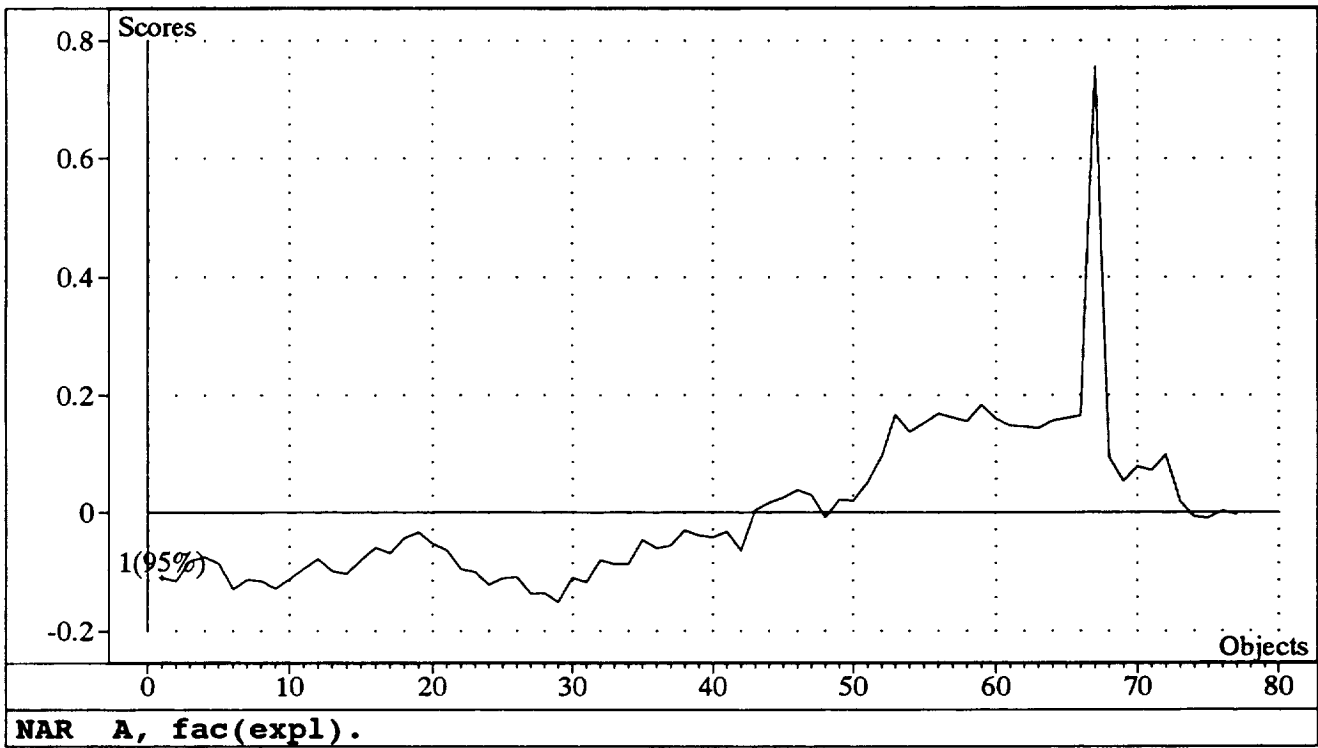


Figure 12b. Model NAR Scores Plot for Factor 1

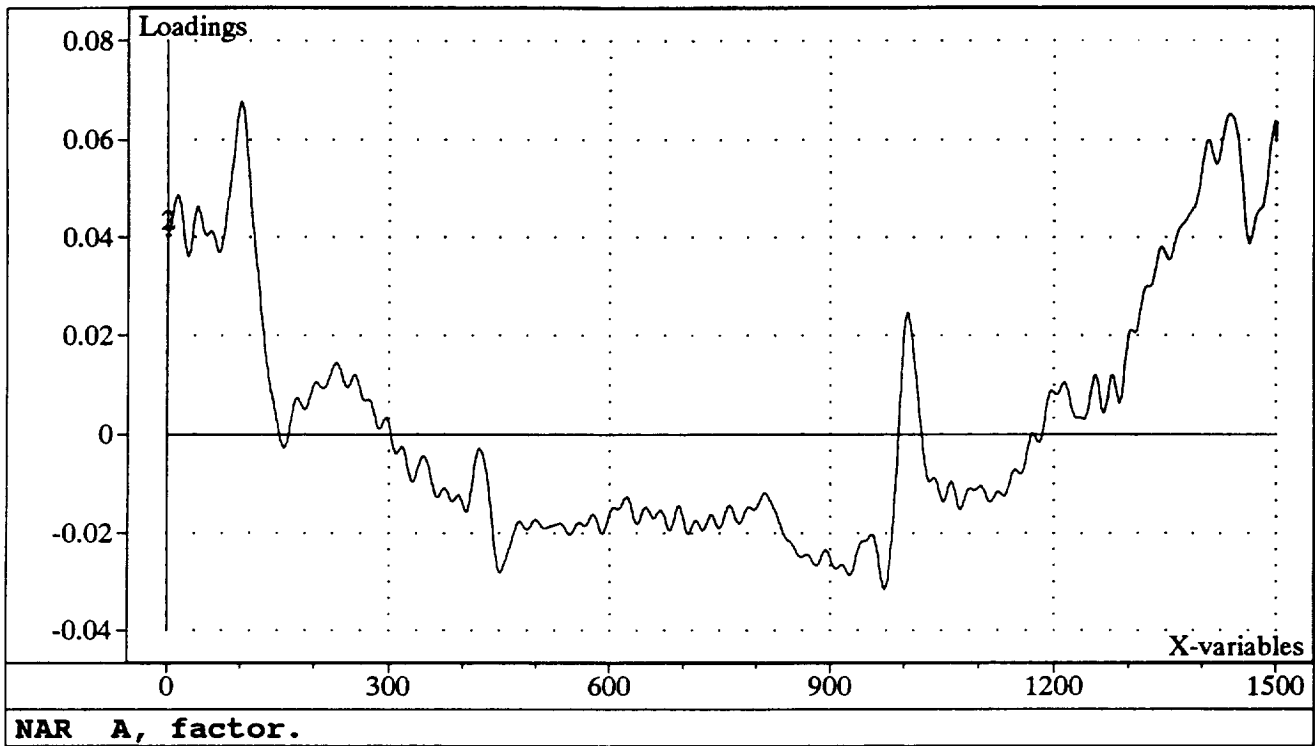


Figure 12c. Model NAR Loadings Plot for Factor 2

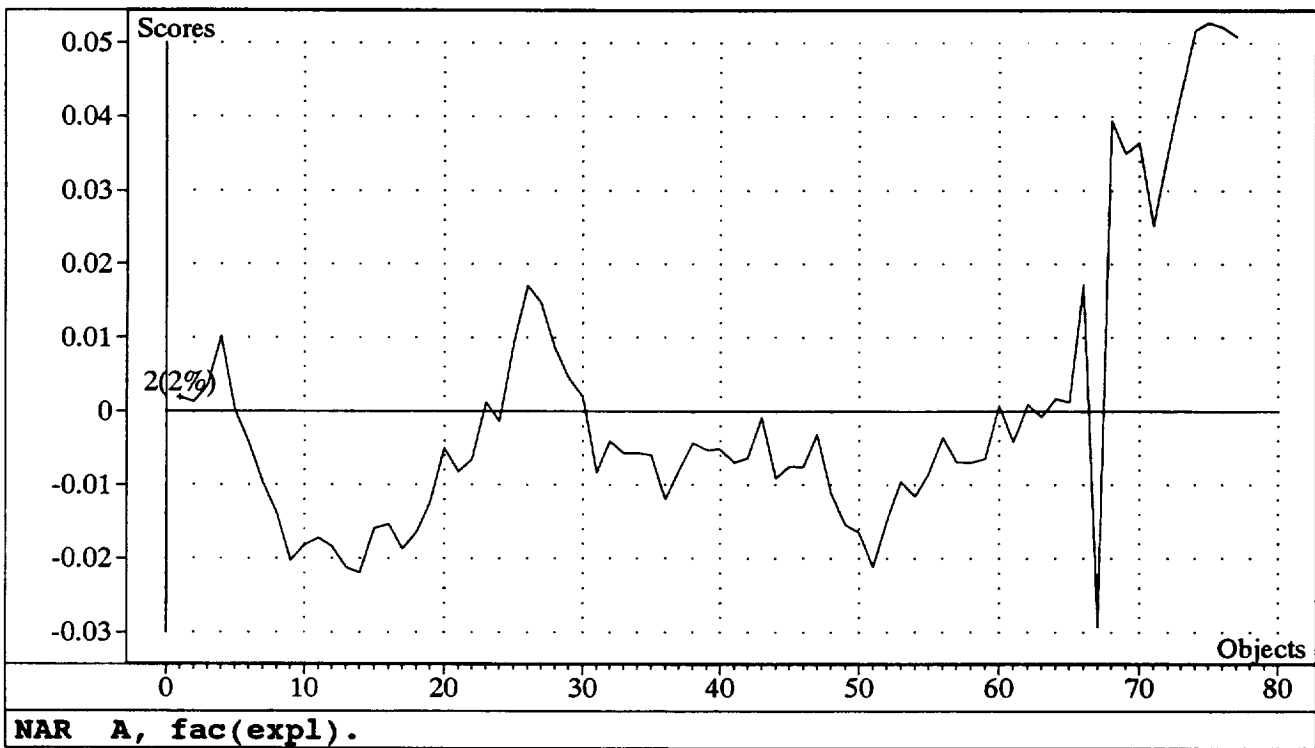


Figure 12d. Model NAR Scores Plot for Factor 2

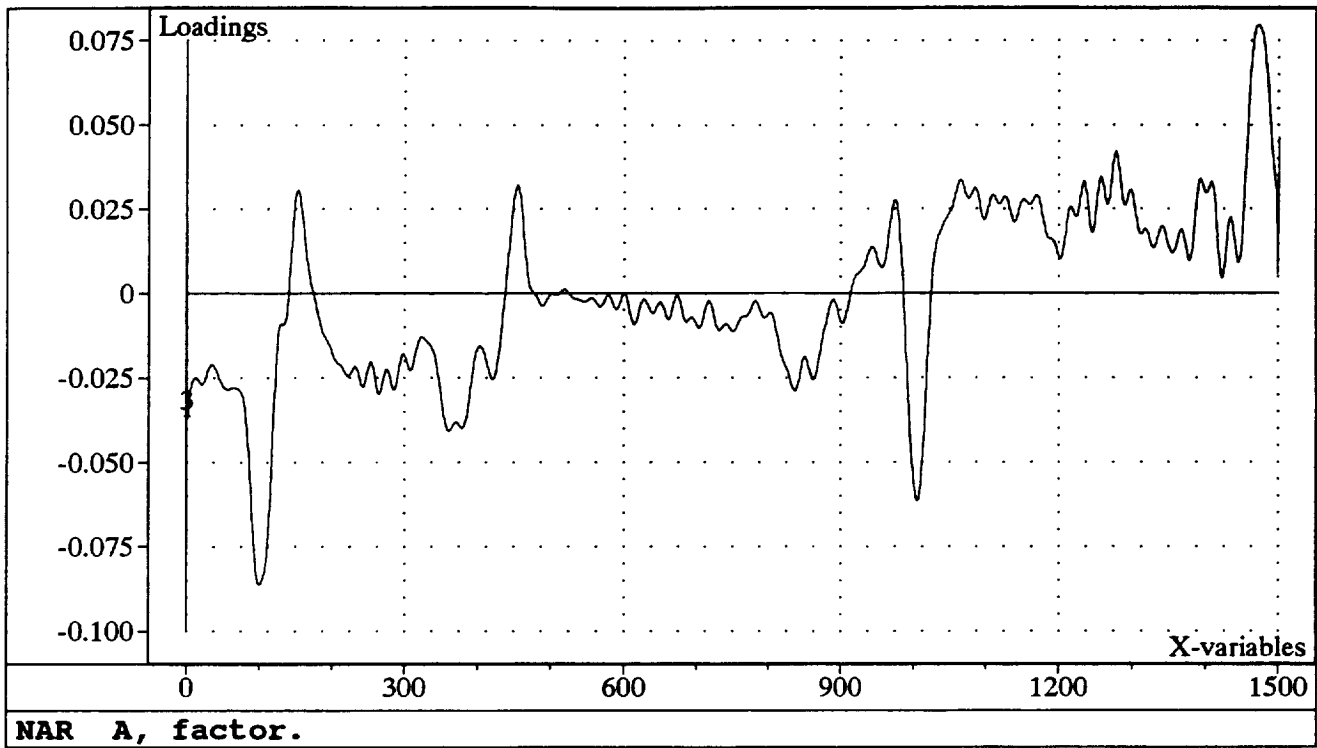


Figure 12e. Model NAR Loadings Plot for Factor 3

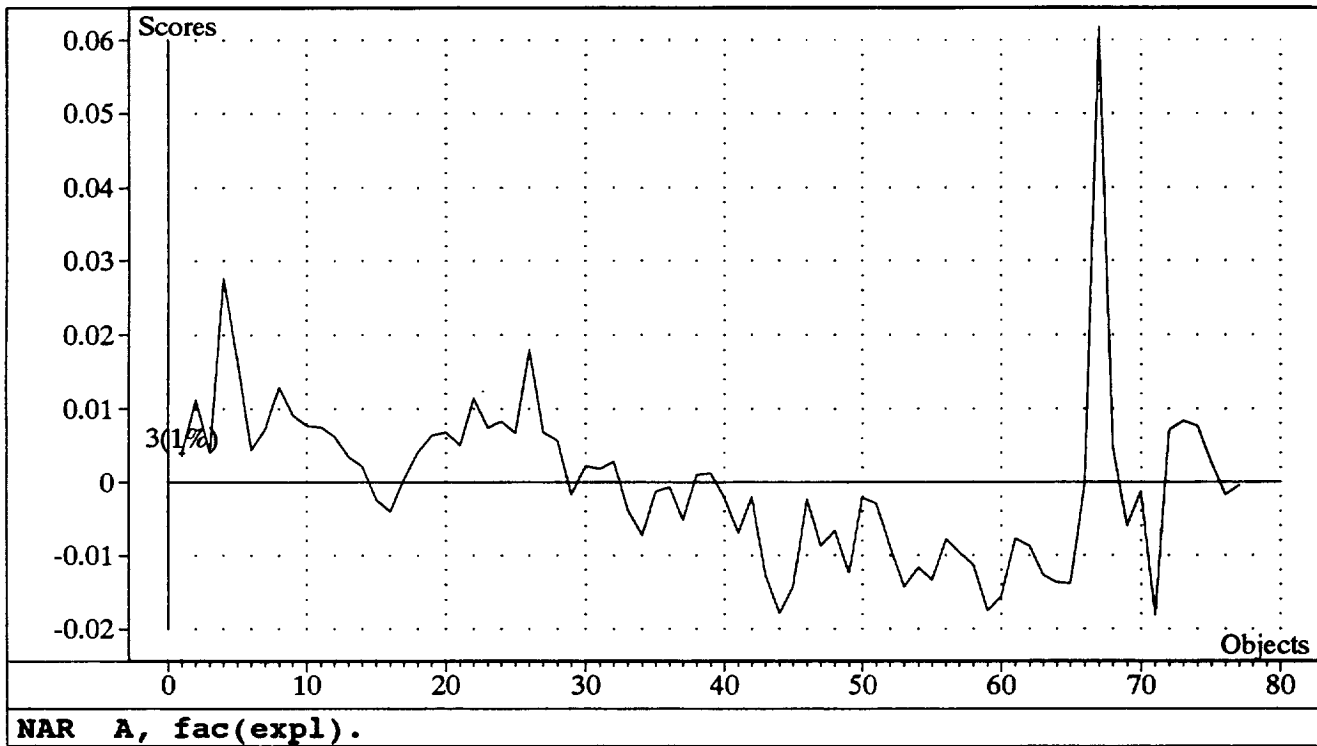


Figure 12f. Model NAR Scores Plot for Factor 3

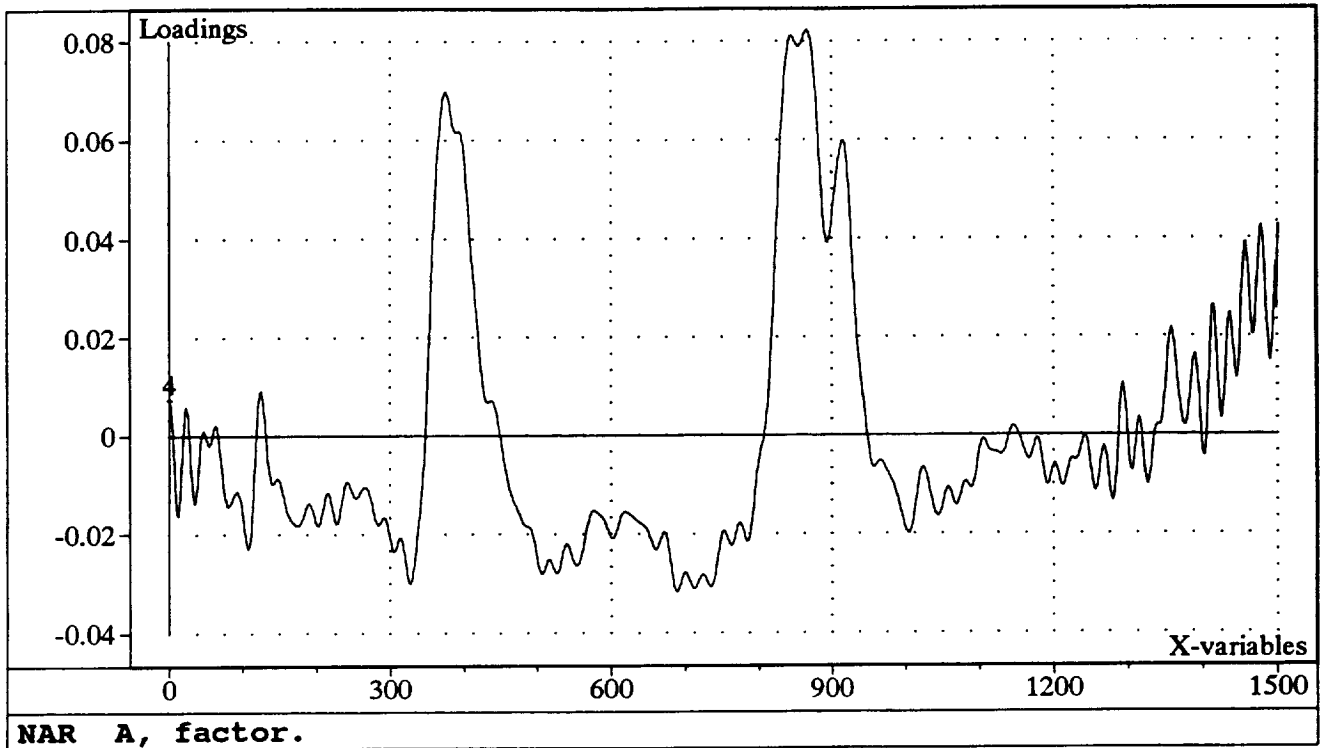


Figure 12g. Model NAR Loadings Plot for Factor 4

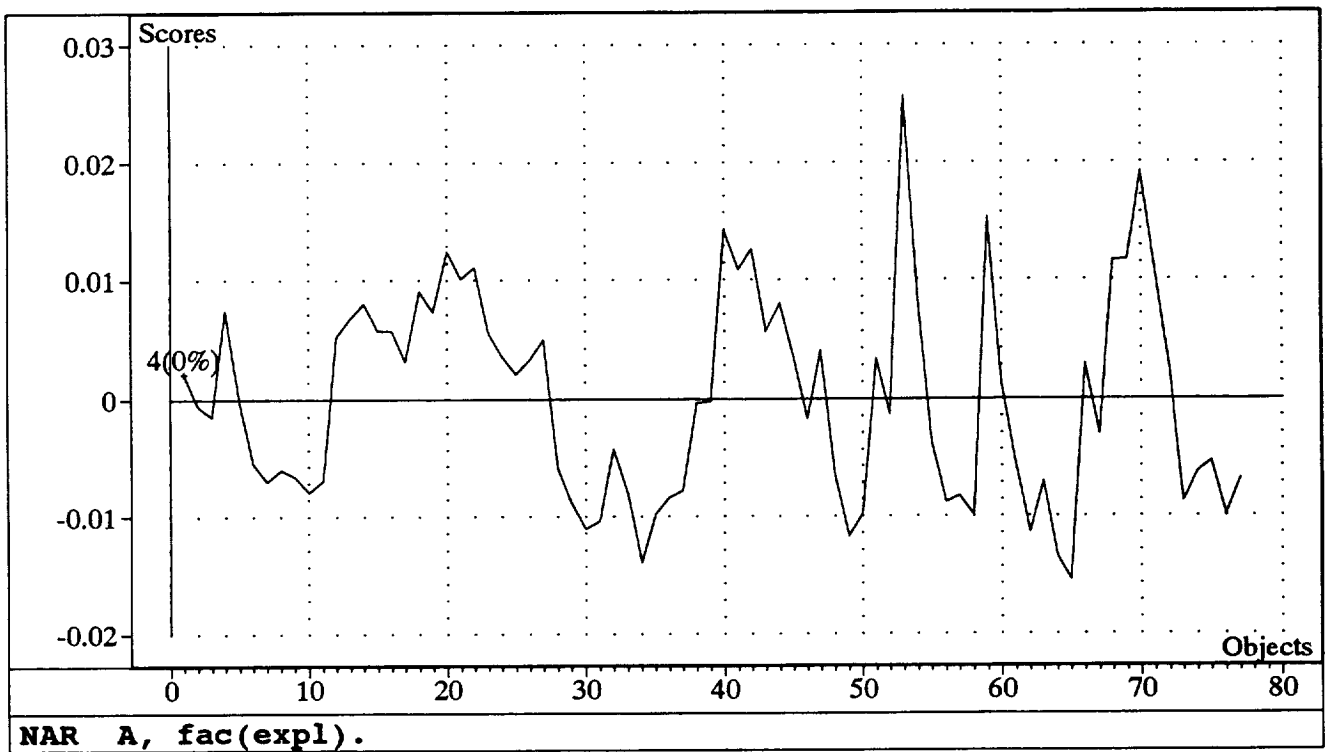


Figure 12h. Model NAR Scores Plot for Factor 4

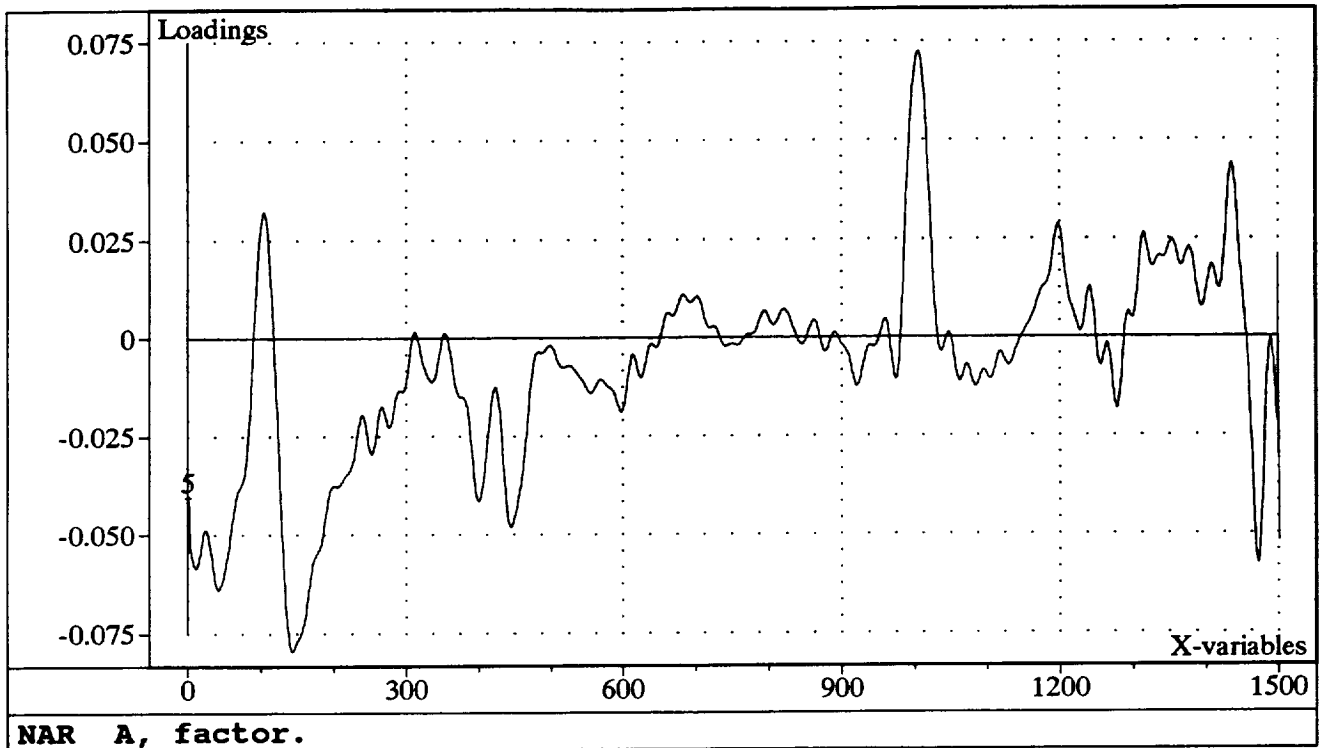


Figure 12i. Model NAR Loadings Plot for Factor 5

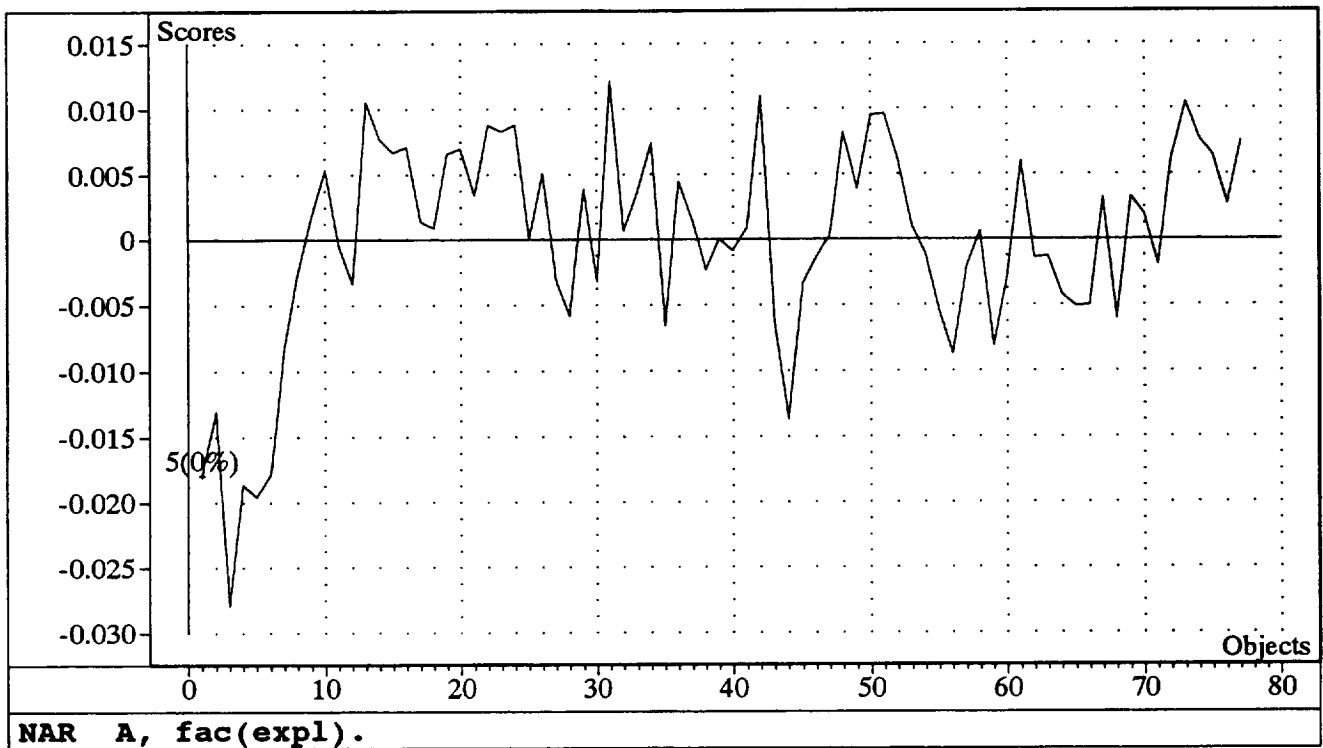


Figure 12j. Model NAR Scores Plot for Factor 5

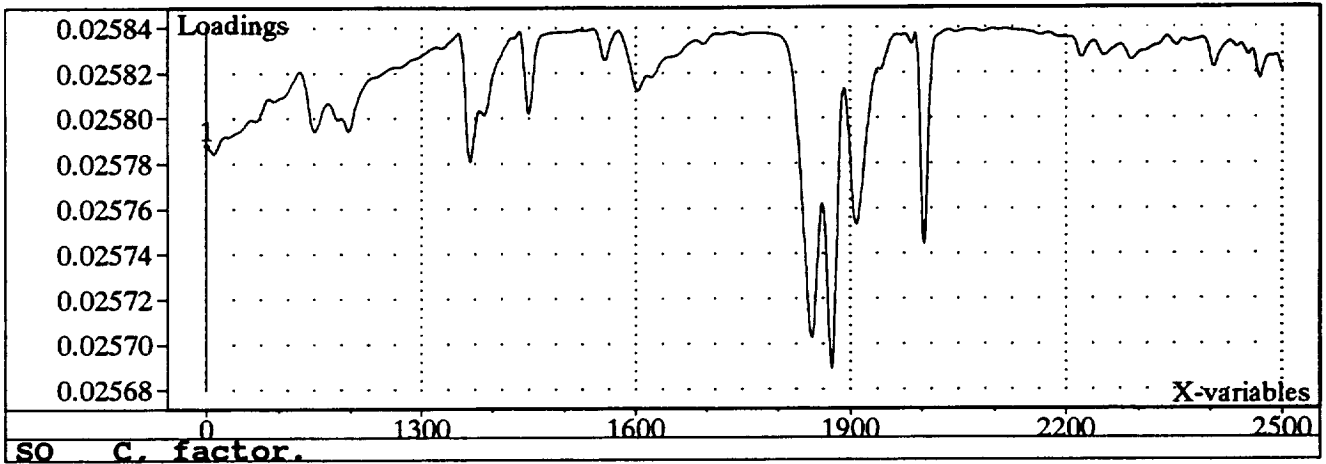


Figure 13a. Loadings Plot for Factor 1

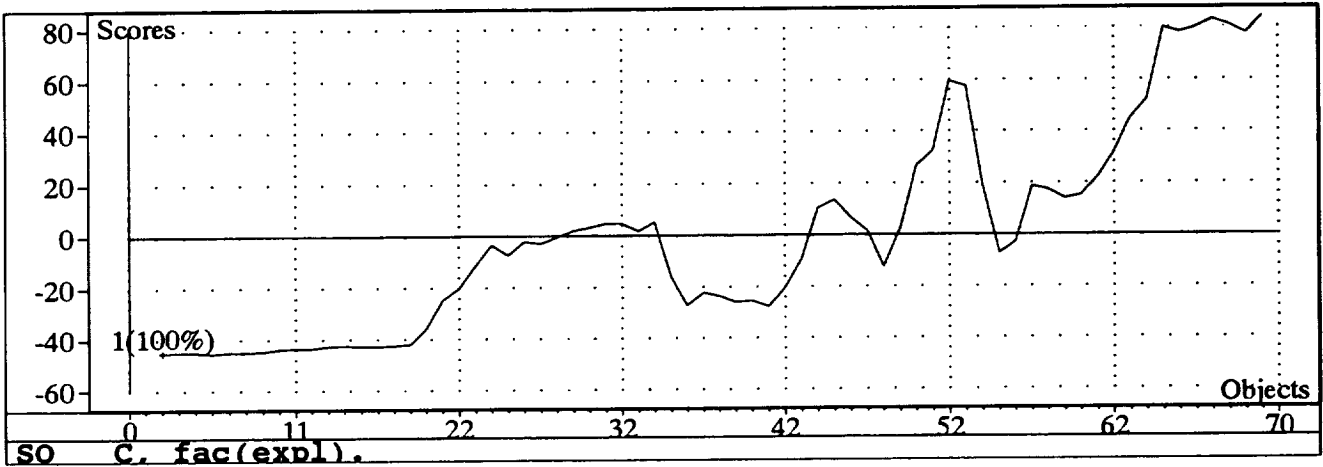


Figure 13b. Scores Plot for Factor 1

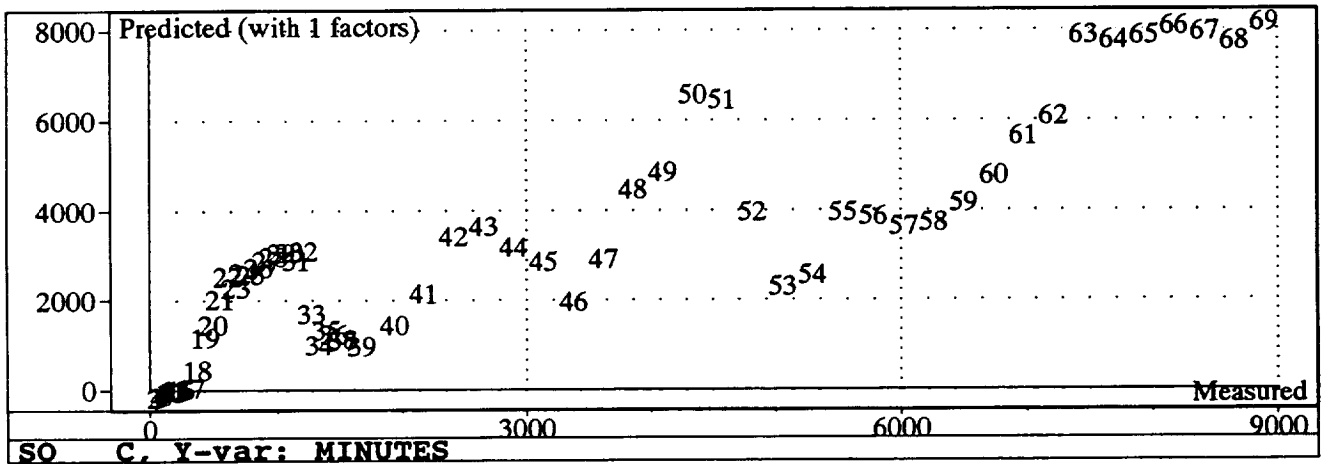


Figure 13c. Predicted with 1 Factor

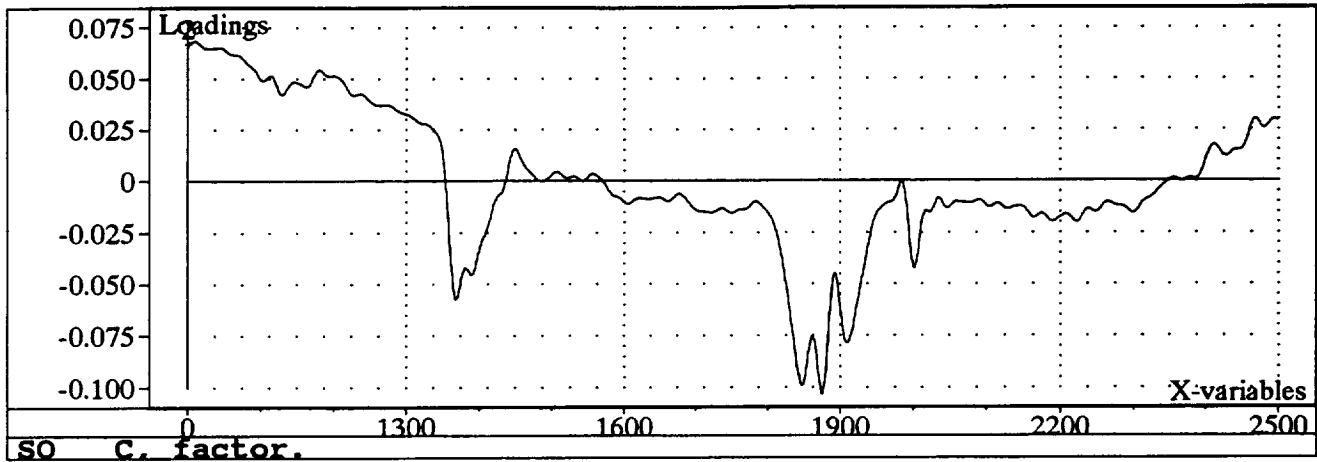


Figure 13d. Loadings Plot for Factor 2

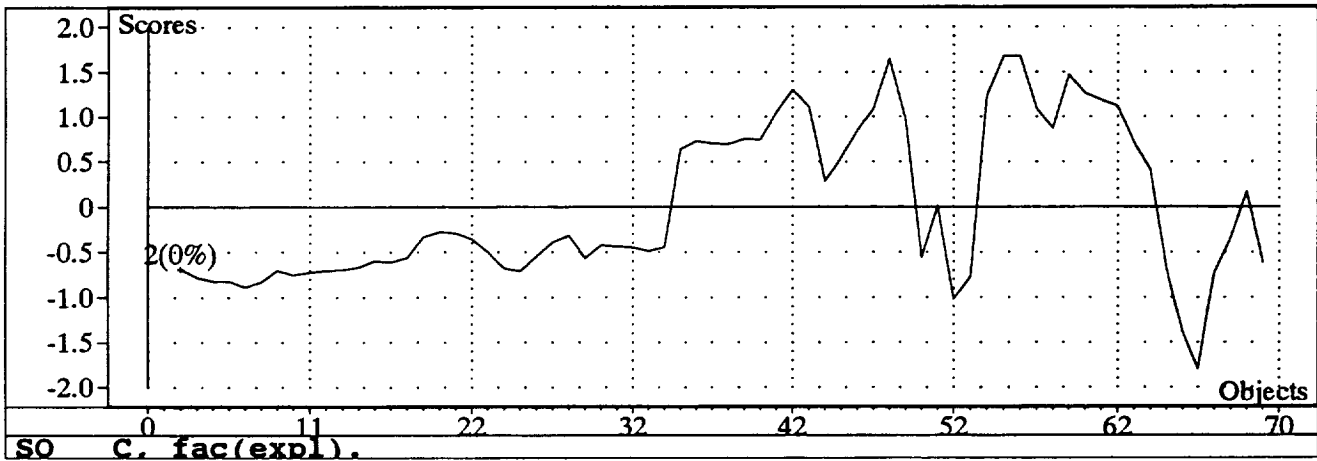


Figure 13e. Scores Plot for Factor 2

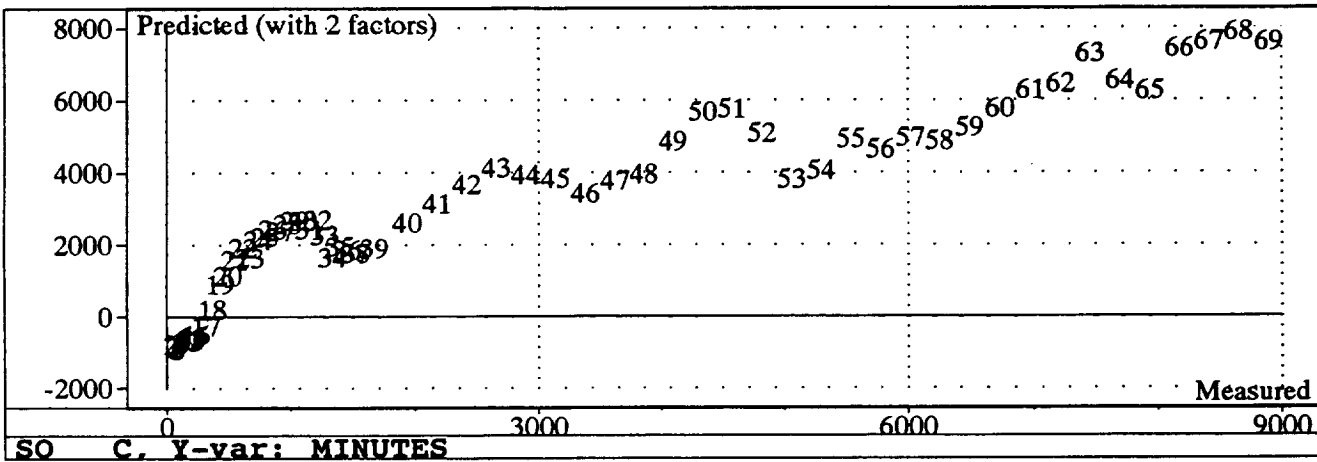


Figure 13f. Predicted with 2 Factors

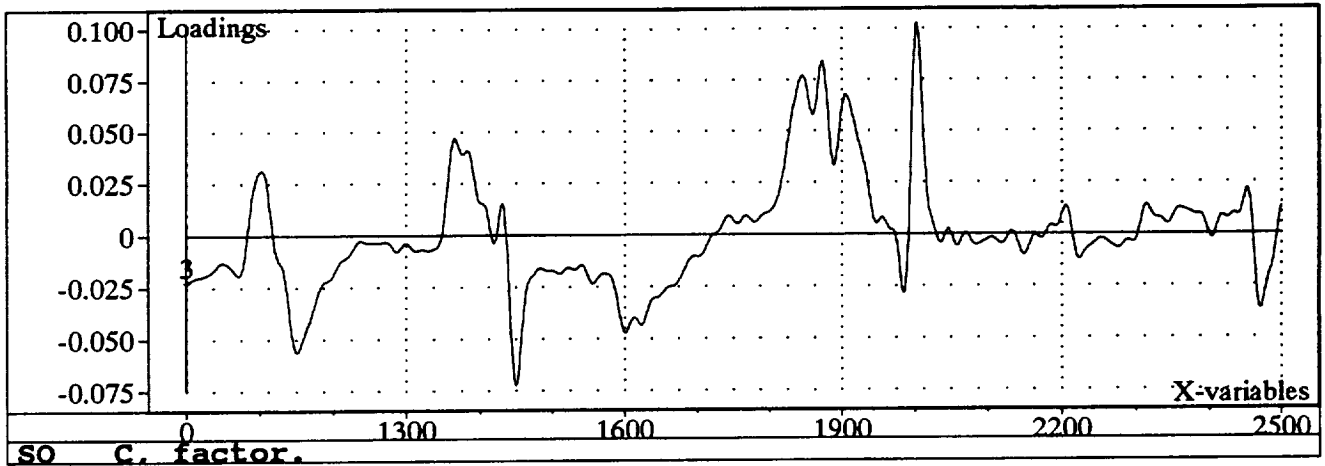


Figure 13g. Loadings Plot for Factor 3

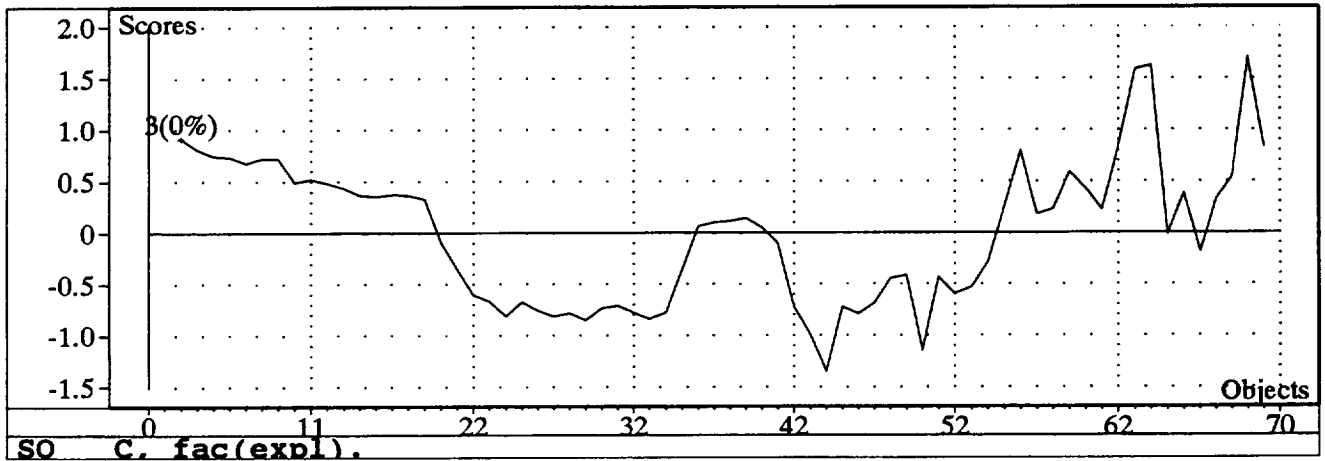


Figure 13h. Scores Plot for Factor 3

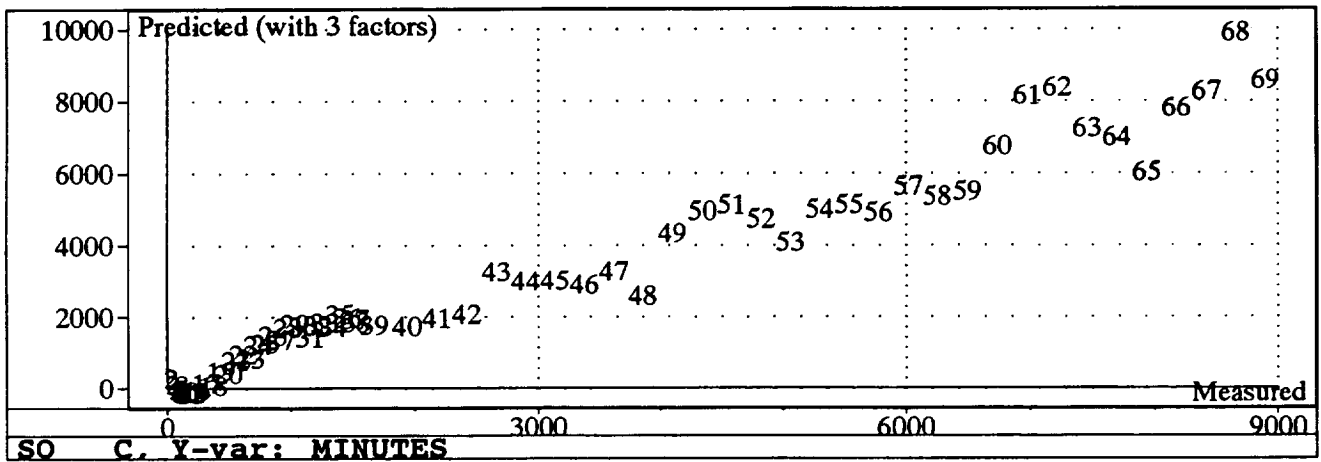


Figure 13i. Predicted with 3 Factors

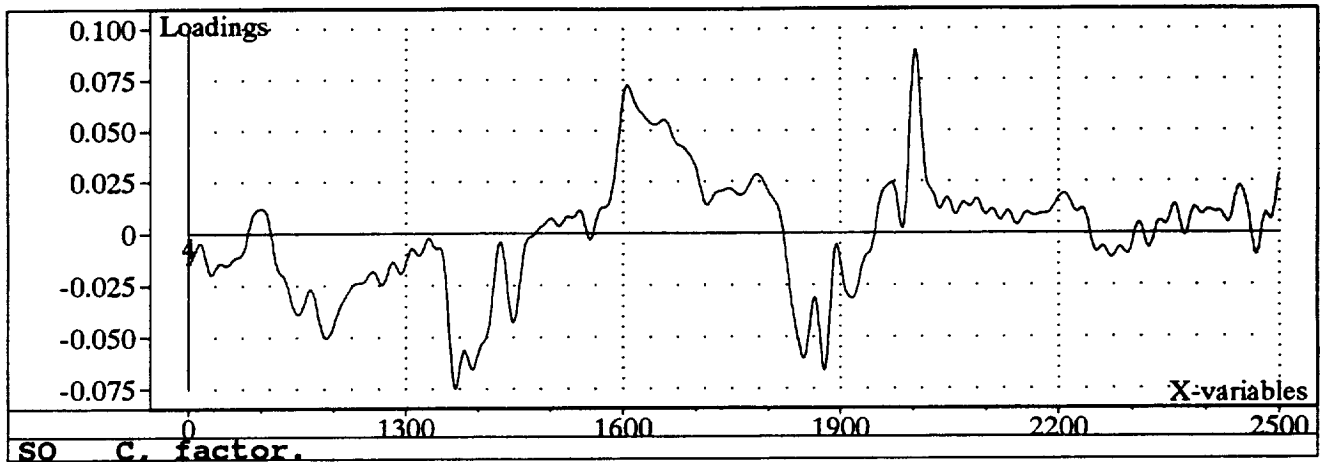


Figure 13j. Loadings Plot for Factor 4

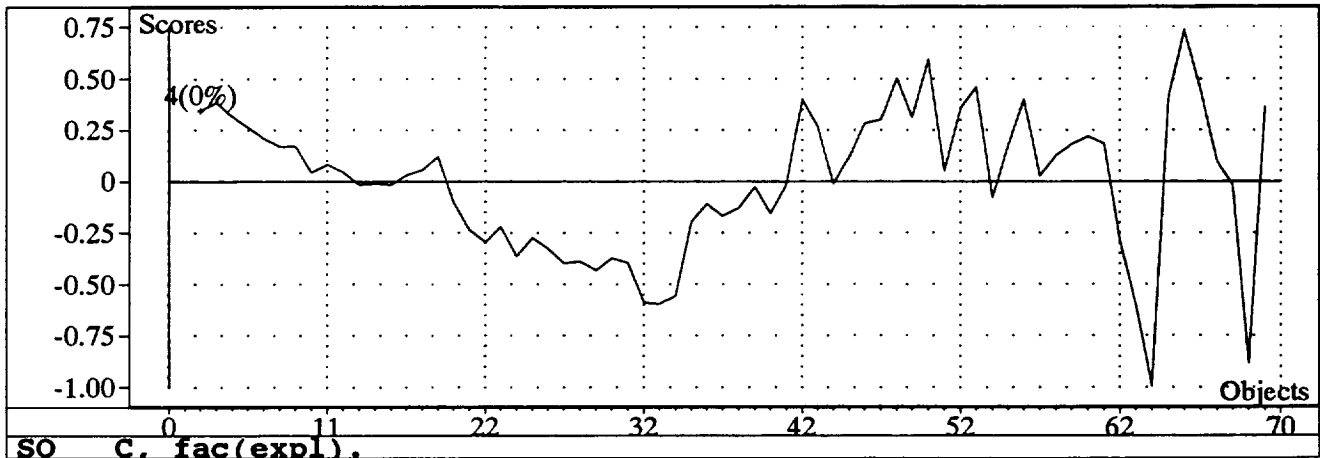


Figure 13k. Scores Plot for Factor 4

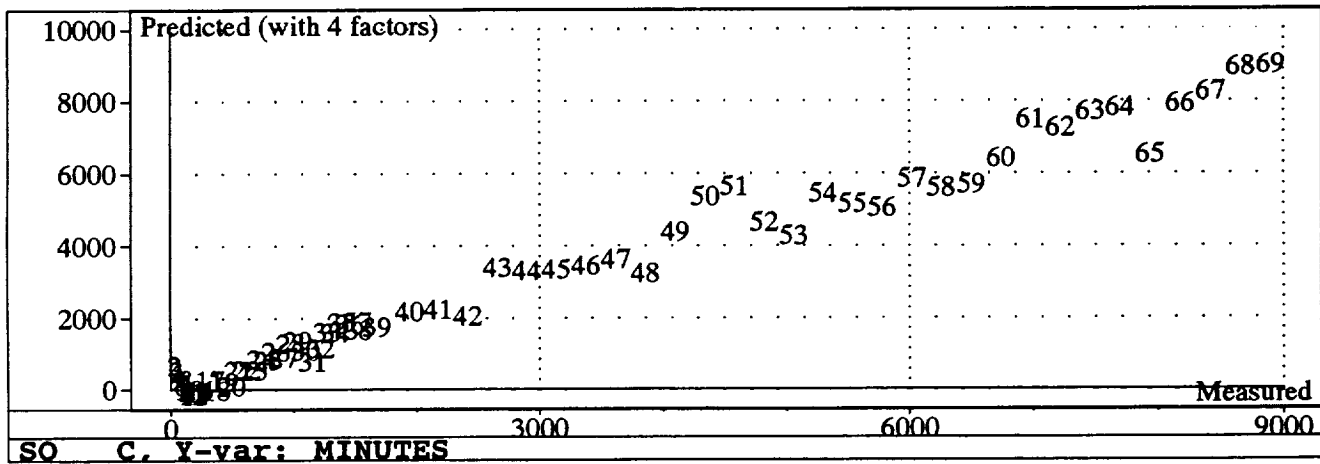


Figure 13l. Predicted with 4 Factors

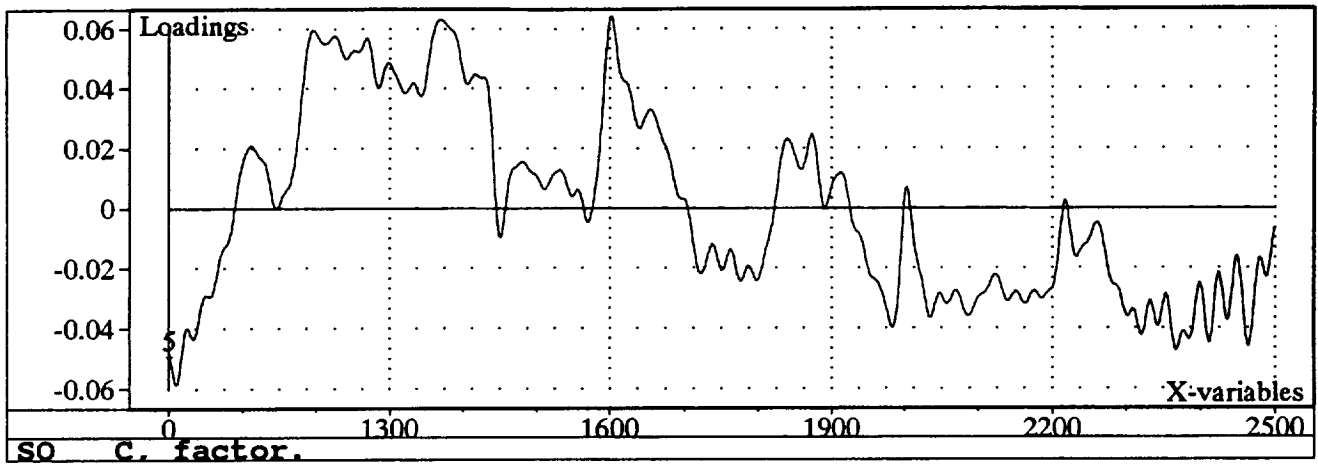


Figure 13m. Loadings Plot for Factor 5

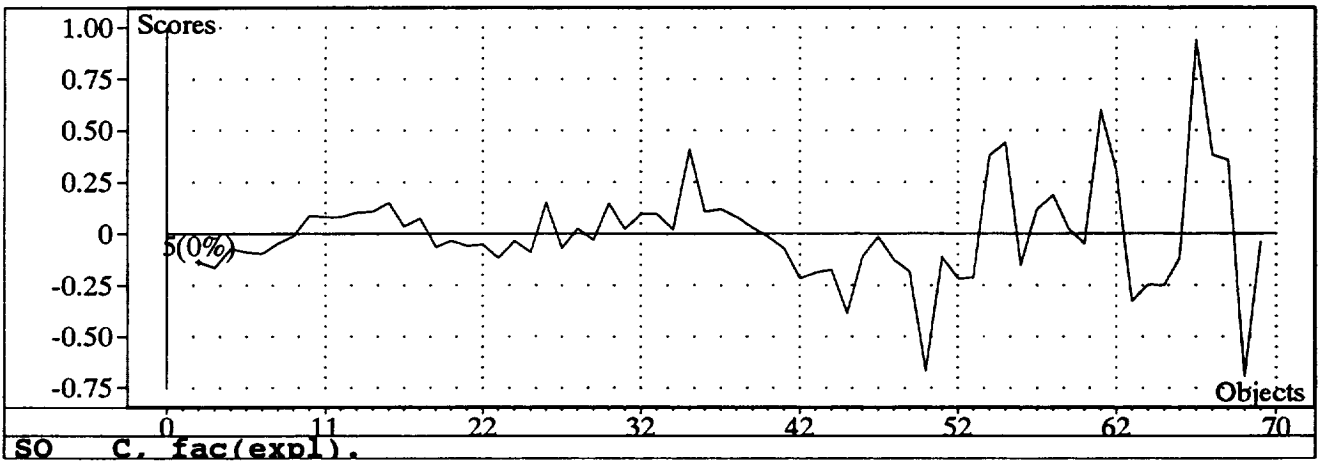


Figure 13n. Scores Plot for Factor 5

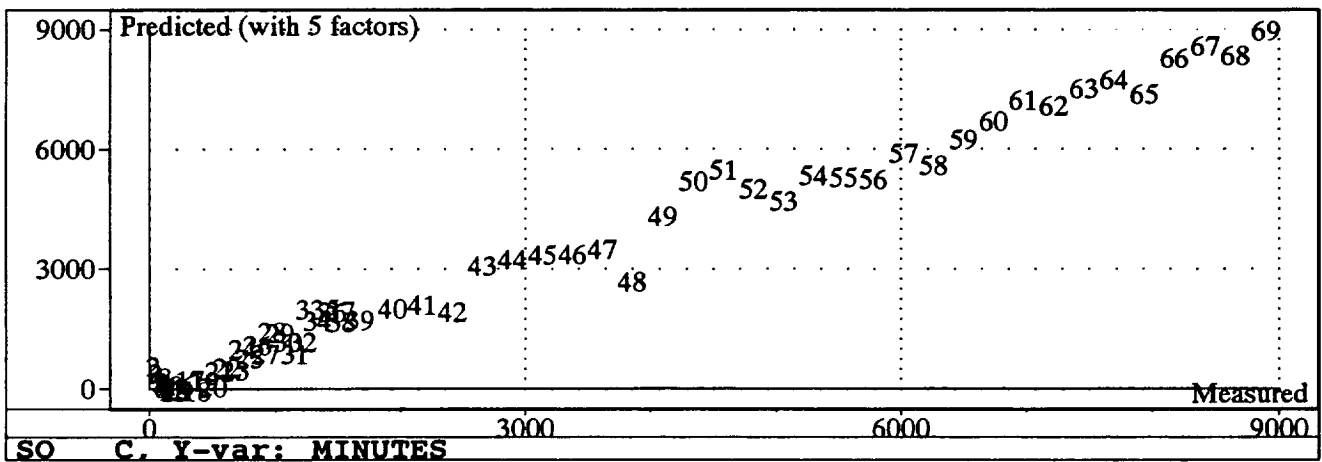


Figure 13o. Predicted with 5 Factors

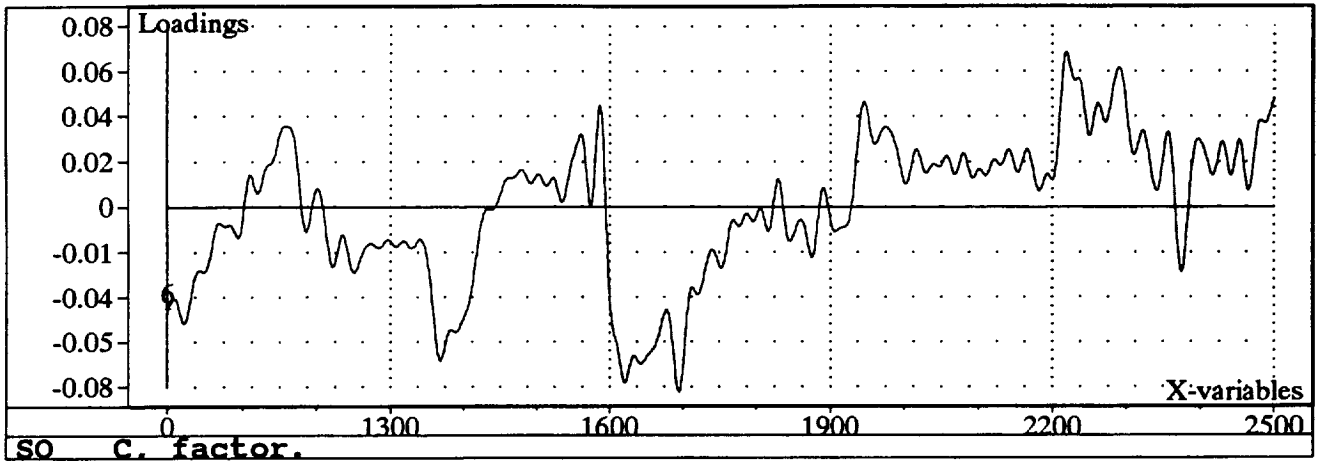


Figure 13p. Loadings Plot for Factor 6

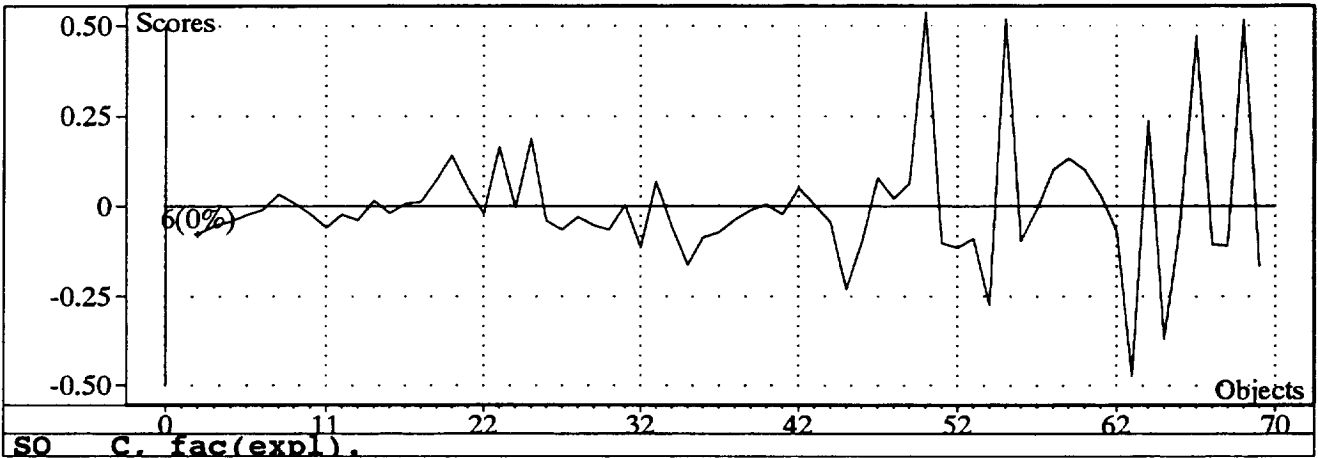


Figure 13q. Scores Plot for Factor 6

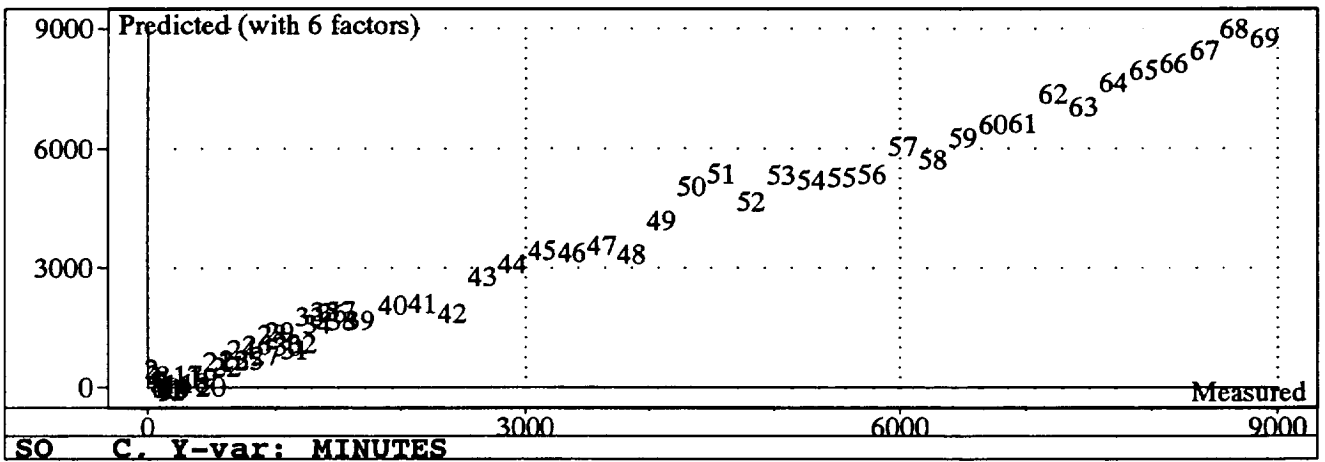


Figure 13r. Predicted with 6 Factors

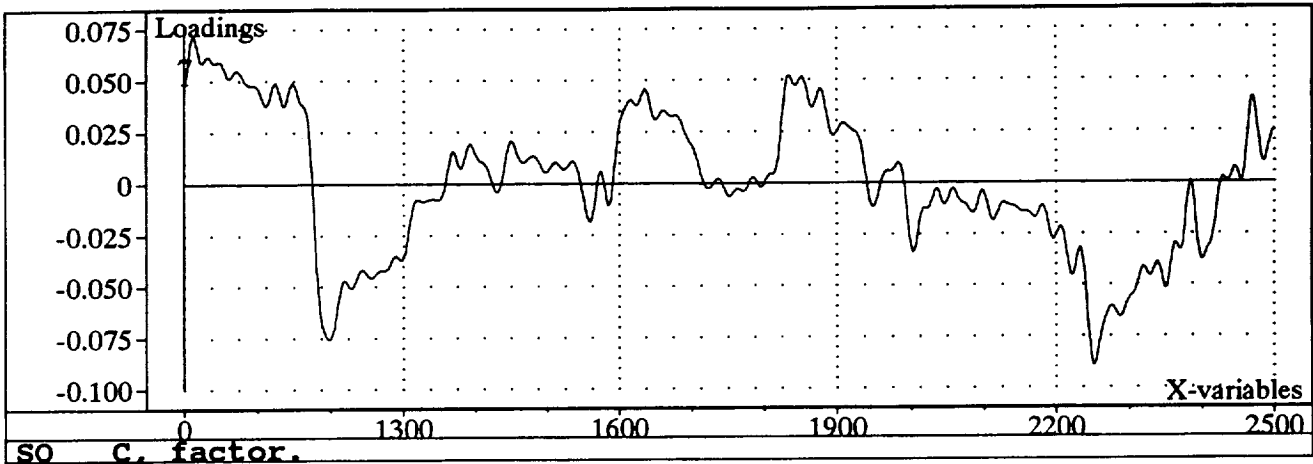


Figure 13s. Loadings Plot for Factor 7

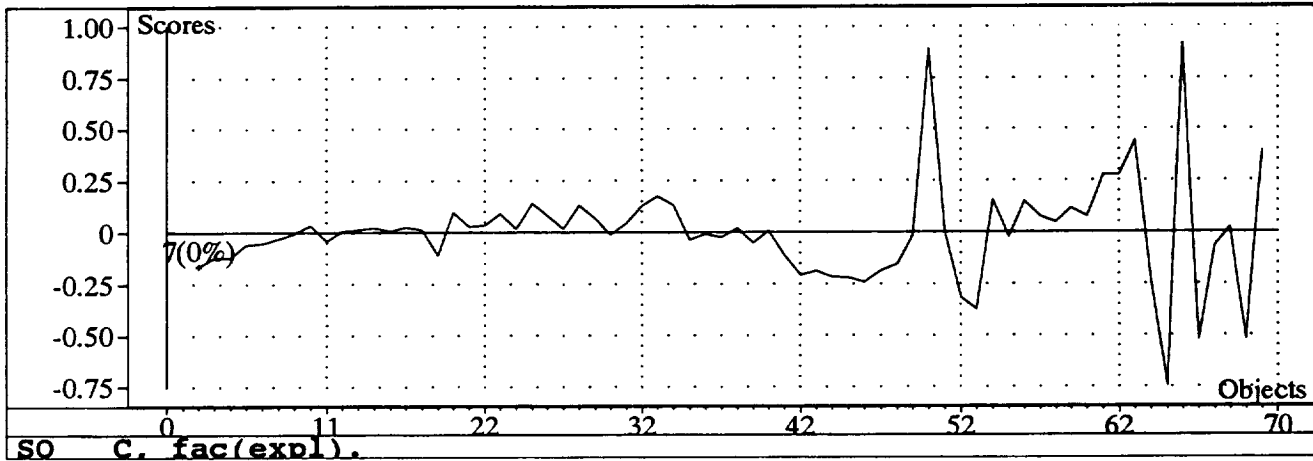


Figure 13t. Scores Plot for Factor 7

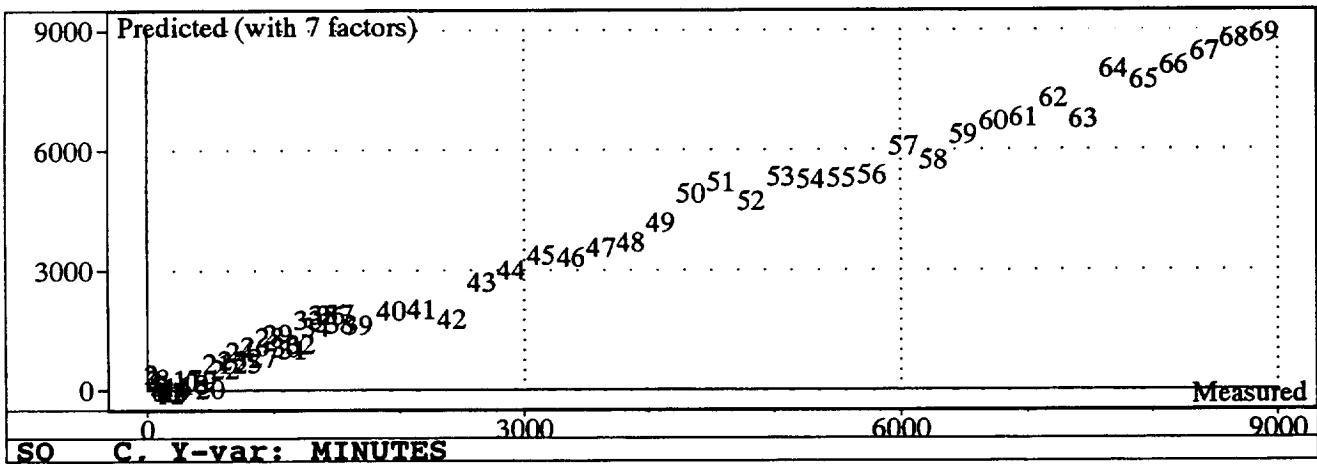


Figure 13u. Predicted with 7 Factors

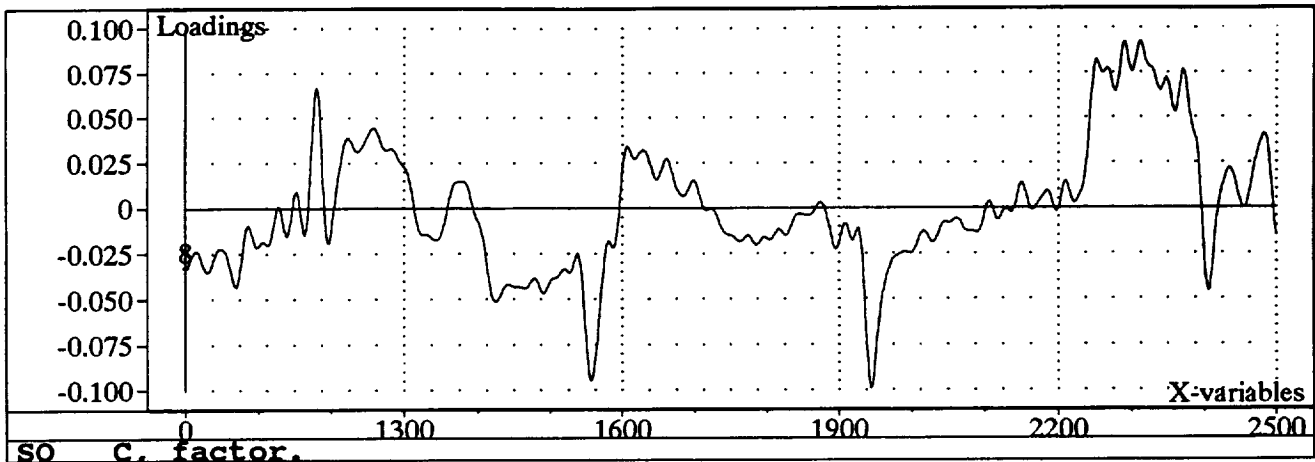


Figure 13v. Loadings Plot for Factor 8

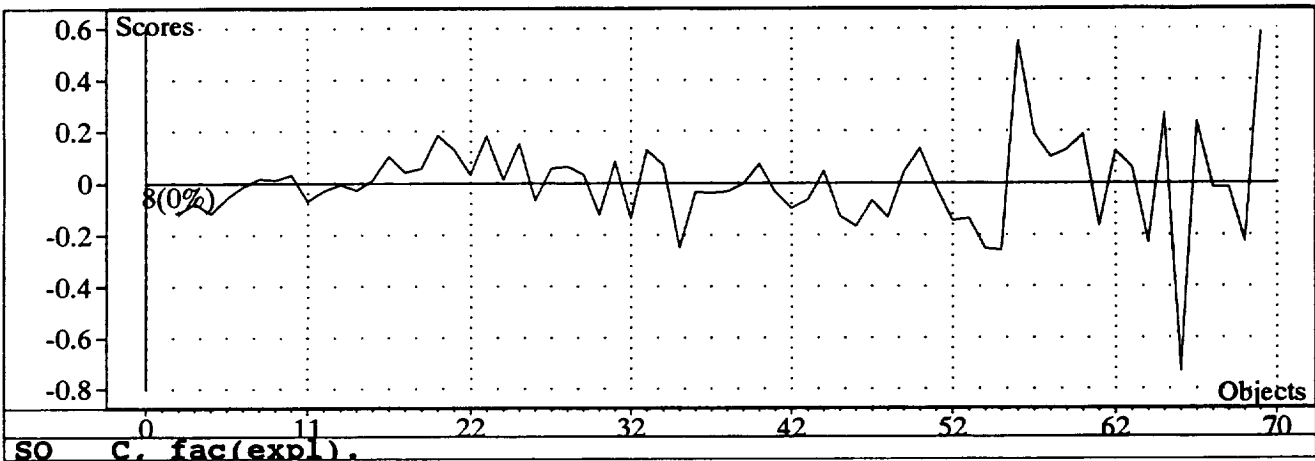


Figure 13w. Scores Plot for Factor 8

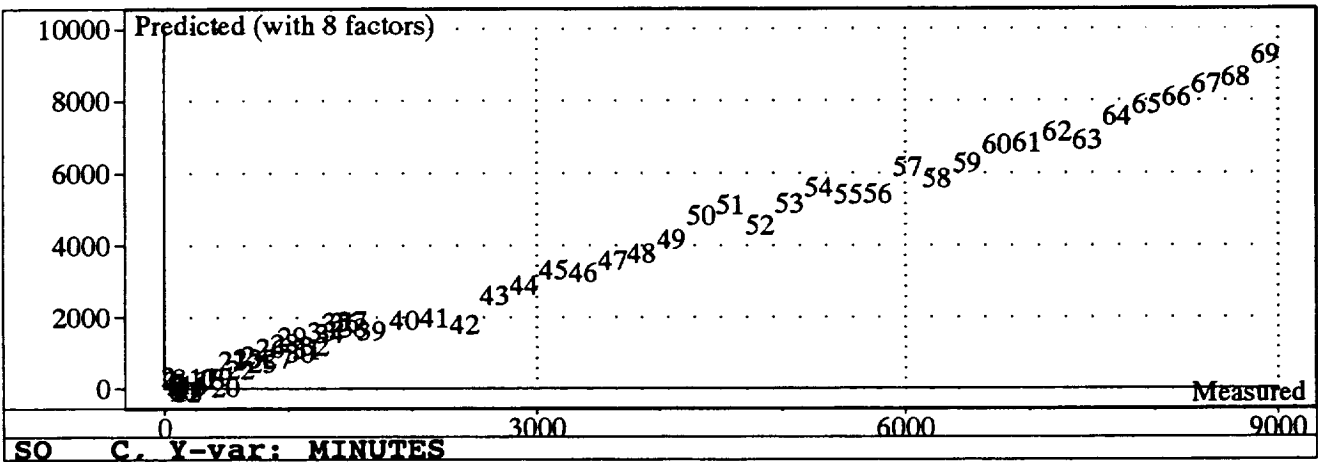
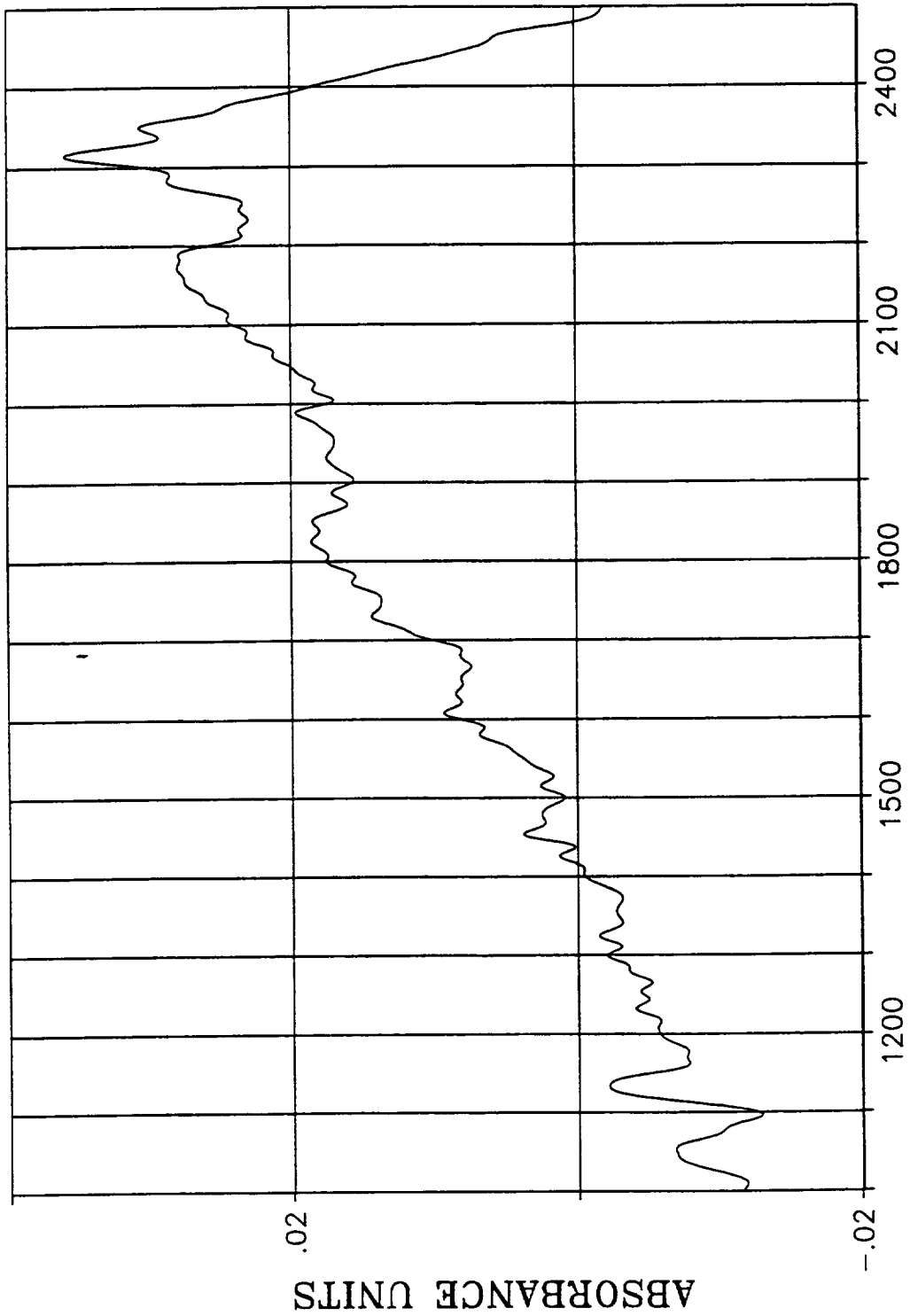


Figure 13x. Predicted with 8 Factors

TABLE V. HD2 Grease Samples

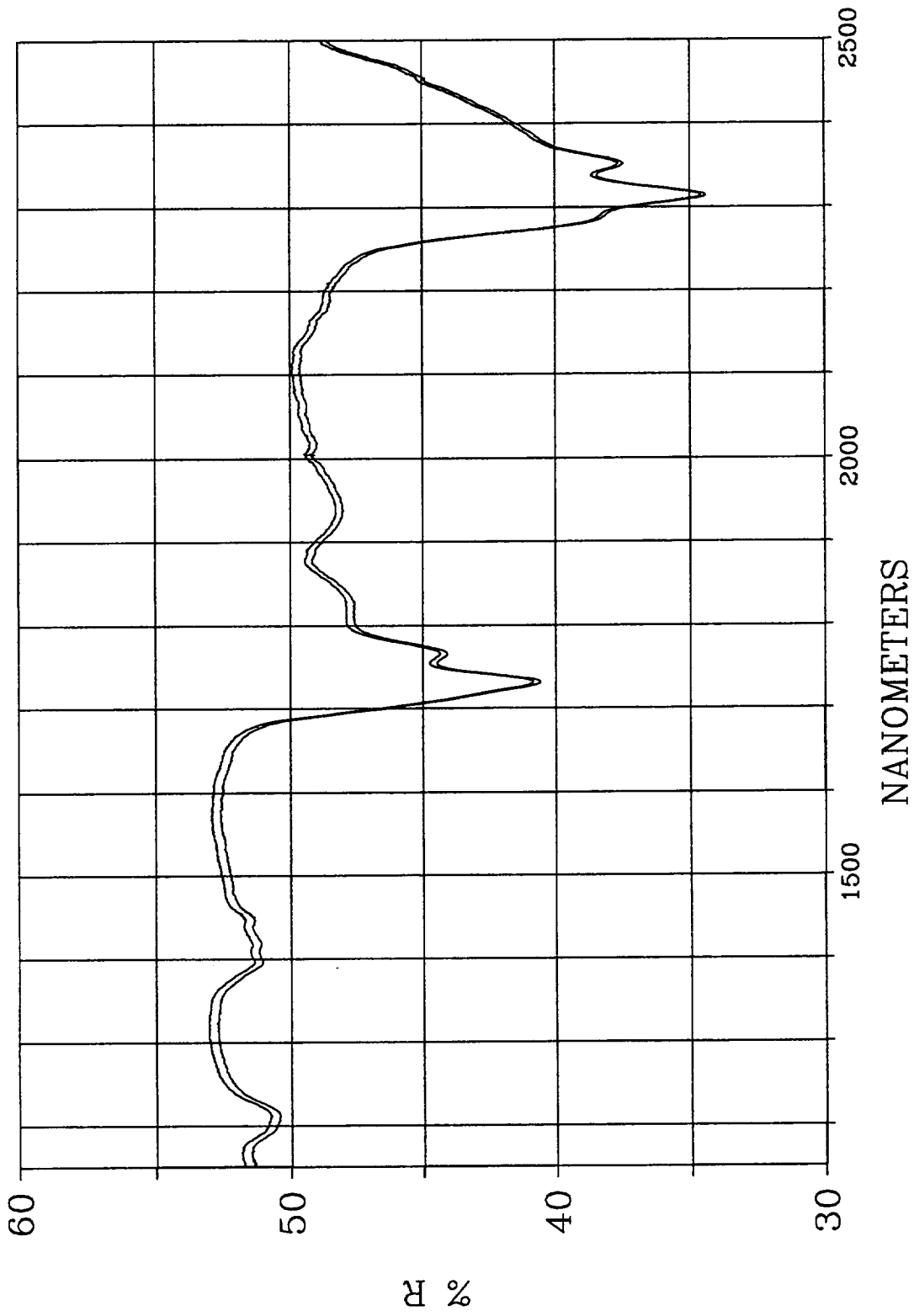
Sample Number	Sample Identification	MG/FT <sup>2</sup>
1	8 18 1	0
2	8 18 2	0
3	8 18 3	0
4	8 18 4	0
5	8 18 5	0
6	8 18 6	0
7	8 24 1	0
8	8 24 2	0
9	8 24 3	0
10	8 24 4	0
11	8 24 5	0
12	8 24 6	0
13	9 2 6	0
14	9 2 7	0
15	8 28 7	5
16	8 28 8	5
17	8 28 9	5
18	8 28 10	5
19	8 28 11	5
20	9 2 1	5
21	9 2 2	5
22	9 2 3	5
23	9 2 4	5
24	9 2 5	5
25	8 24 7	10
26	8 24 8	10
27	8 24 9	10
28	8 24 10	10
29	8 24 11	10
30	9 3 1	10
31	9 3 2	10
32	9 3 3	10
33	9 3 4	10
34	8 18 7	20
35	8 18 8	20
36	8 18 9	20
37	8 18 10	20
38	8 18 11	20
39	9 3 5	20
40	9 3 6	20
41	9 3 7	20

42	9 4 1	20
43	9 4 2	20
44	9 4 3	30
45	9 4 4	30
46	9 4 5	30
47	9 4 6	30
48	9 4 7	30



**NANOMETERS**  
**HD2 ATR SPECTRUM WA9136**  
**ESMOOTH 30**

Figure 14



HD2 SPREAD ON ALUMINUM

Figure 15

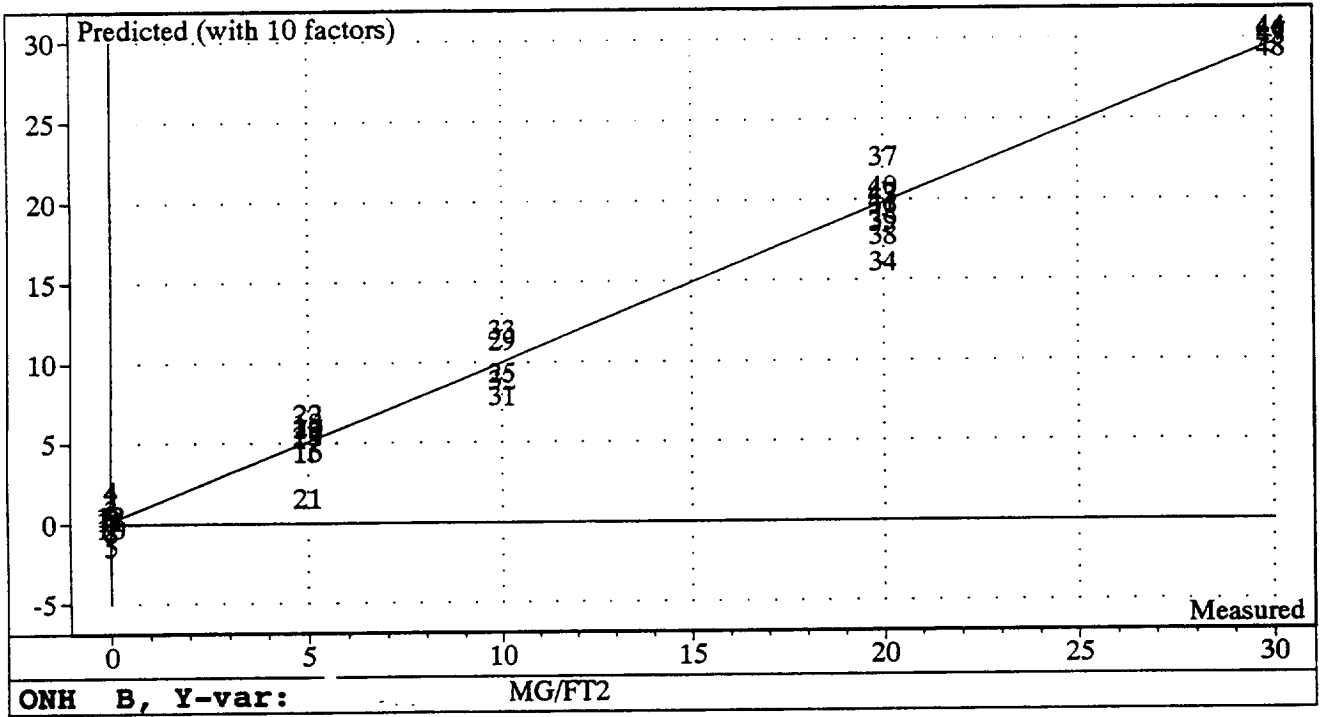


Figure 16a. Model ONH Predicted with 10 Factors

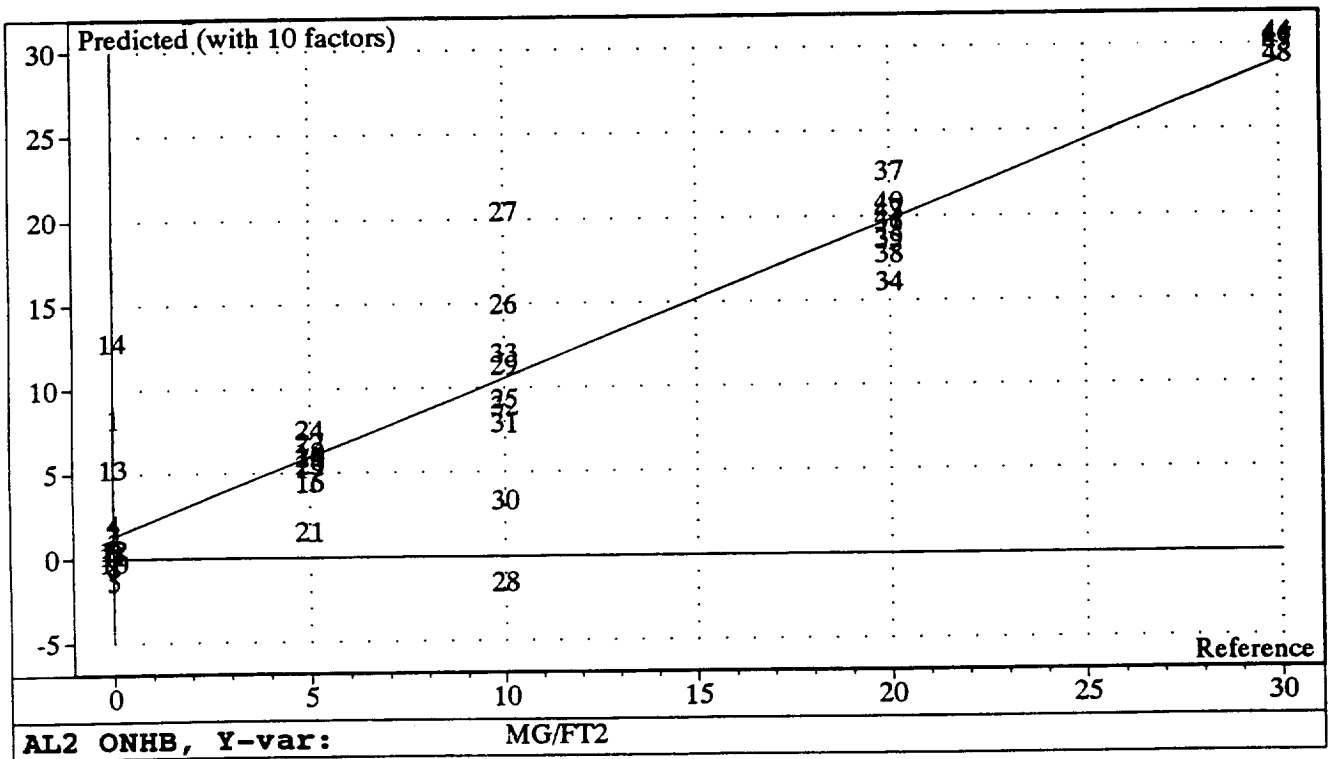


Figure 16b. Model AL2 Predicted with 10 Factors

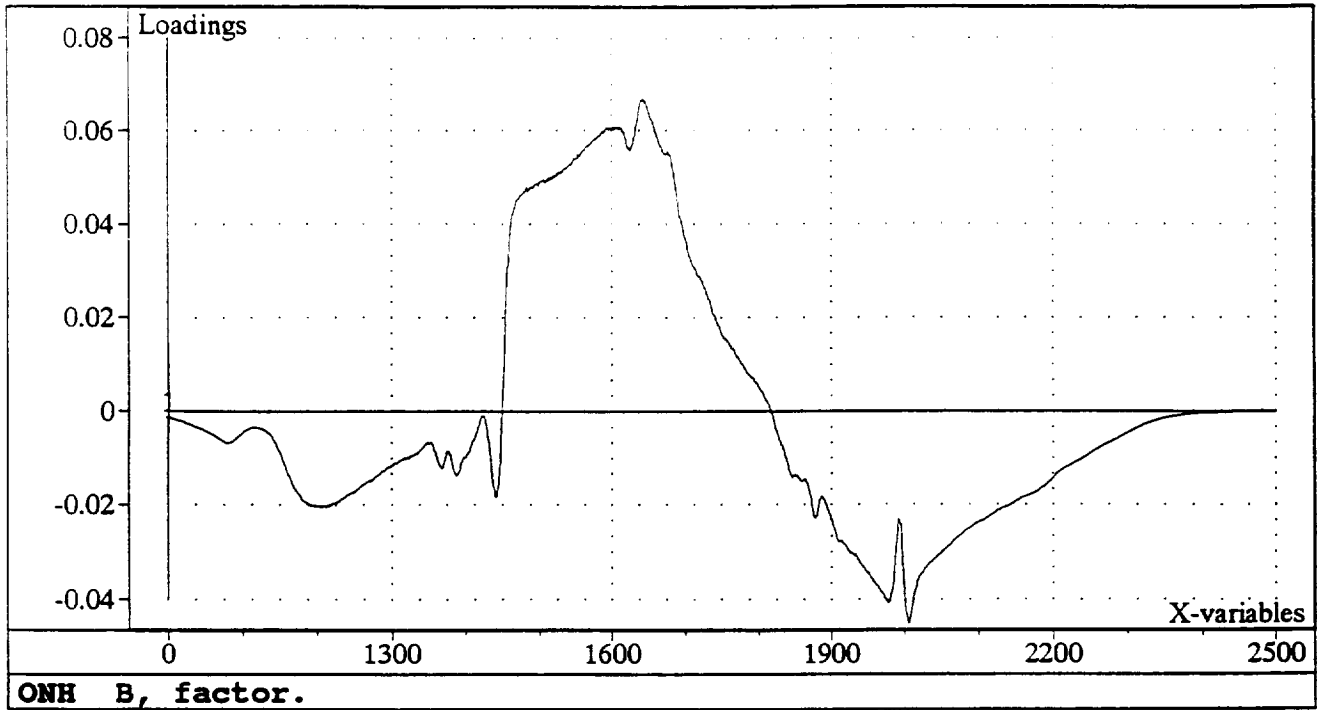


Figure 17a. Model ONH Loadings Plot for Factor 1

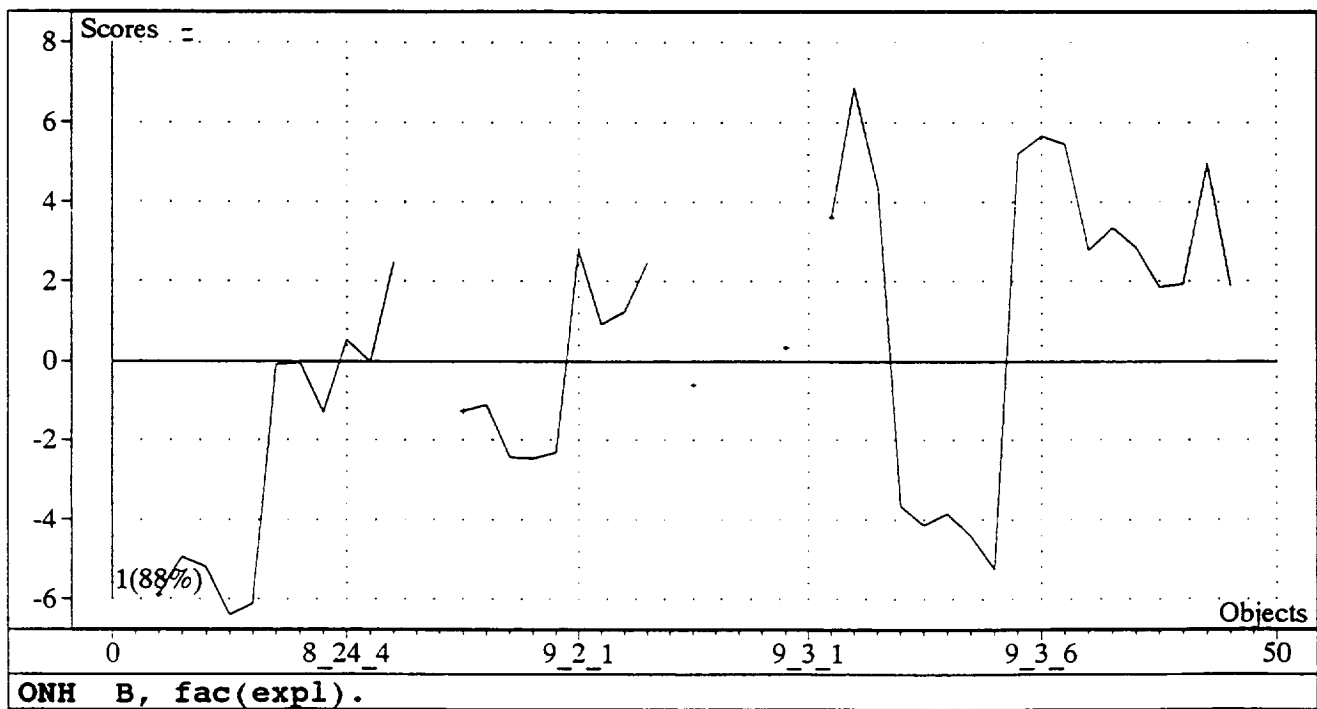


Figure 17b. Model ONH Scores Plot for Factor 1

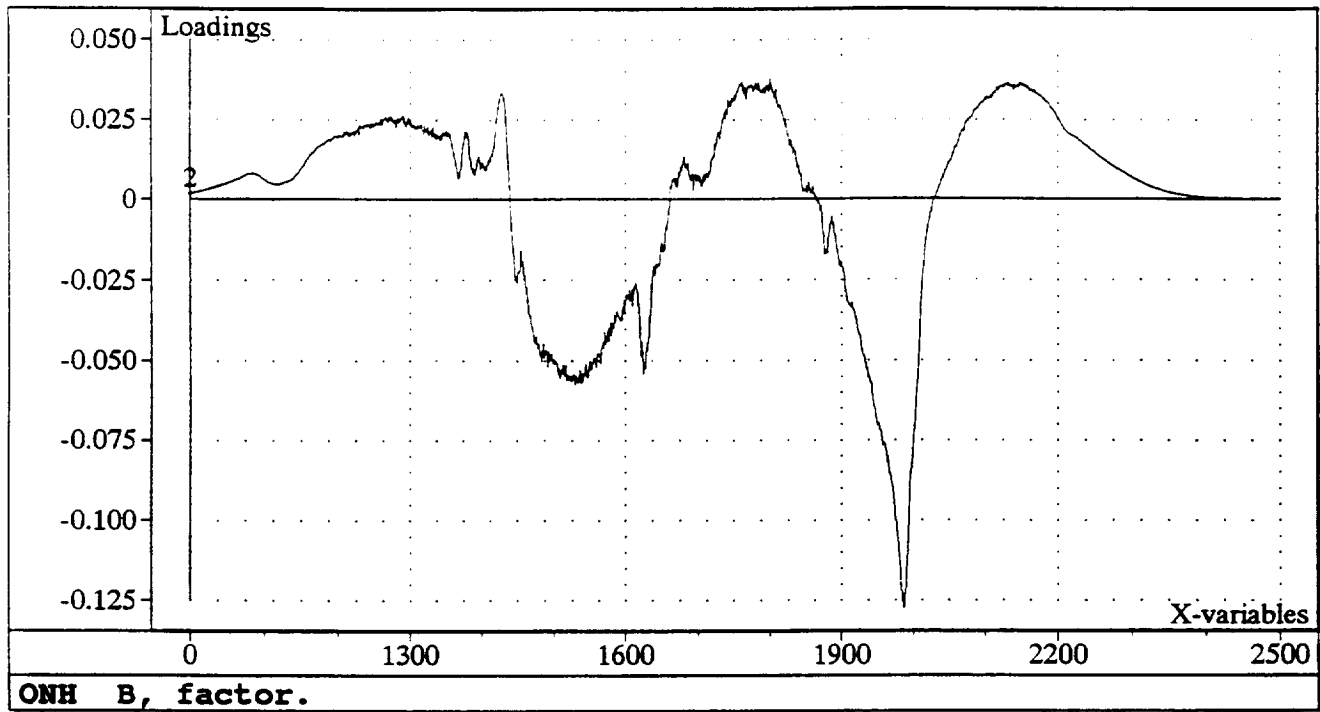


Figure 17c. Model ONH Loadings Plot for Factor 2

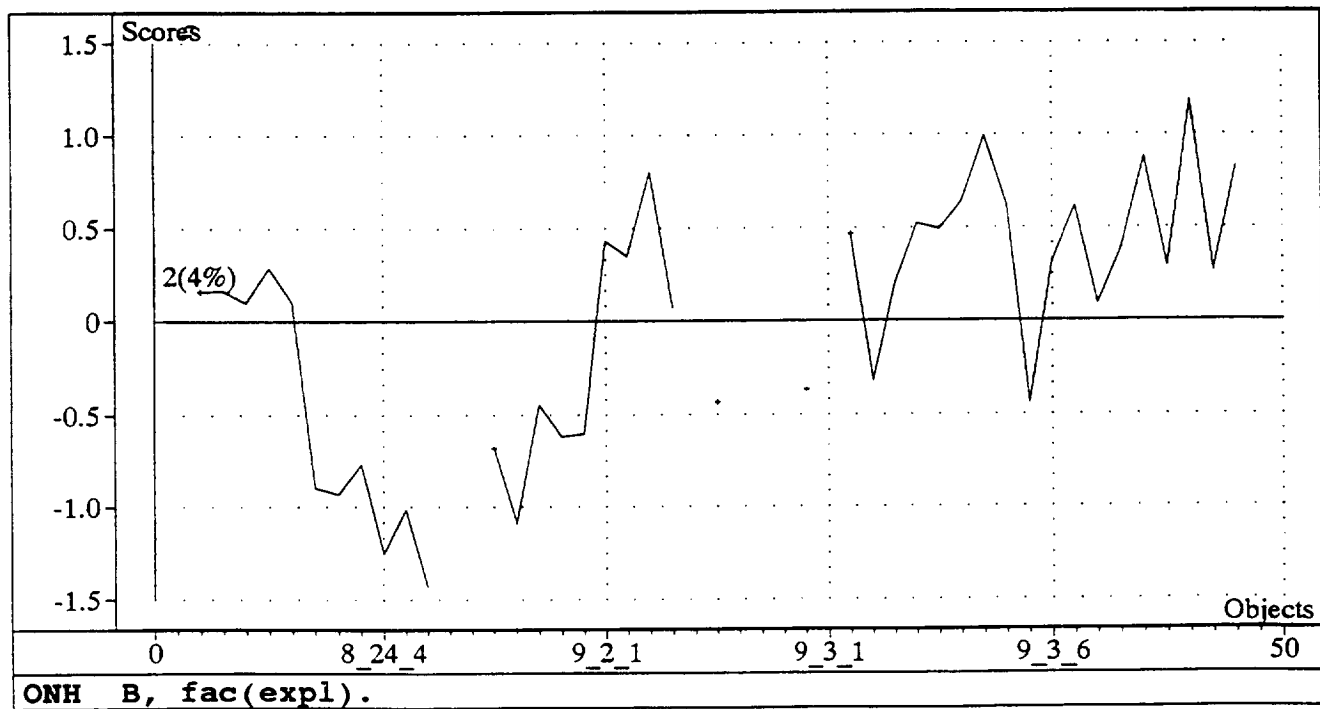


Figure 17d. Model ONH Scores Plot for Factor 2

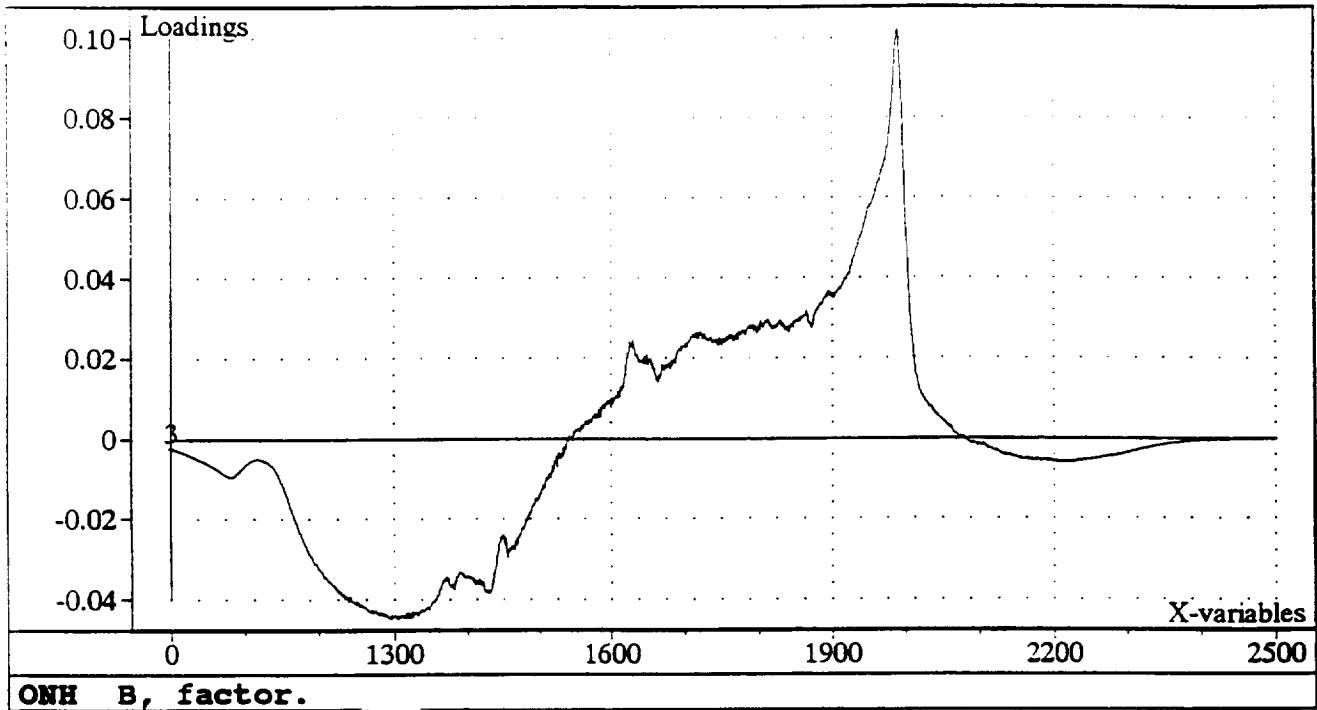


Figure 17e. Model ONH Loadings Plot for Factor 3

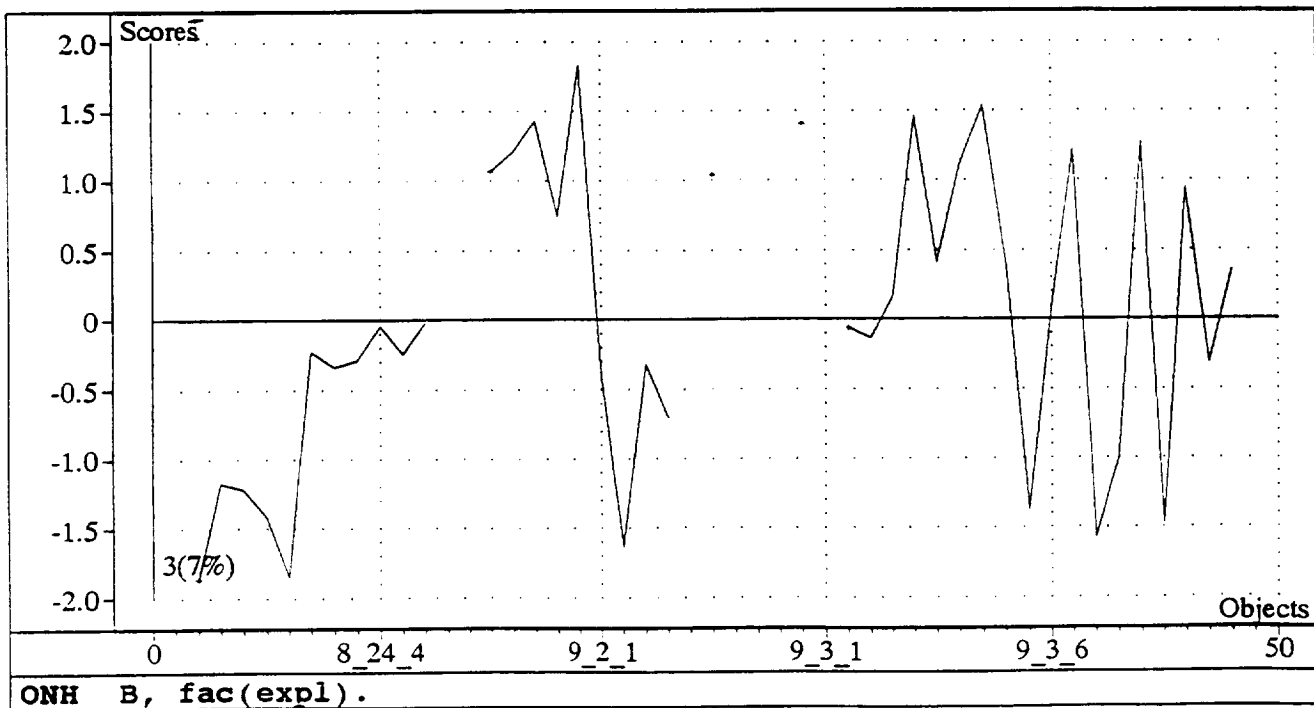


Figure 17f. Model ONH Scores Plot for Factor 3

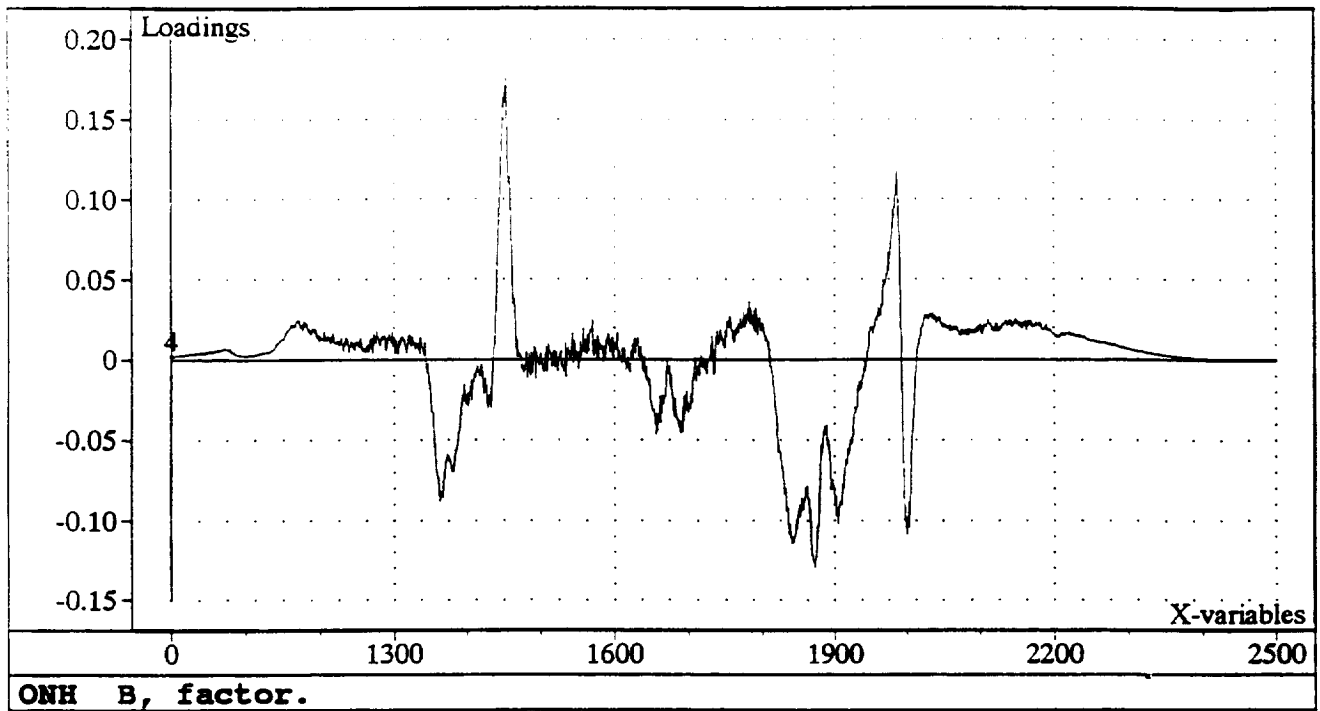


Figure 17g. Model ONH Loadings Plot for Factor 4

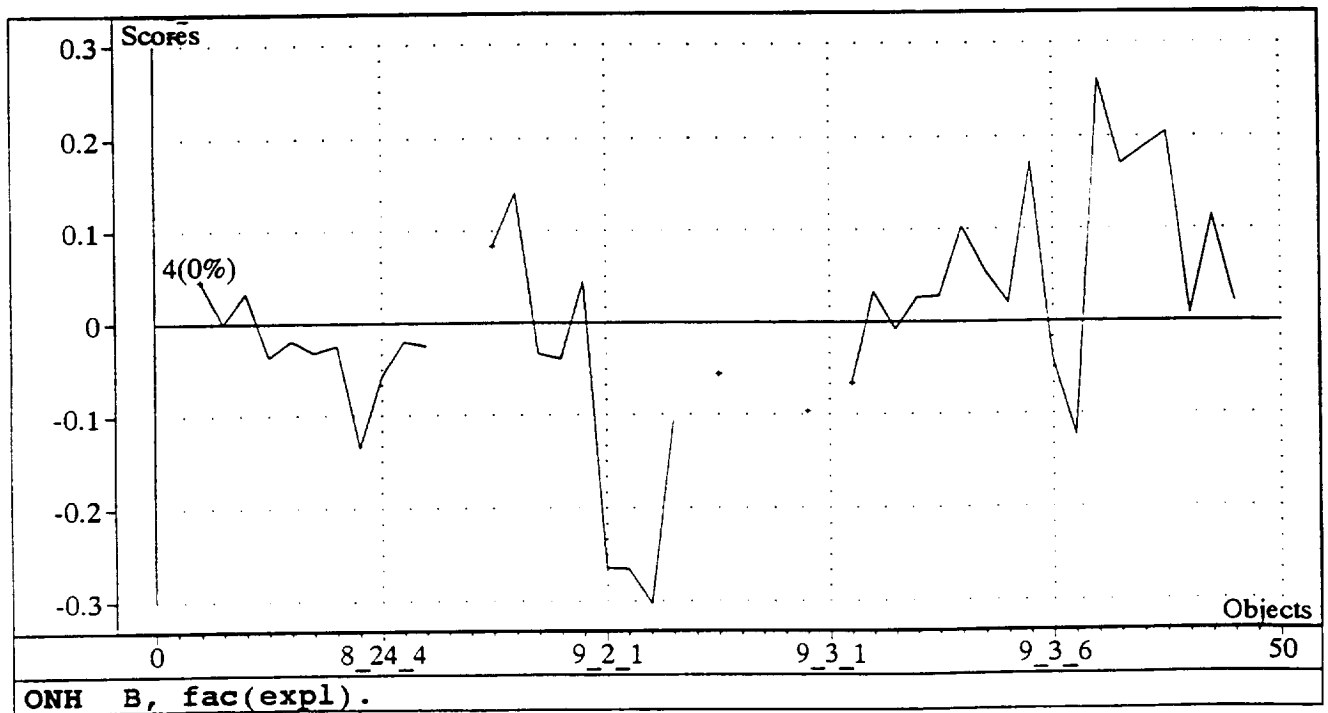


Figure 17h. Model ONH Scores Plot for Factor 4

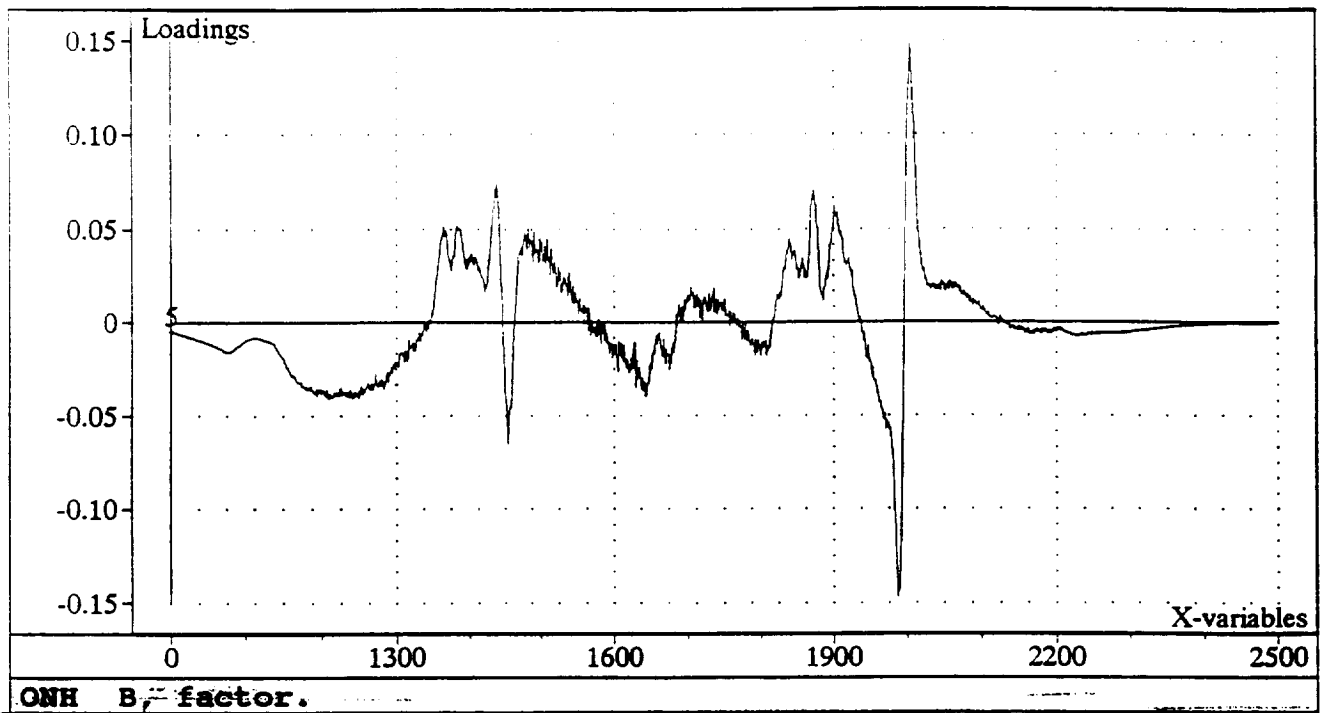


Figure 17i. Model ONH Loadings Plot for Factor 5

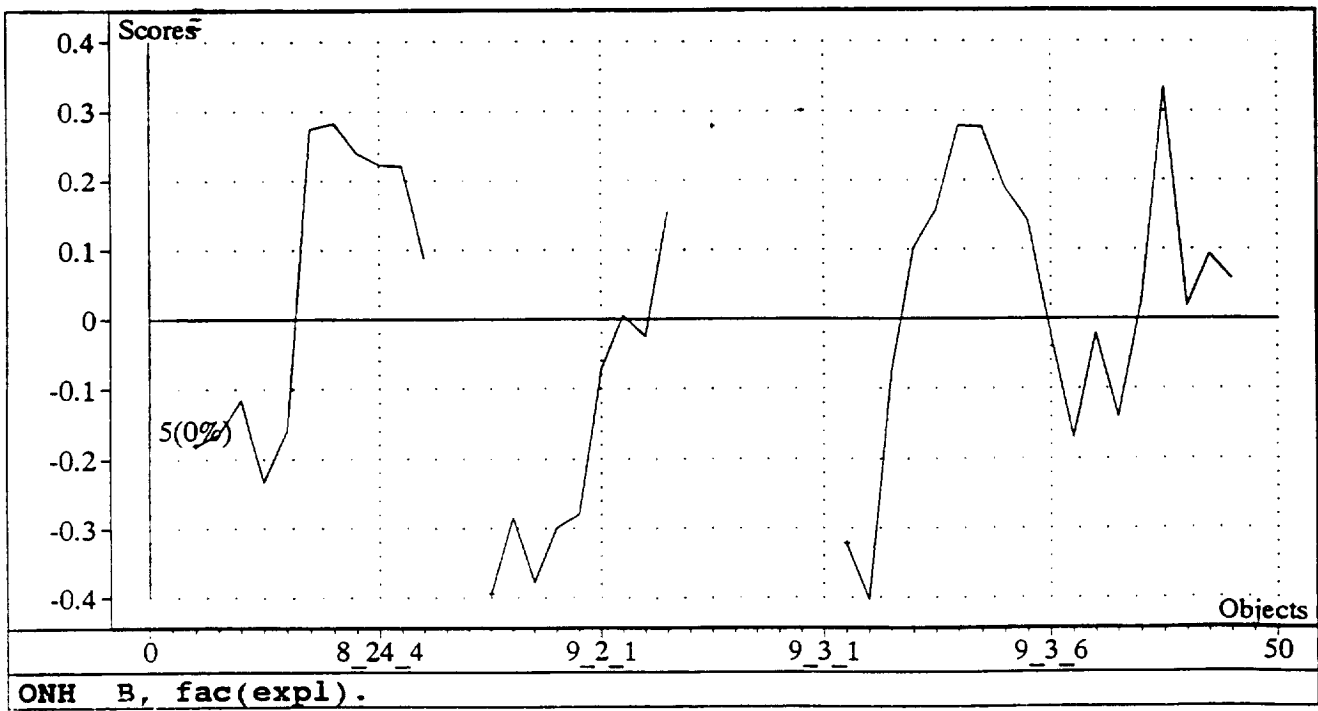


Figure 17j. Model ONH Scores Plot for Factor 5

## 6.5 Observations related to the reflected energy from the surfaces

Initial observations were made using a front surface mirror as the reference surface. We soon learned that a mirror is not an appropriate reference for a steel surface. A series of observations were made illuminating the surface with a collimated beam and placing the receiving fiber in the region that specular reflection would be expected. The patterns are shown in Figures 18a through 18f. Note that the mirror gave a specular reflection as expected. Reflection patterns are shown for BaSO<sub>4</sub> that is usually considered a diffuse standard for reflection. Reflection patterns for D6AC steel at several angles are shown in Figures 18c through 18f. Specular reflection accounts for a large percentage of the reflected energy.

The UV data reported for the study of contaminants was obtained at 45°-45° using the reflection apparatus described above. The remainder of the data was obtained at approximately 0°-0° using a Guided Wave 19 fiber probe. This probe use nine fibers to illuminate the surface and 10 fibers to receive the reflected energy. The 10 fibers are configured to match the slit entrance to the detector.

When the collimated beam was being used to illuminate and observe the samples, very rigid alignment was required. If the sample was not at the correct distance from the probe, large differences were observed for off axis illumination. Distance is not as critical for the 0-0 probe. Recently we have found that alignment normal to the surface is very critical for this probe.

Specular reflection is believed to account for most of the signals observed during these experiments. For example during the sequence studies, we noted that the energy from the sample increased initially, then would decrease. This observation hypothesis would be consistent with an hypothesis that the surface becomes glazed as a film forms on the surface or as reaction takes place at the bottom of the pits on the surface.

Reflection spectroscopy has been used to measure surface roughness. It is possible that some of the variance which is being observed is measuring surface roughness. A controlled study where roughness is measured by an independent method should be beneficial for a complete interpretation of the data.

Figure 18. Reflection patterns observed from various surfaces.

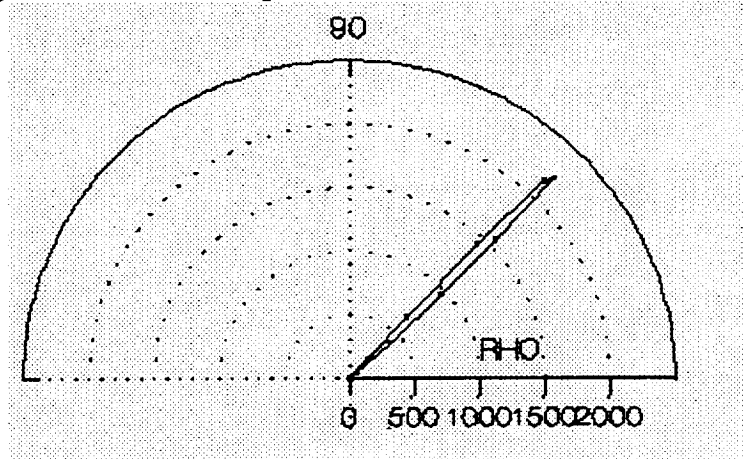


Figure 18a Mirror Surface at 45°

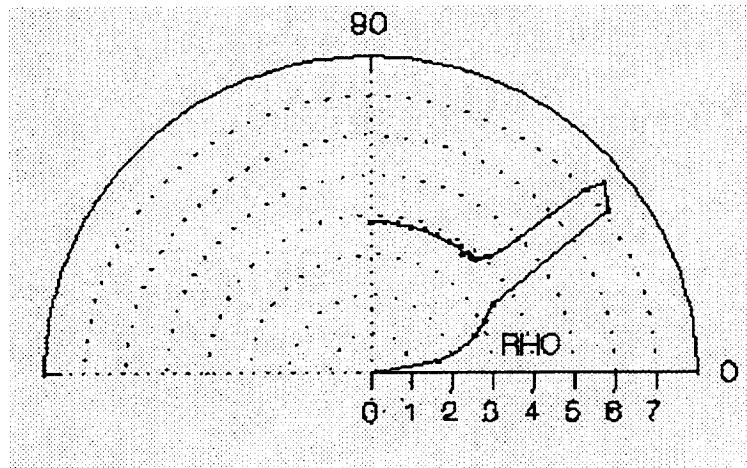


Figure 18b. Packed Barium sulfate at 45°

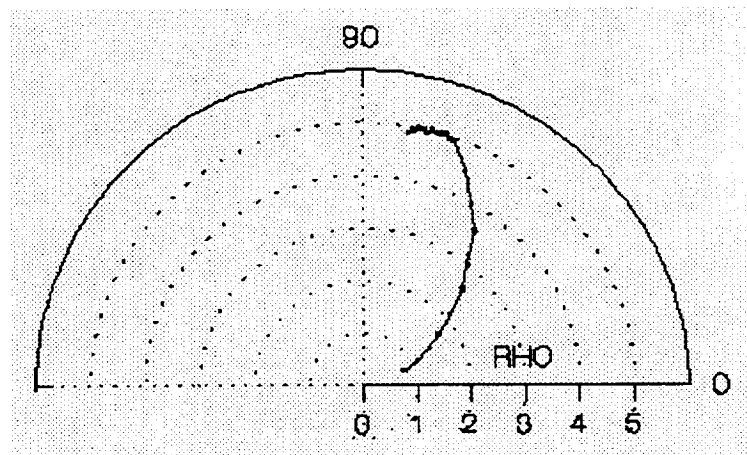


Figure 18c. D6AC steel plate at 12°

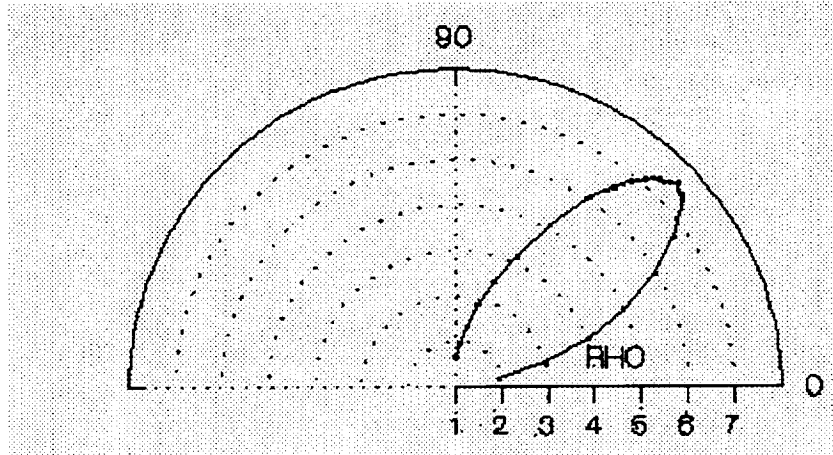


Figure 18d. D6AC steel plate at 45°

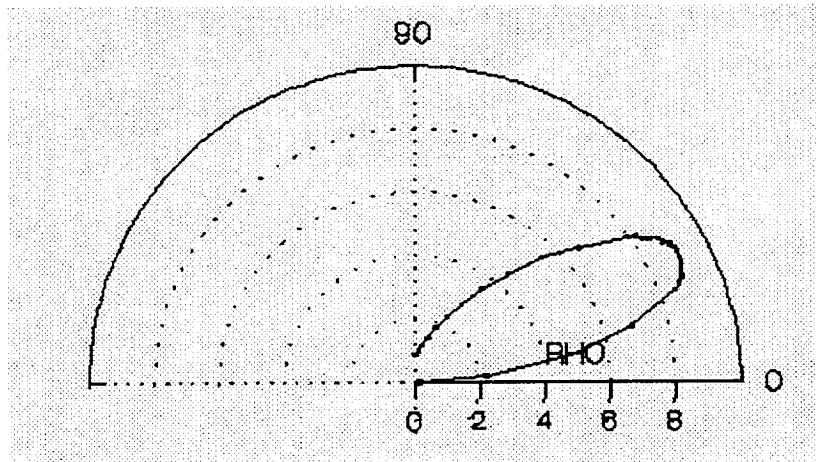


Figure 18e. D6AC steel plate at 60°

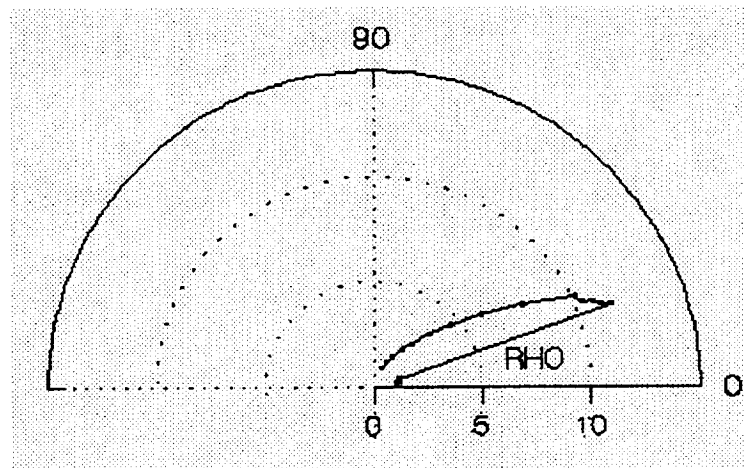


Figure 18f. D6AC steel plate at 70°

## 7.0 Conclusions

During the course of this research, we have worked with several types of data sets. The first spectra were recorded using samples of compounds or contaminants similar to HD2 grease. Since the spectrum of each compound could be obtained, it was possible to resolve the compositions of mixtures of the compounds. As each set of environmental chamber experiments were examined and the accumulated set of spectral observations grew, it became evident that the technology we were using should also allow for the detection and identification of the species resulting from oxidation and/or hydrolysis of D6AC steel. Much of the data that we have used was obtained as sequential spectra recorded during extended periods in the environmental chamber tests.

Since reproducibility is a necessity, the data were first examined as a series. For these studies absorbance units were calculated by subtracting spectra of all later periods from the initial spectrum in the series. Factor analysis was performed to determine the number of components involved. Two to six were usually found. PCR and PLS2 were used in an attempt to determine if the components always occurred in the same sequence. Models from each series were used with the spectra from other series to determine if the order predicted were the same as the observed order, i.e., one order can be used to predict the order of samples in another series.

In the analysis of these experiments, the time the predictions are not the same as the observed values. For example, when using the data obtained at  $\sim 70^{\circ}$  to predict the data at  $140^{\circ}\text{F}$  the predicted times are much greater than the observed times. This can be construed as encouraging, since most chemical reactions proceed at a faster rate when the temperature is raised. This observation is reinforced when we find that the  $40^{\circ}\text{F}$  samples have lower values than predicted. We are encouraged that the same chemistry is involved. There is some evidence that there is an induction period as a species begins to form, which is then followed by a fairly rapid reaction.

Throughout all the analyses of the D6AC surface spectra, we find reappearing spectral features. We are encouraged to continue to work to identify the molecular species and the mechanisms for the oxidations and other reactions that are occurring on the D6AC surface.

## 8.0 Optimization of the use of NIR for quality assurance

Building on the past experiences using NIR spectrophotometry coupled with chemometric procedures investigations directed toward optimization of the use of NIR spectrophotometry should be pursued. The following tasks are recommended.

1. Optimization of the techniques for examining surfaces. Primary emphasis for this task would be measurement of corrosion products and organic contaminants on steel and aluminum surfaces using a microprobe. The currently available 9/10 probe and Guided Wave Model 260 Spectrophotometer will be used to optimize experimental parameters and provide data for the optimization of data reduction using multivariate algorithms.

2. Integration with materials analyses. Previous work with an ATR probe has indicated that NIR spectrophotometry can be used to measure ratio of ingredients during processing and that the data can be used to predict the physical properties of a material, for example bond strength of the cured matrix, at the conclusion of the next processing step. The spectrophotometer will be available for Task 1 to measure the properties of the surface. ATR spectra would be taken of the matrix applied to the metal surface. The predicted strength of the bond would be compared to the measured strength. Surface roughness measurements should also be investigated.

3. Computerization of data reduction. New versions of the Guided Wave software and Unscrambler II include microlanguages adaptable to "script" procedures. Matlab is also available and includes script capability. Programs can be provided so that data is immediately available during test thus providing an opportunity for immediate action.

4. Optimization of probe designs. Concurrent with Task 1 and 2 new probes would be designed that optimize the data that is obtained. Hopefully, the newer Guided Wave INSIGHT spectrophotometer will be available. This spectrophotometer has a much higher processing capability and more importantly, a noise level at 0 AU of less than 20 microabsorbance units. Recent tests have indicated that the average of 32 spectra has a noise level of 4 microAU. These 32 spectra can be taken quicker than 1 spectrum with the Model 260, thus a further indication of how technology is improving our ability to monitor processes.

## 9.0 Acknowledgements

A number of students and staff have assisted in carrying out this research project. Ms. Yadilett Garlington, Ms. Bianca Brindley, Mr. Brian Benson, Mr. Markus Heilbrotter, and Morgan Wang, all contributed to some part of this activity. Each is to be commended for their assistance.

## 10.0 References

1. Martens, H. and T. Naes, *Multivariate Calibration*, Wiley, New York, 1989.
2. *Handbook of Military Infra-red Technology*, Office of Naval Research 1966.
3. Weyer, L. G. "Near-Infrared Spectroscopy of Organic Substances," *Applied Spectroscopy Review* 21 (1985), 1-43.
4. Massart, D.L., et. al. *Chemometrics: a textbook*, Elsevier, New York, 1988.
5. Malinowski, E. R., *Factor Analysis in Chemistry*, Wiley , New York, 1991.
6. DeNoyer, Lin and Dodd, Jack, "Square Tools," *Spectrum Squares Associates*, Ithaca, N.Y. 1992.

7. Hauffe, K., *Oxidation of Metals*, Plenum Press, New York, 1965.
8. Hecht, H.G., *Infrared-Spectroscopy*,
9. Greenler, R.G., *Jour Chem Phys* 44 (1966) pp 310 - 315.
10. Greenler, R.G., *Jour Chem Phys* 50 (1969) pp 1963 - 1968.
11. Greenler, R.G., *Surface Scien* 69 (1977) pp 647-652.
12. Allara, D.L., et. al., *Macromolecules* 11 (1978) pp 1215 - 1220.
13. Martens, H. and B. Alsberg, *Analytical Applications of Spectroscopy II*, Roy Soc. of Chem, Cambridge, 1991, pp 221 - 239.
14. Naes, T. and T. Isaksson, *Computer-Enhanced Analytical Spectroscopy*, vol. 3, Plenum Press, New York, 1992, pp 69 - 94.
15. Ares, J., *Anal. Chem. Acta*, 268 (1992) pp 135 - 144.

## APPENDIX. Study of mixtures of four hydroxyl containing compounds

As indicated previously analyses of spectra of mixtures of known compounds is straightforward. Several methods are suitable for determining the calibration matrix. Since we were interested in the wavelengths at which the OH group absorbs, a set of 8 mixtures was prepared using methanol, ethanol, isopropanol, and glycerol. (Table 6 shows the mole percentage of each alcohol sample) The NIR spectra were recorded for the same wavelength region as used for the other studies in this report (Table 7 shows some groups and their wavelengths). The raw data is presented in Figure 19a through 19l. A calibration model was set up using PLS2 from UNSCRAMBLER with this data and the spectra of the pure alcohols. The compositions were expressed in mole fractions of the mixture. This reduces the degrees of freedom by one since the mixtures must add to 1.0. Figures 20a through 20k show the predicted results vs the known compositions.

Even though the loadings can not be considered "real" spectra it is informative to compare the loadings to the spectra of the pure materials. Factor 1 and Factor 2 are compared to methanol and glycerol in Figure 21a and 21b. Figure 22 shows that glycerol is explained largely by the variance from Factor 1. Looking at the chemical formula for glycerol,  $\text{CH}_2\text{OH-CHOH-CH}_2\text{OH}$ , it is clear that it contains all of the chemical vibrations that occur due to C-C, C-H, or O-H vibrations that may occur in the selected alcohols. Because the vibrations in glycerol comprise the variations common to all of the pure alcohols in the mixtures, it is evident that Factor 1 would be most similar to the spectrum of glycerol. Figure 23a through Figure 23h are the loadings and Figure 23a through Figure 23h are the scores.

All the prior work presented in this report, except for the contaminant study, was based on unknown chemistry. Hence, we felt that an informative experiment based on known mixtures would assist in building confidence in Unscrambler II as a calibration tool. Consequently, the following study was performed to verify that the components of a known mixture can be resolved.

TABLE VI. MOLE PERCENTAGE OF RESPECTIVE ALCOHOL

	OBJECTS	Methanol	Ethanol	Propanol	Glycerol
SOL 01	1	1	0	0	0
SOL 02	2	0	1	0	0
SOL 03	3	0	0	1	0
SOL 04	4	0	0	0	1
SOL 05	5	0.59	0.41	0	0
SOL 06	6	0.66	0	0.35	0
SOL 07	7	0	0.57	0.43	0
SOL 08	8	0.4	0.28	0.21	0.11
SOL 09	9	0.45	0.31	0.24	0
SOL 10	10	0.25	0.35	0.4	0
SOL 11	11	0.53	0.19	0.28	0
SOL 12	12	0.55	0.25	0.1	0.11

TABLE VII. Some Groups and Their Wavelengths

<i>Group</i>	<i>Overtone</i>	<i>Wavelength</i>	<i>Intensity</i>
C-H	1	1700 nm	strong
	2	1100 nm	medium
O-H	1	1400 nm	strong
C-C	3	1750 nm	very weak
	4	1400 nm	not detectable <sup>1,2</sup>
C-H	1	1600 - 1800 nm	N/A
	2	1100 - 1250 nm	
	1 <sup>st</sup> Set Combinations	2000 - 2400 nm	
	2 <sup>nd</sup> Set Combinations	1300 - 1450 nm	weaker
O-H	1	1400 - 1416 nm	strong
	2	1000 nm	weaker
	Combination bands	2000 nm	weaker <sup>3</sup>

<sup>1</sup>Wheeler, Owen H., "Near Infrared Spectra of Organic Compounds," Chemical Review, 59, 629-666 (1959).

<sup>2</sup>Approximate theoretical wavelengths of overtones.

<sup>3</sup>Weyer, L.G., "Near-Infrared Spectroscopy of Organic Substances," Applied Spectroscopy Reviews, 21(1&2), 1-43(1985).

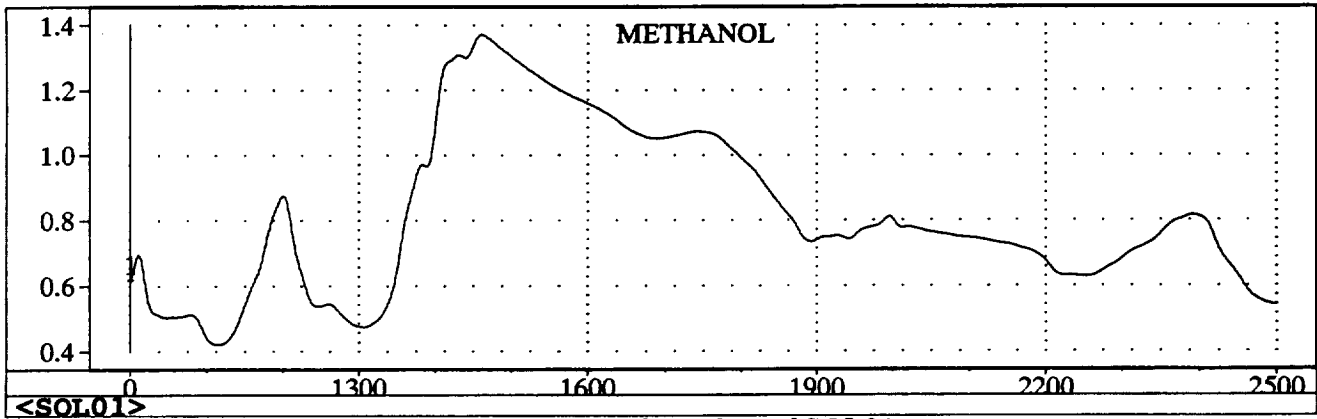


Figure 19a. Raw data of SOL01

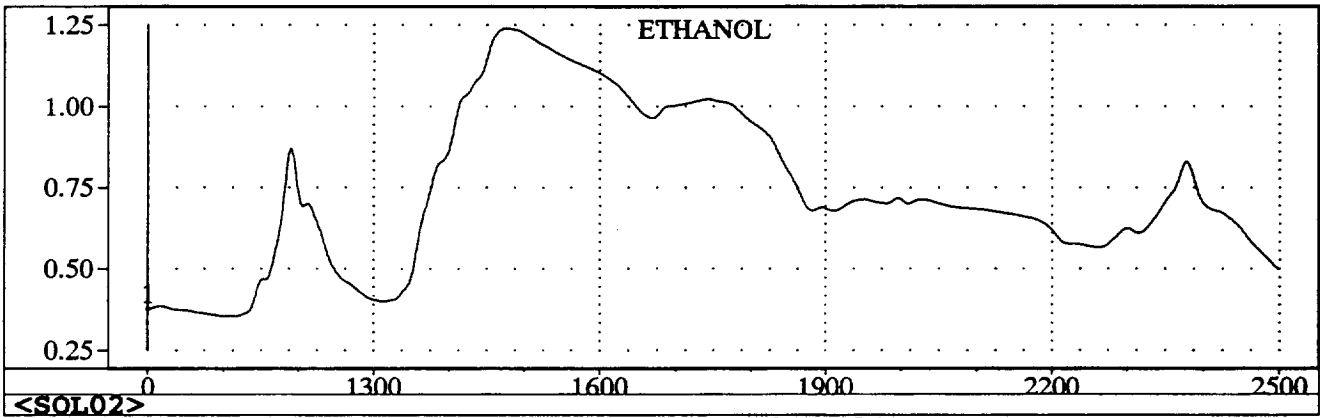


Figure 19b. Raw data for SOL02

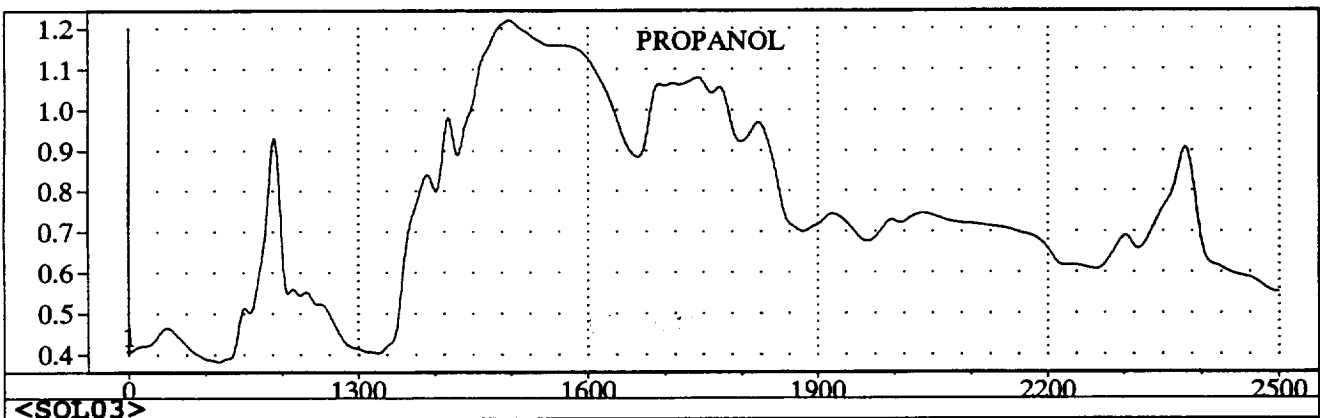


Figure 19c. Raw data of SOL03

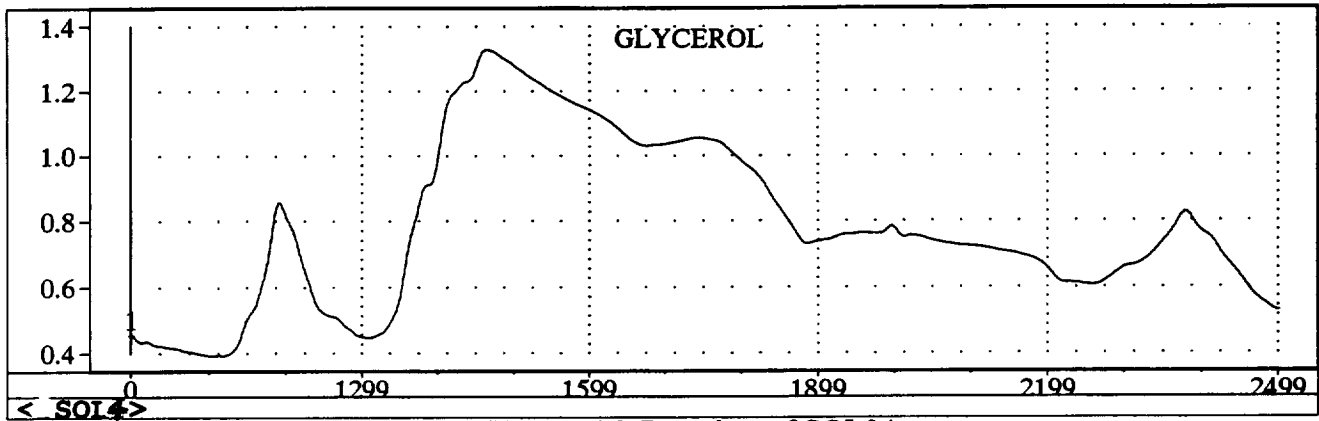


Figure 19d. Raw data of SOL04

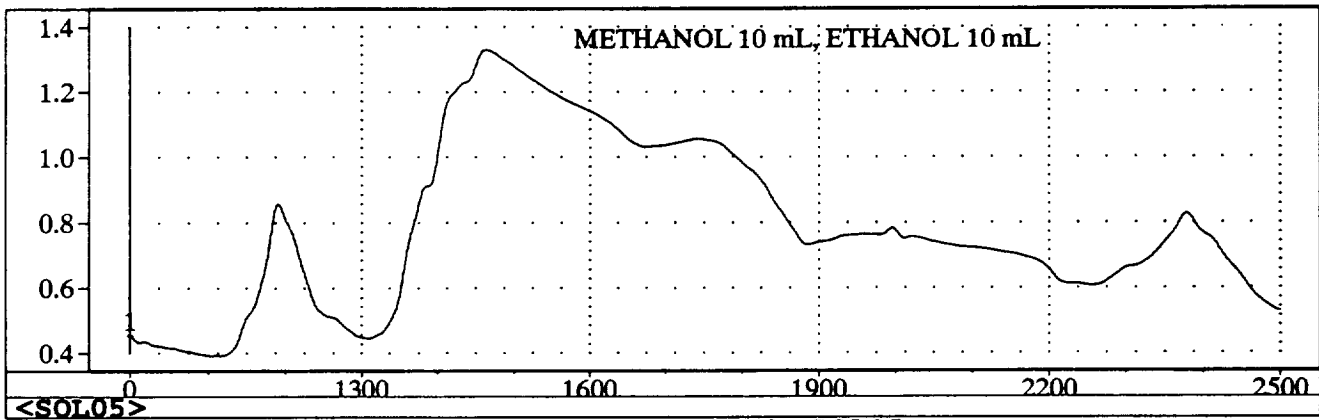


Figure 19e. Raw data for SOL05

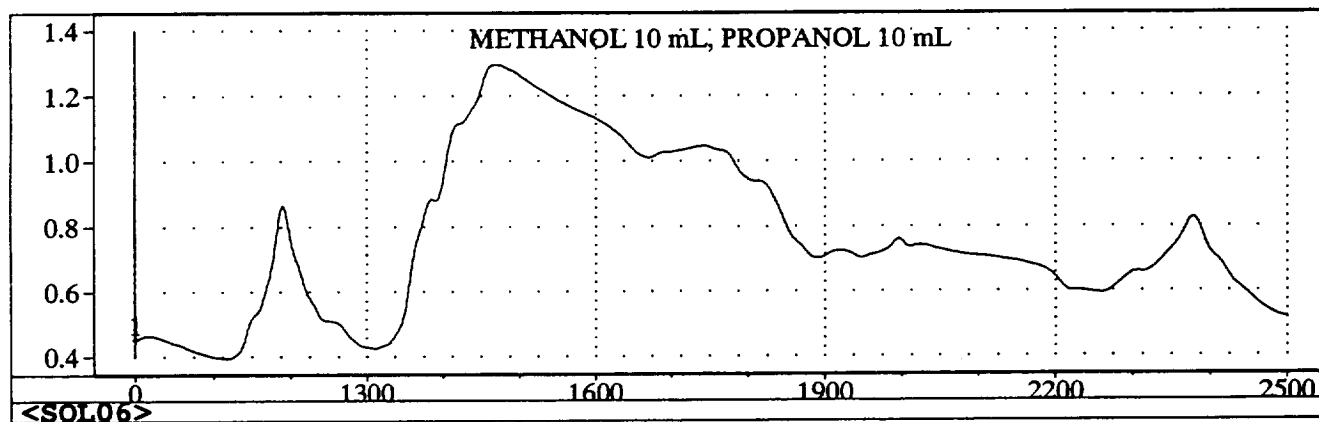


Figure 19f. Raw data of SOL06

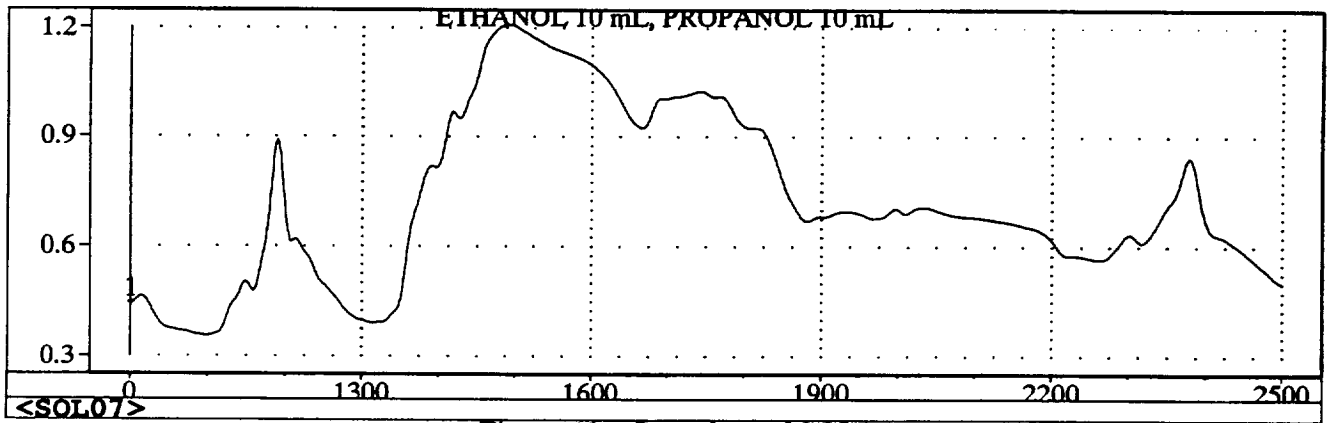


Figure 19g. Raw data of SOL07

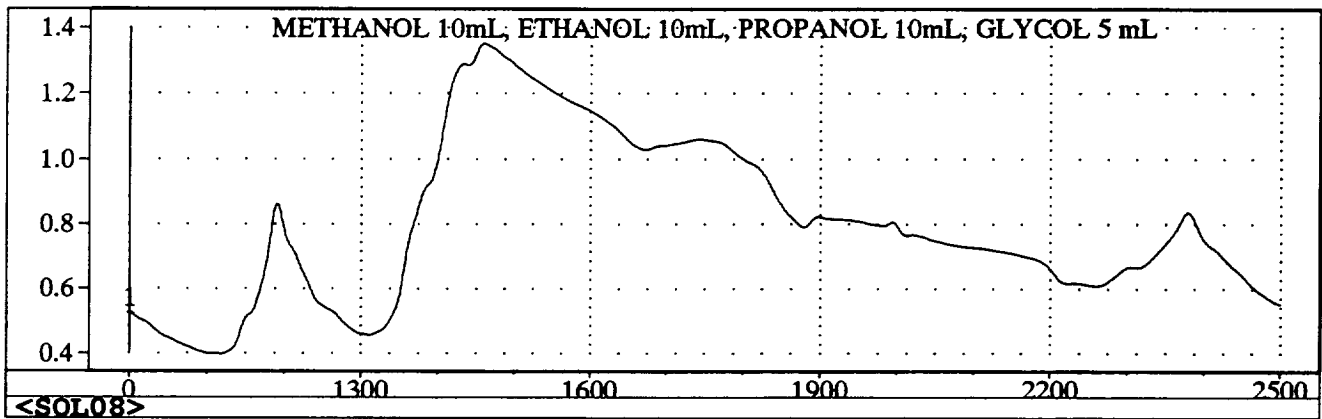


Figure 19h. Raw data for SOL08

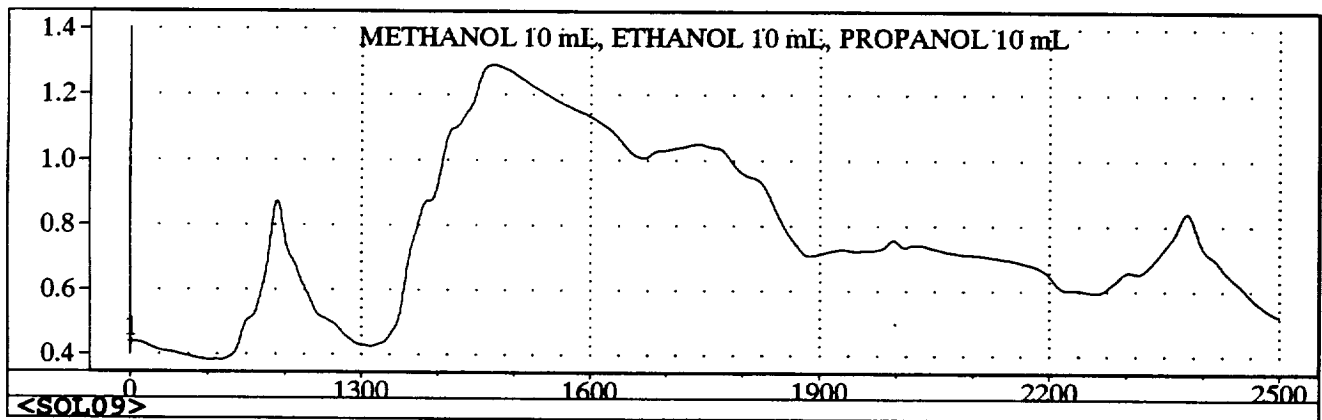


Figure 19i. Raw data of SOL09

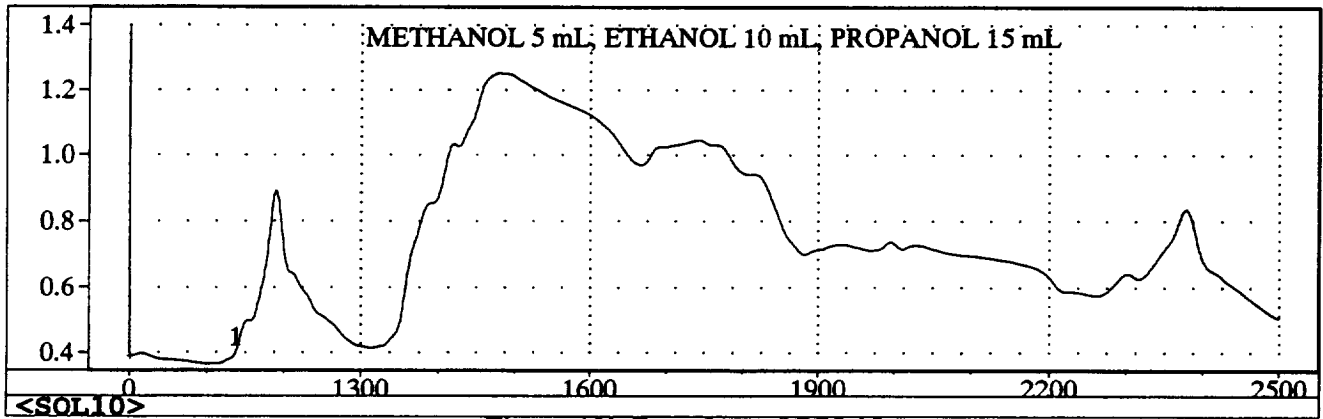


Figure 19j. Raw data of SOL10

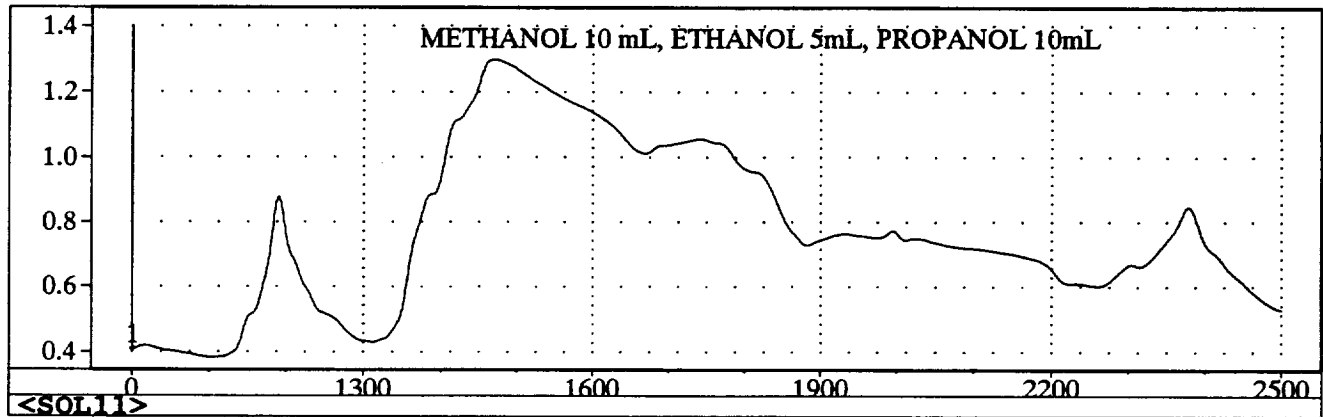


Figure 19k. Raw data for SOL11

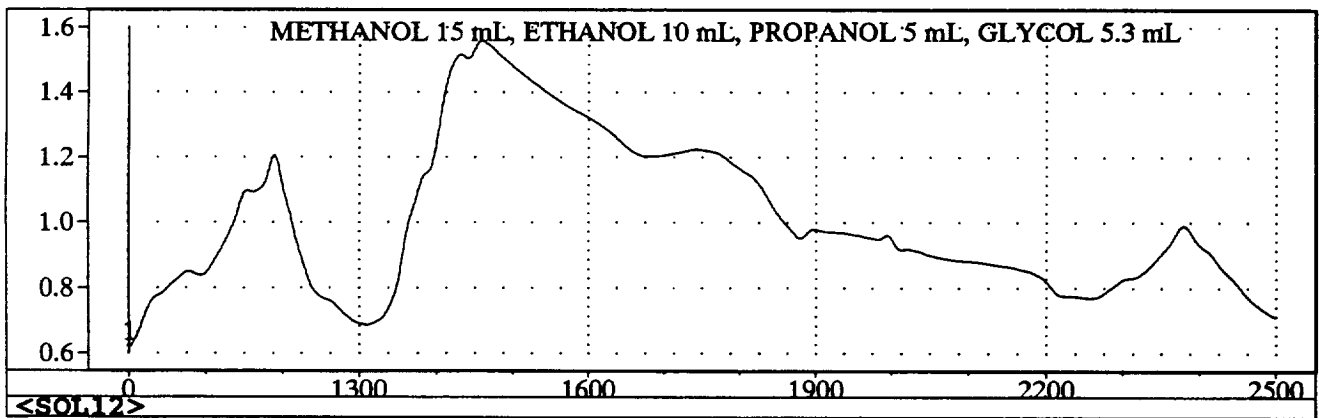


Figure 19l. Raw data of SOL12

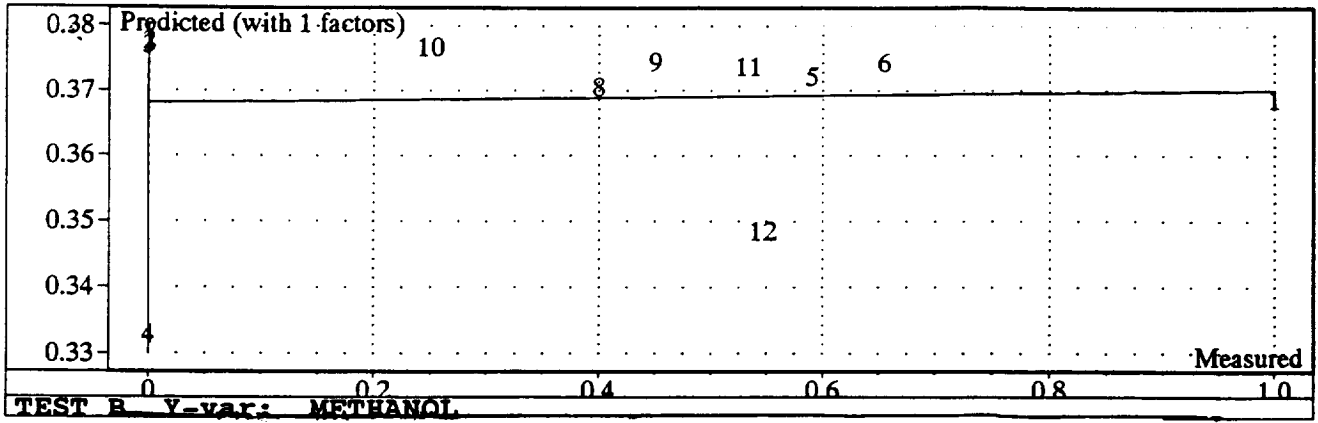


Figure 20a. Predicted vs. known compositions of Methanol using 1 factor

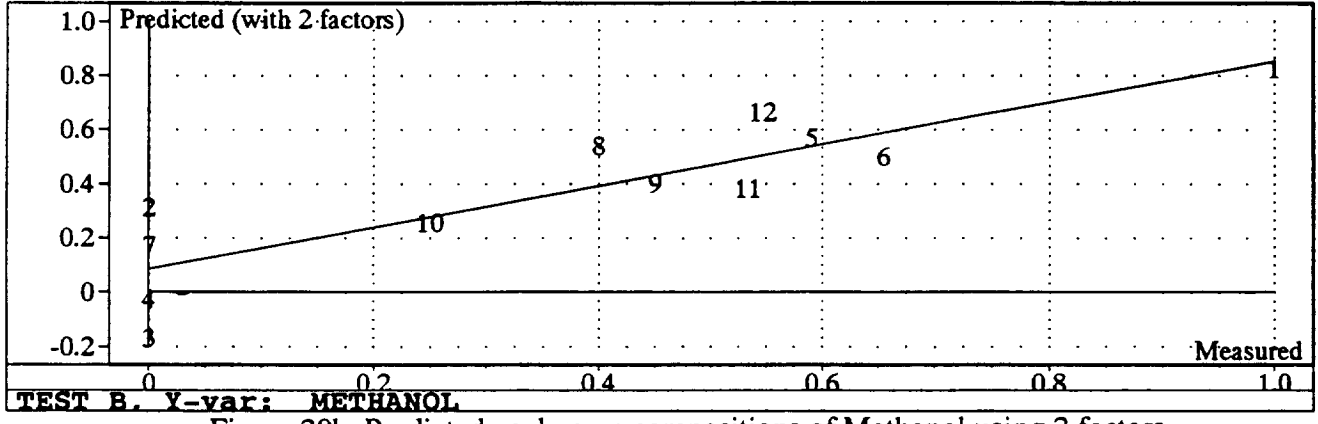


Figure 20b. Predicted vs. known compositions of Methanol using 2 factors

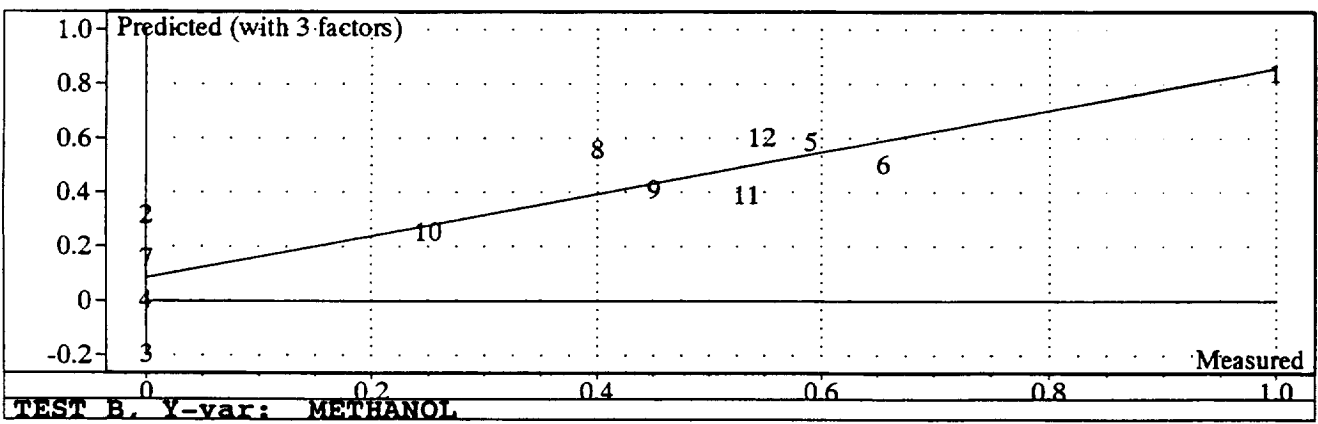


Figure 20c. Predicted vs. known compositions of Methanol using 3 factors

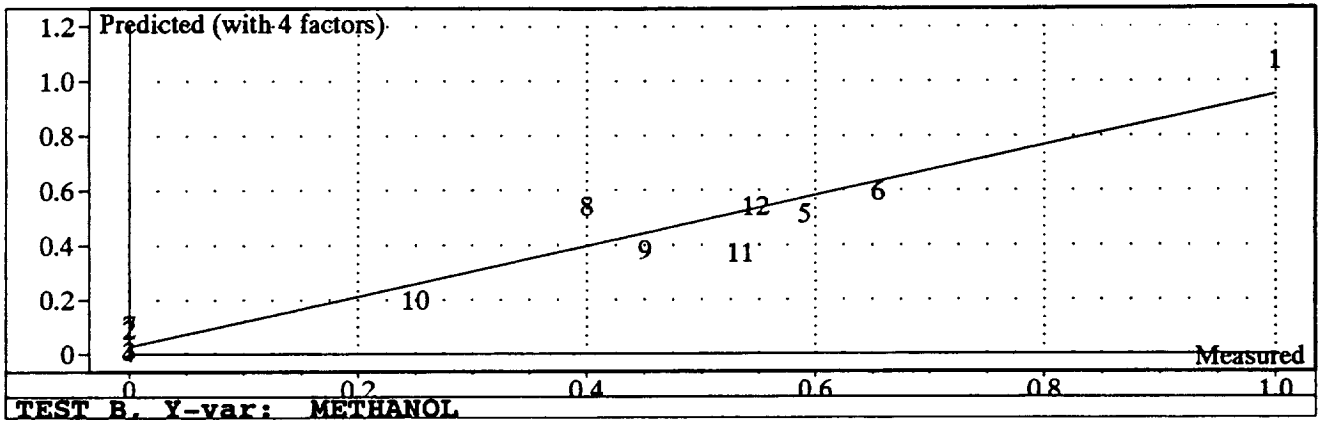


Figure 20d. Predicted vs. known compositions of Methanol using 4 factors

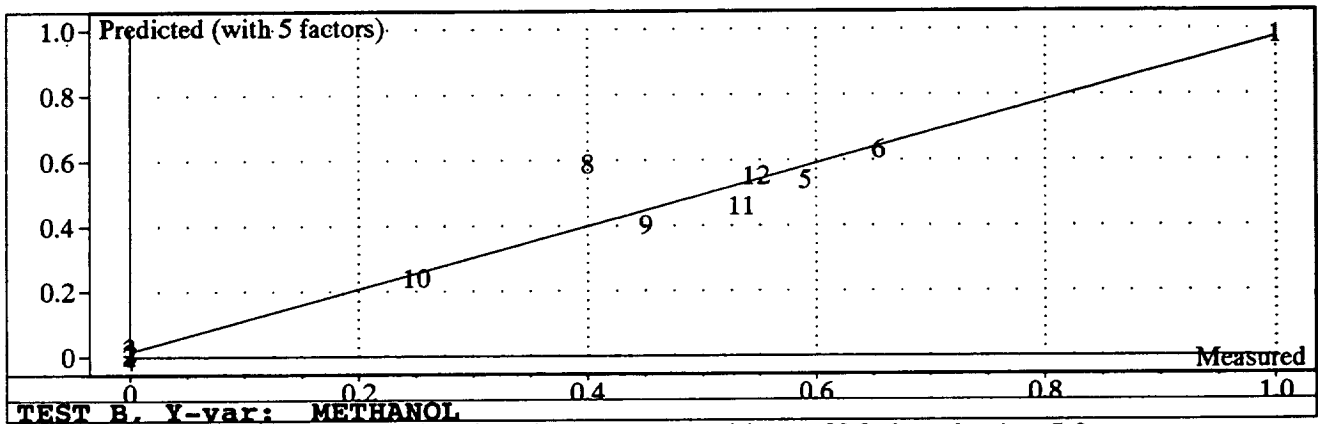


Figure 20e. Predicted vs. known compositions of Methanol using 5 factors

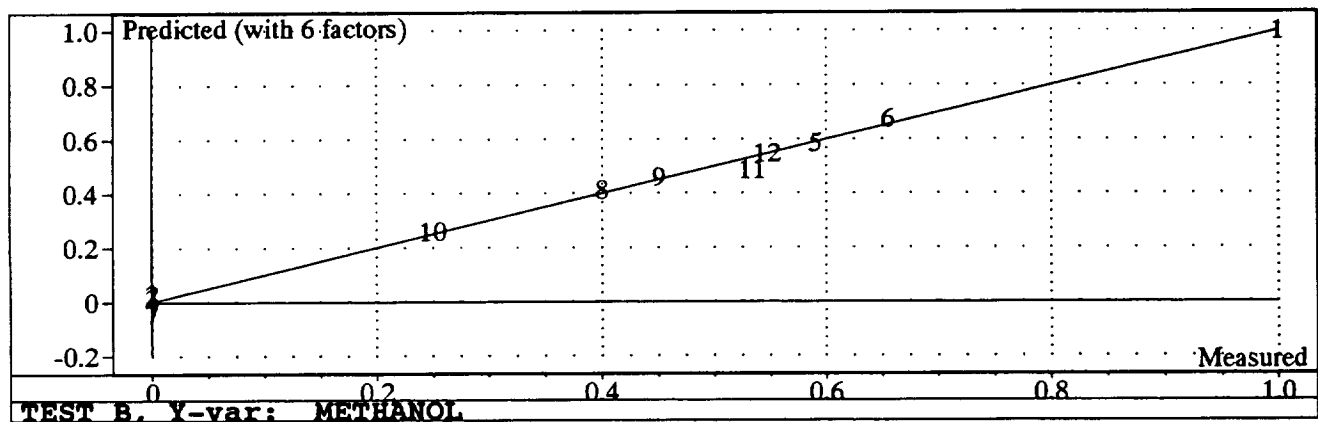


Figure 20f. Predicted vs. known compositions of Methanol using 6 factors

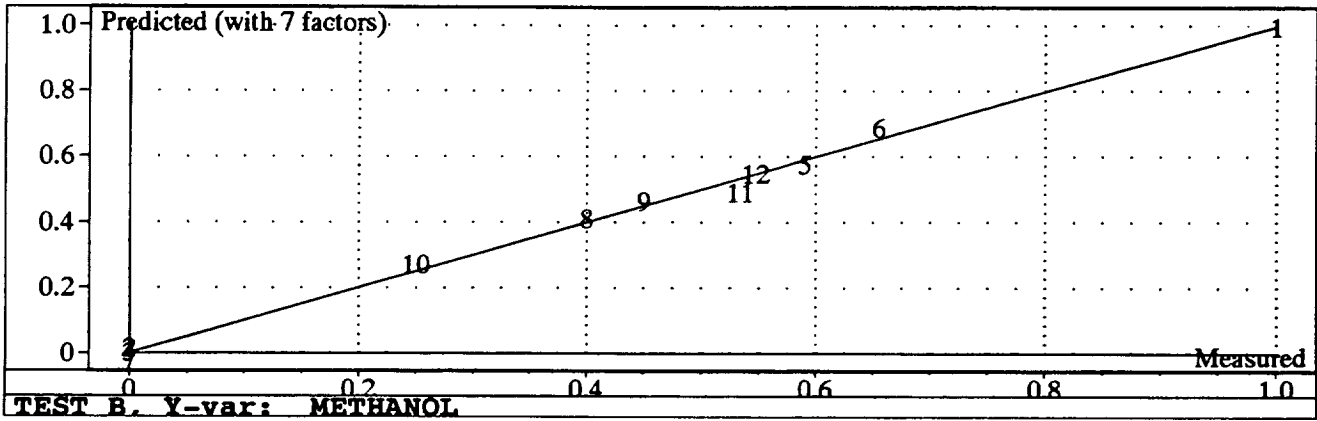


Figure 20g. Predicted vs. known compositions of Methanol using 7 factors

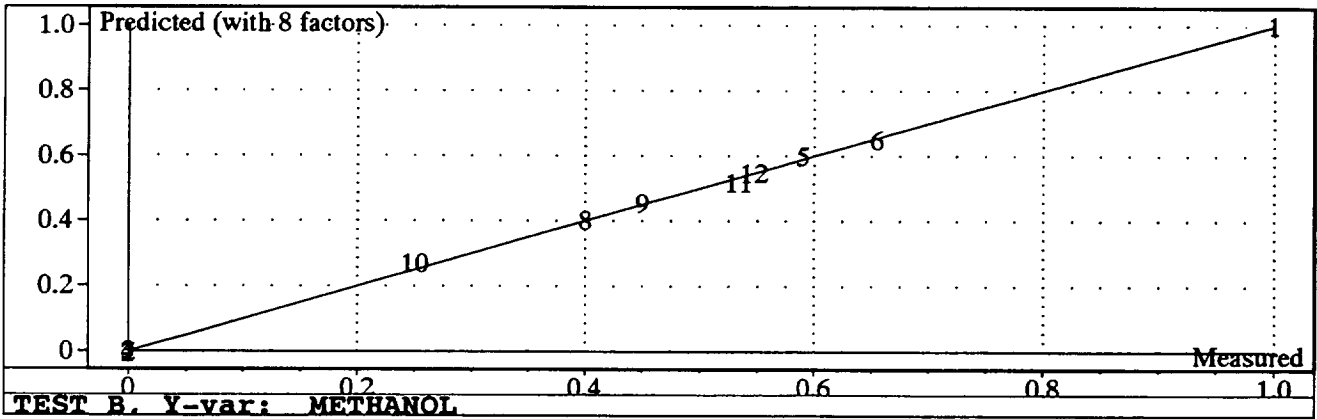


Figure 20h. Predicted vs. known compositions of Methanol using 8 factors

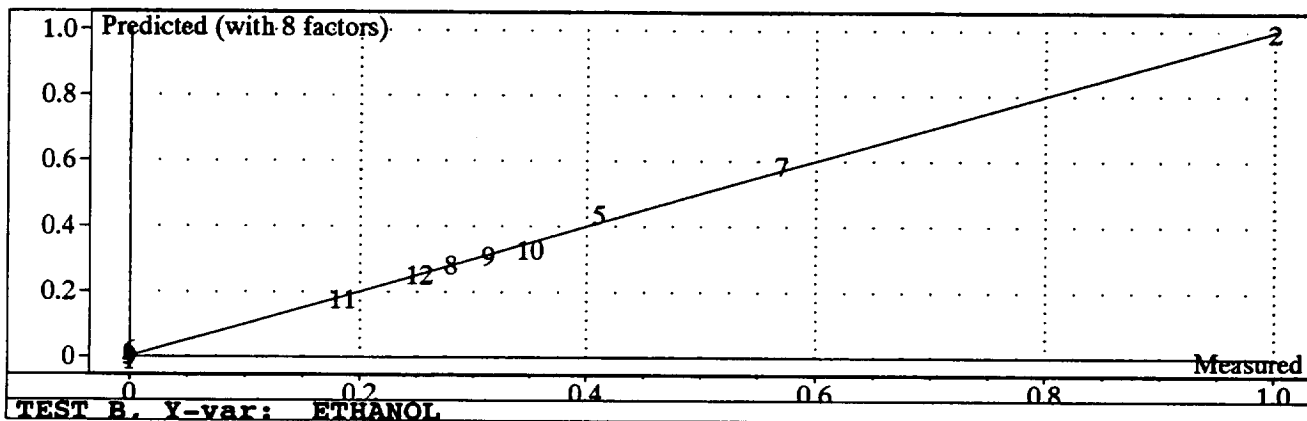


Figure 20i. Predicted vs. known compositions of Ethanol using 8 factors

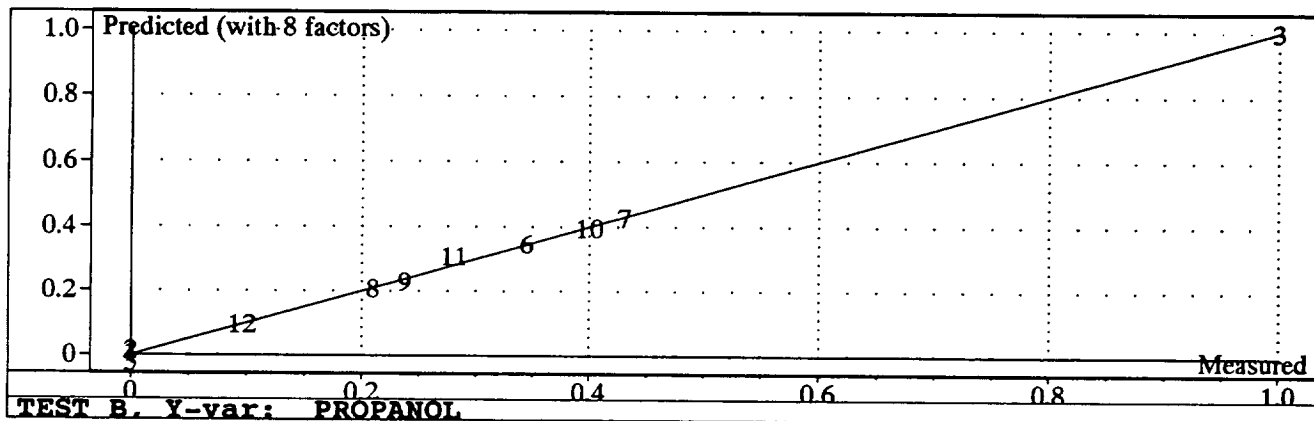


Figure 20j. Predicted vs. known compositions of Propanol using 8 factors

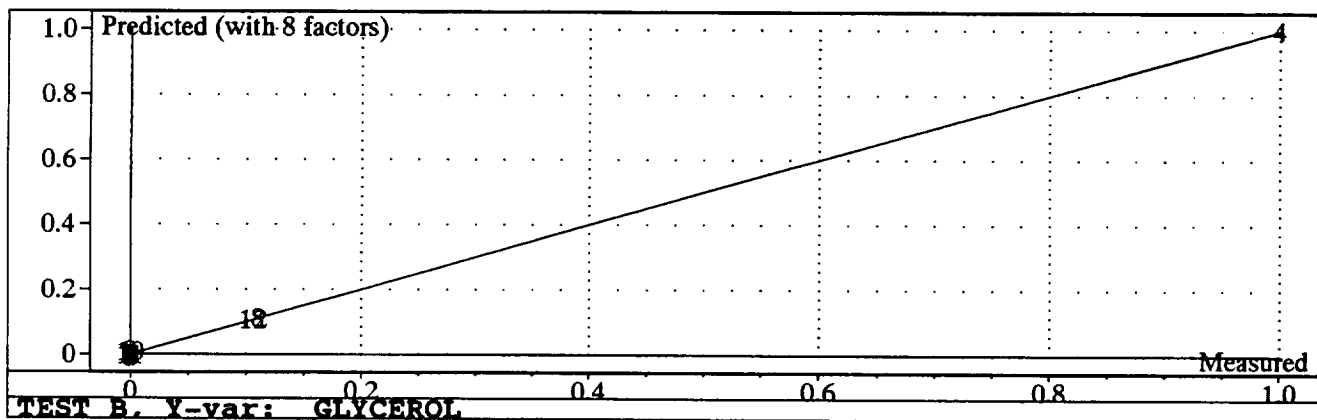


Figure 20k. Predicted vs. known compositions of Glycerol using 8 factors

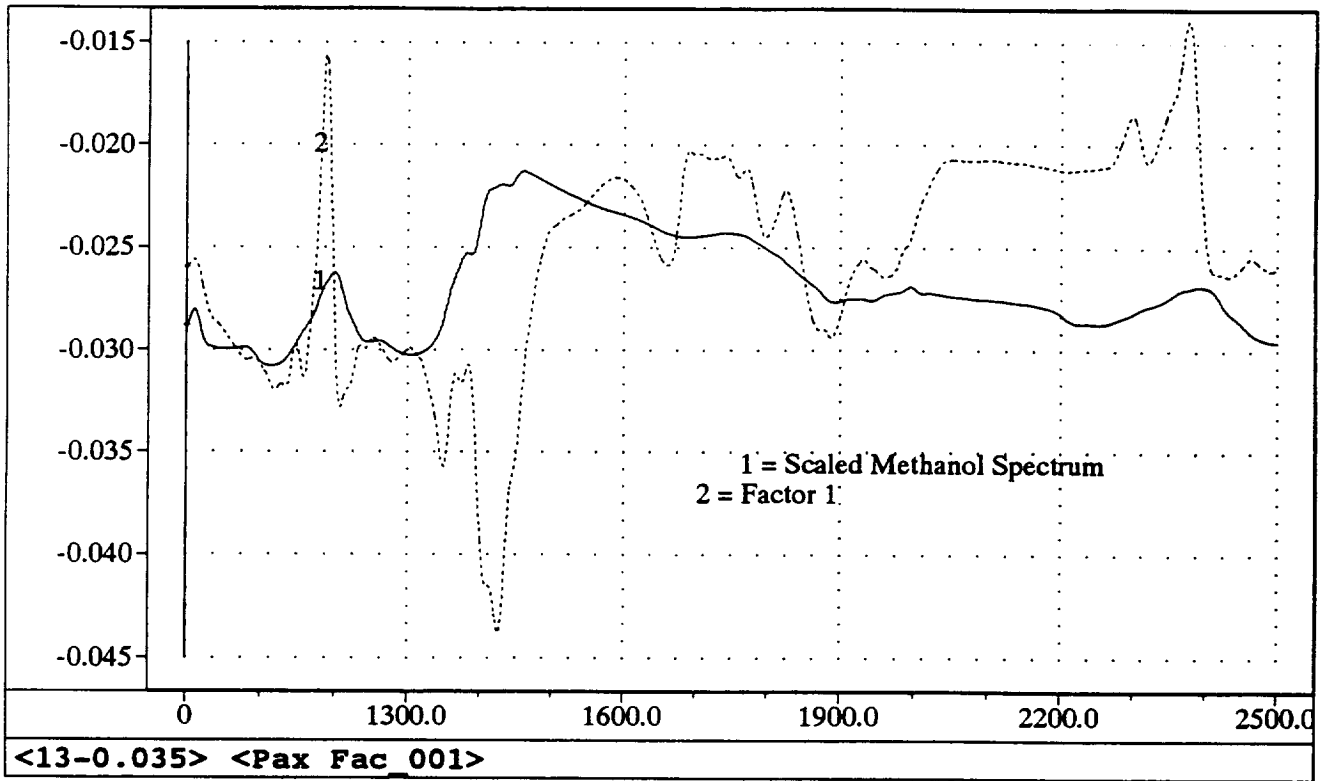


Figure 21a. Methanol spectrum compared to Factor 1

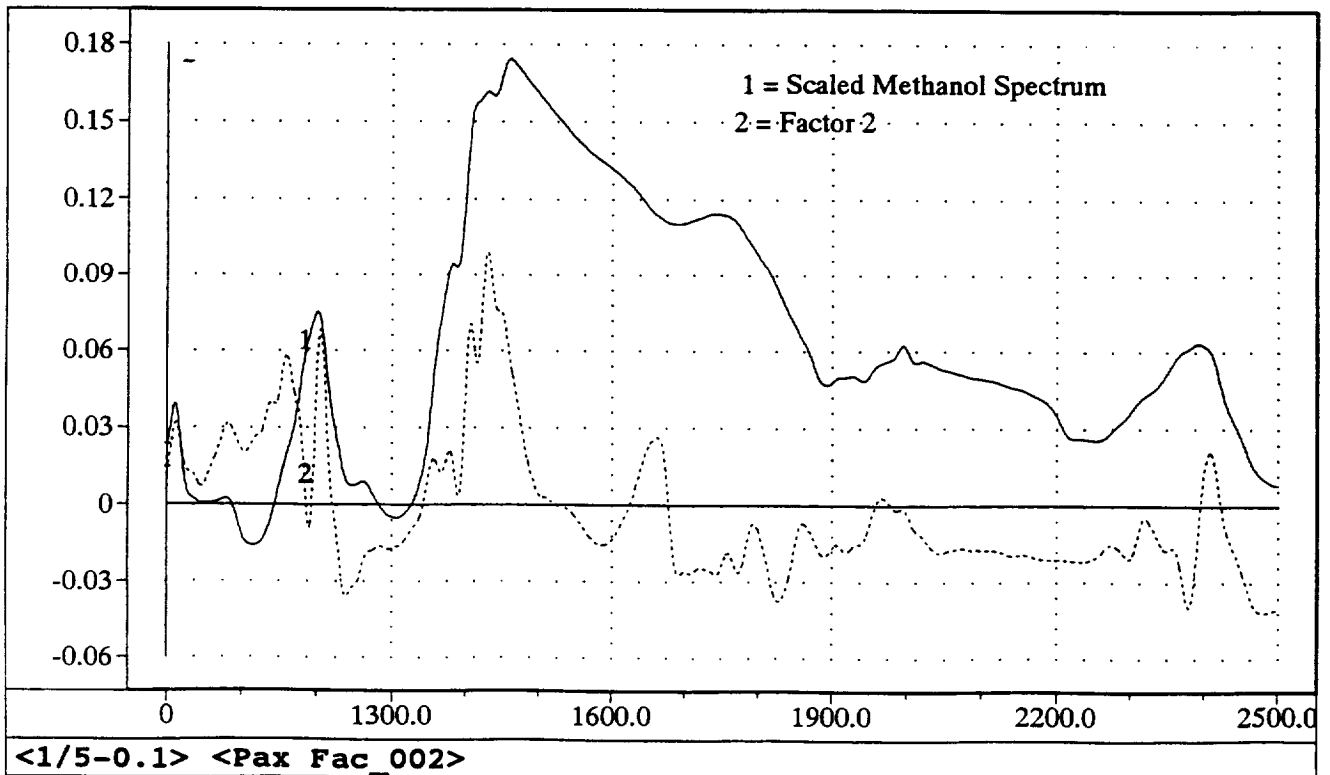


Figure 21b. Methanol spectrum compared to Factor 2

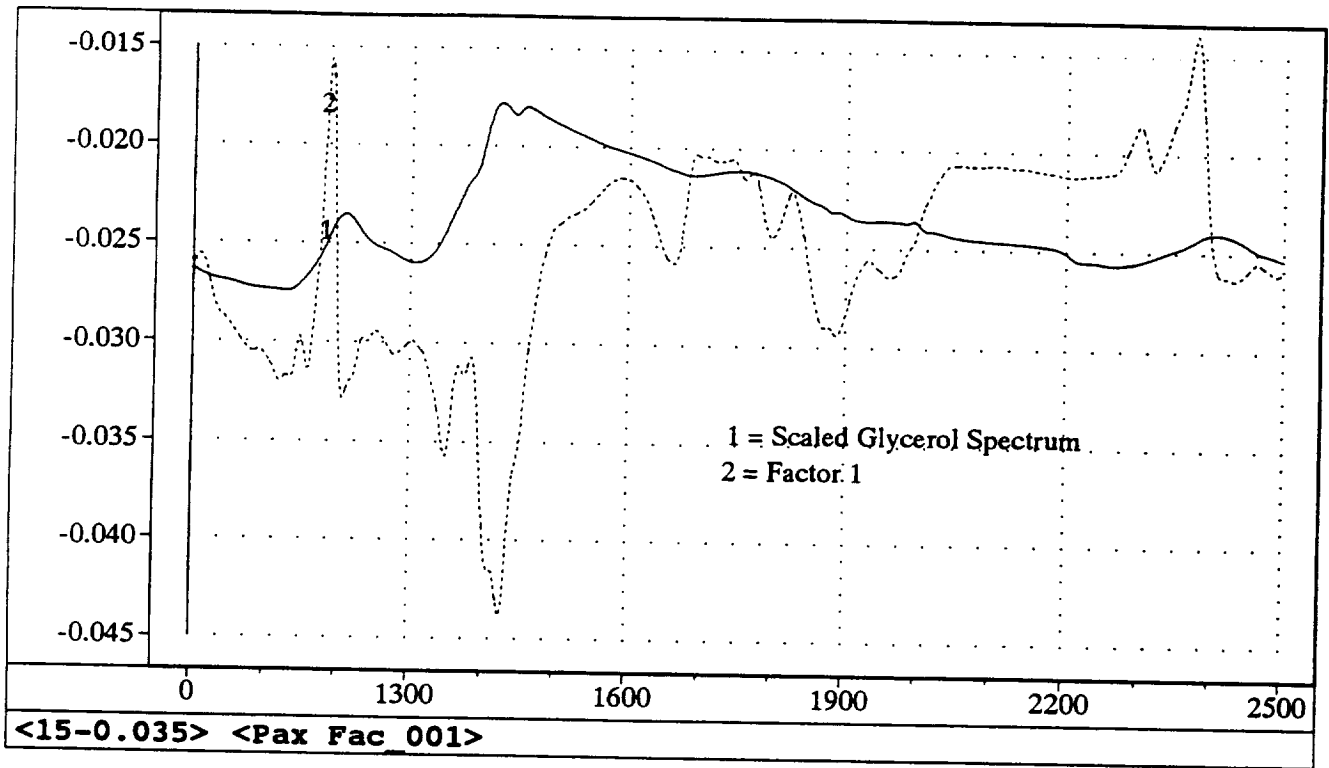


Figure 21c. Glycerol spectrum compared to Factor 1

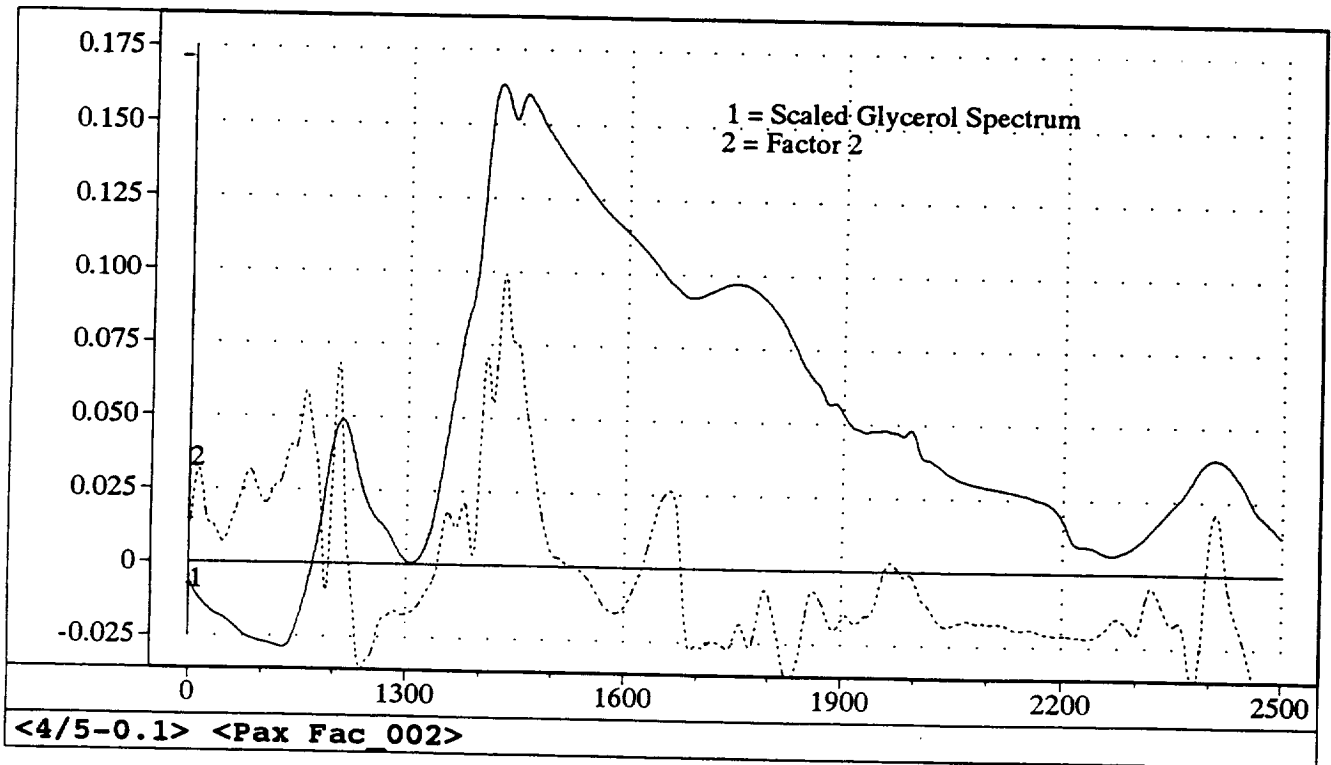


Figure 21d. Glycerol spectrum compared to Factor 2

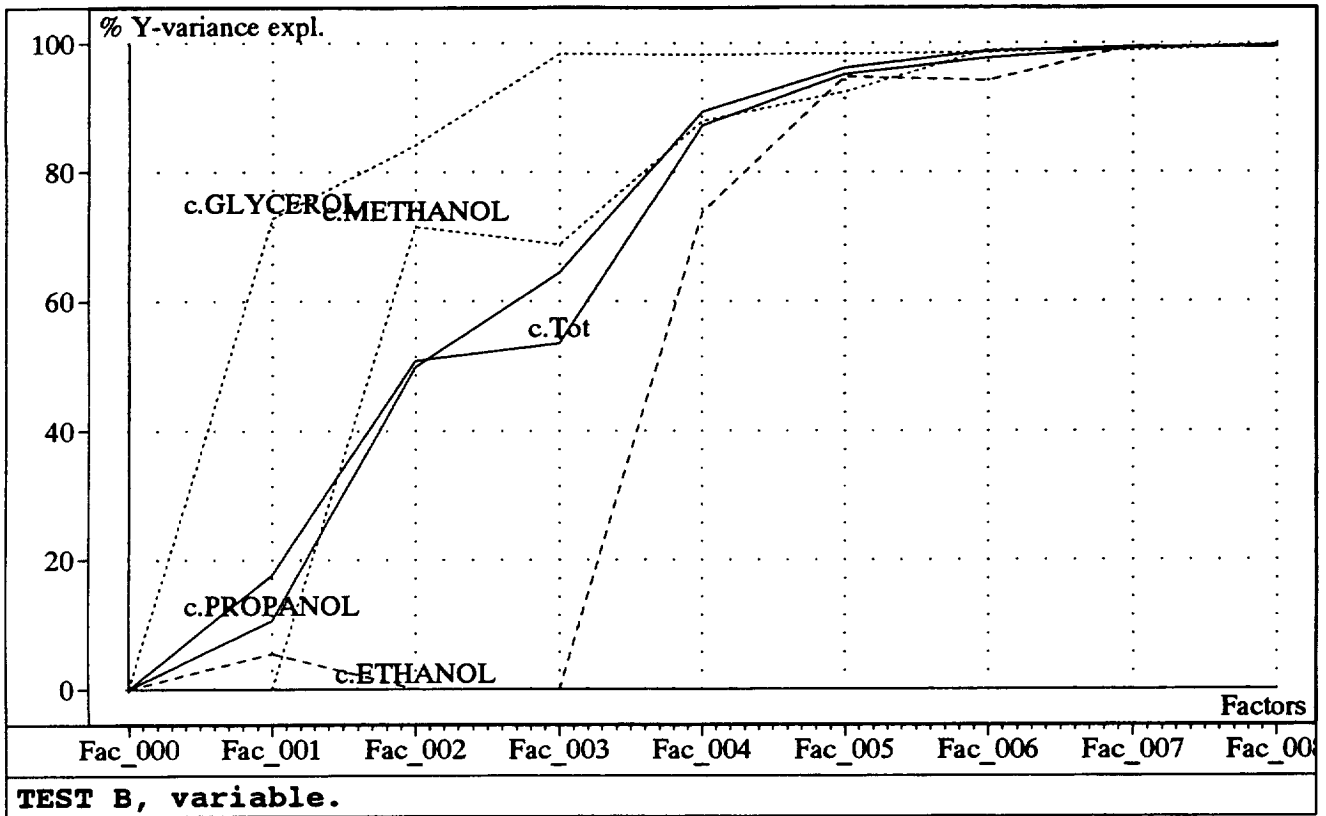


Figure 22. Percent Variance Explained

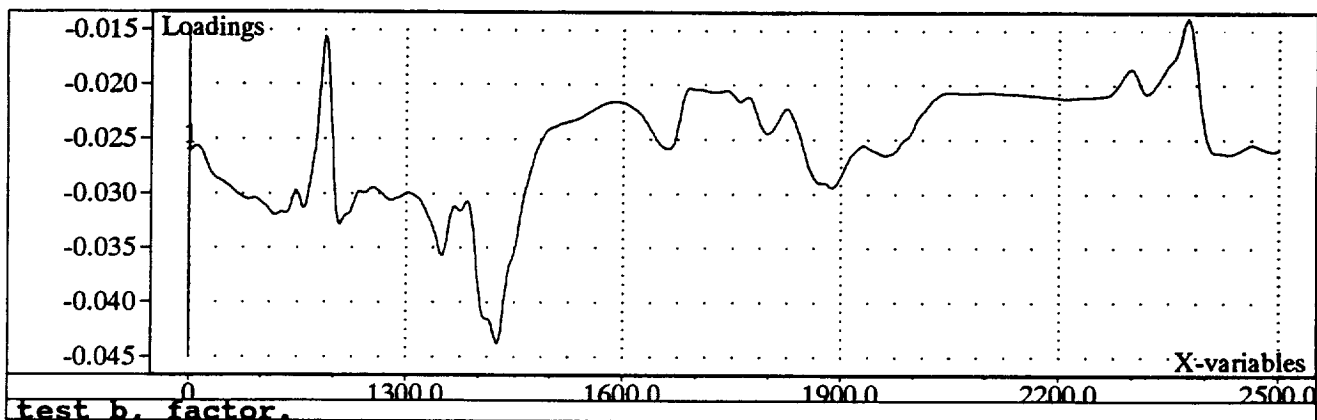


Figure 23a. Factor 1 of Hydroxyl Mixture Set

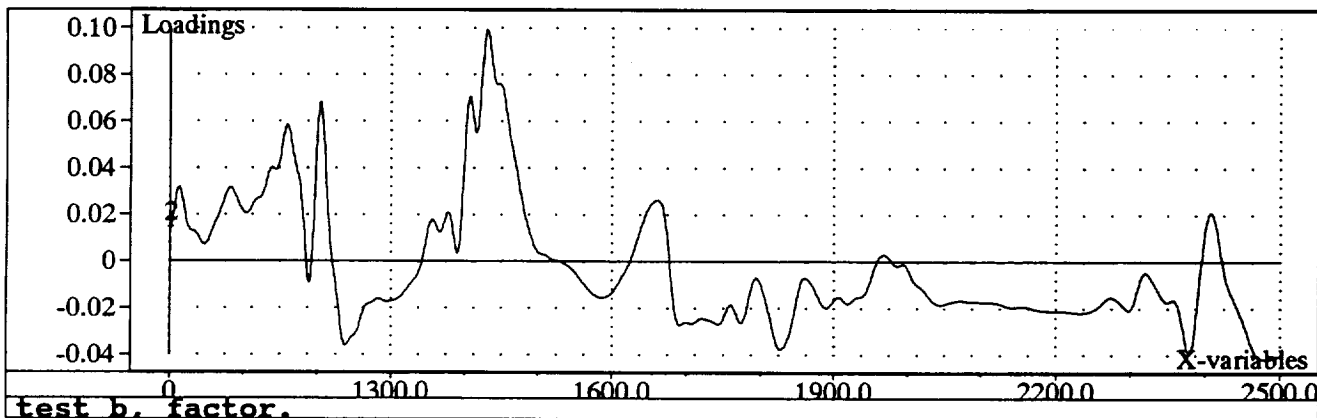


Figure 23b. Factor 2 of Hydroxyl Mixture Set

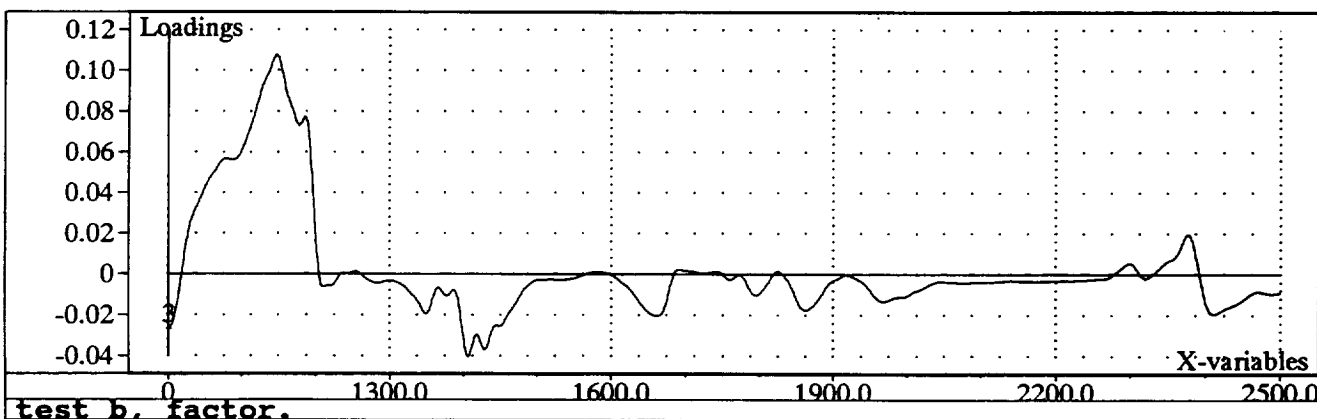


Figure 23c. Factor 3 of Hydroxyl Mixture Set

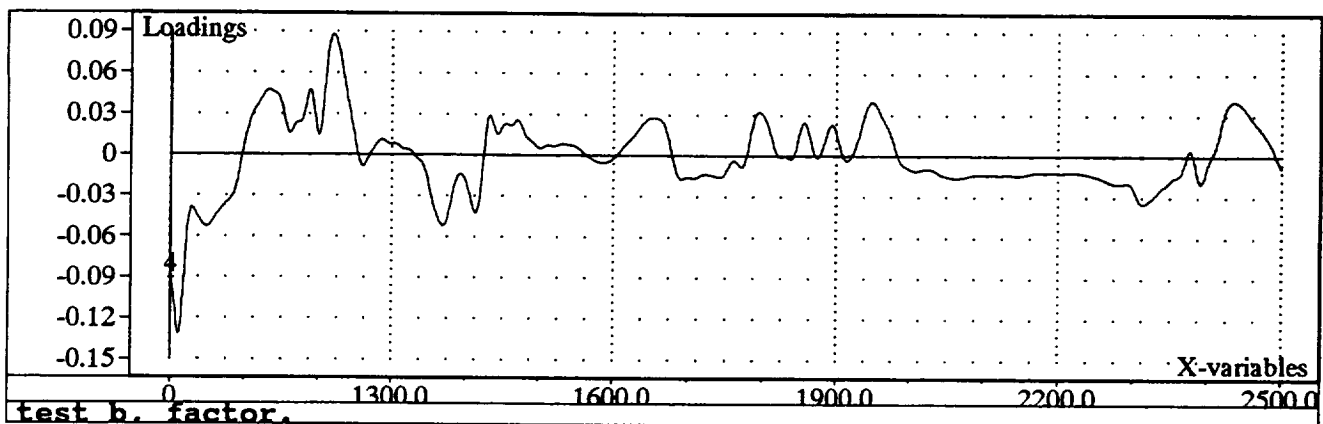


Figure 23d. Factor 4 of Hydroxyl Mixture Set

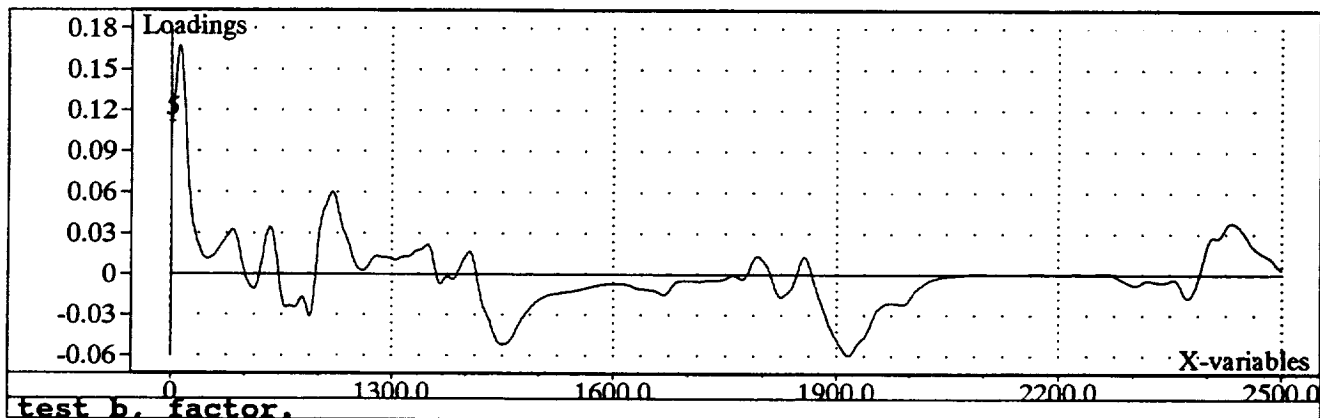


Figure 23e. Factor 5 of Hydroxyl Mixture Set

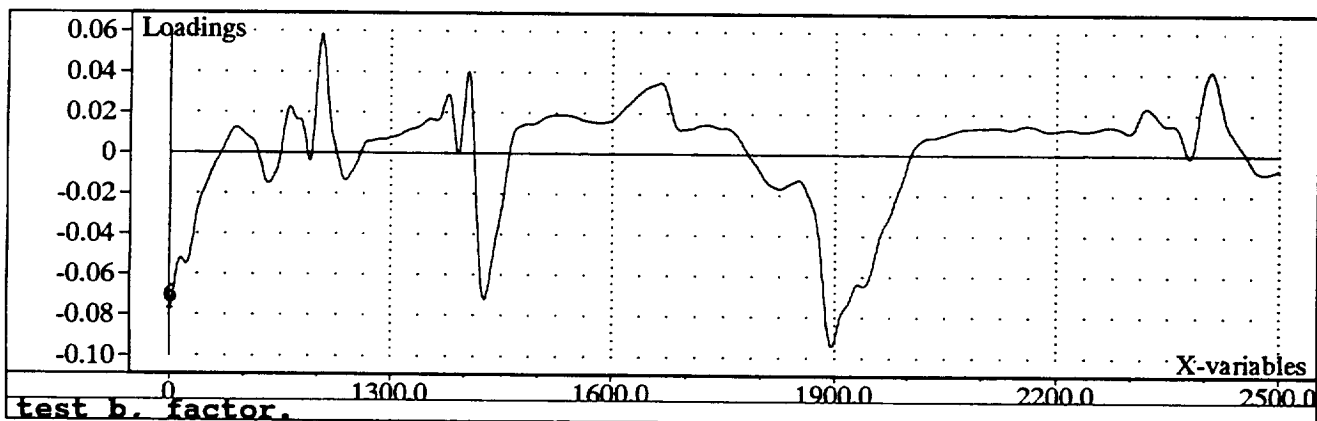


Figure 23f. Factor 6 of Hydroxyl Mixture Set

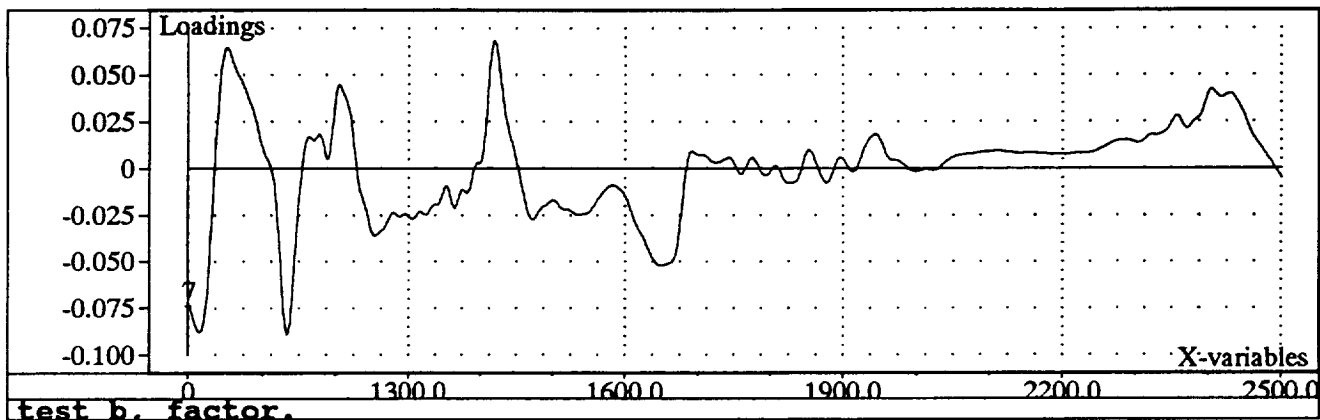


Figure 23g. Factor 7 of Hydroxyl Mixture Set

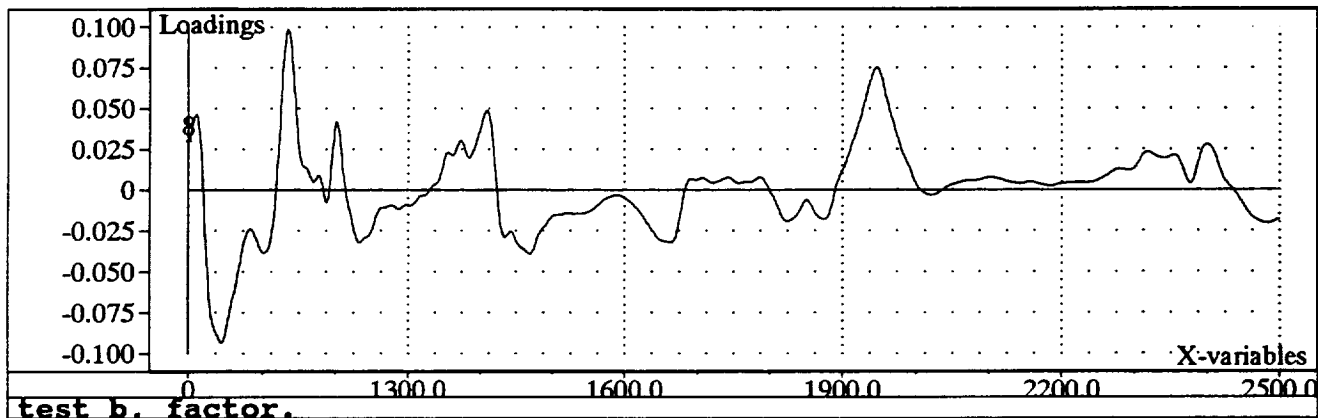


Figure 23h. Factor 8 of Hydroxyl Mixture Set

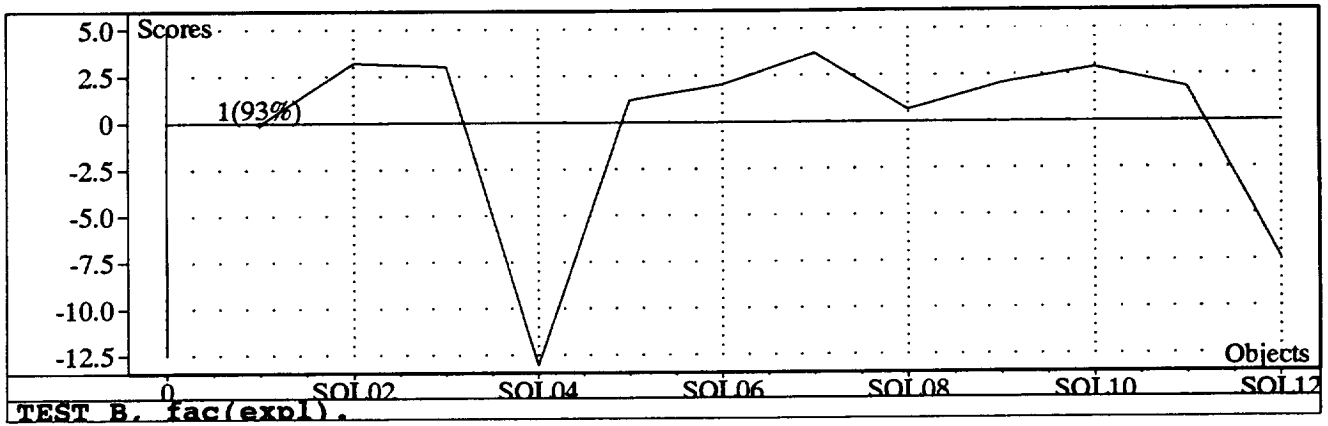


Figure 24a. Scores for Factor 1 of Hydroxyl Mixture Set

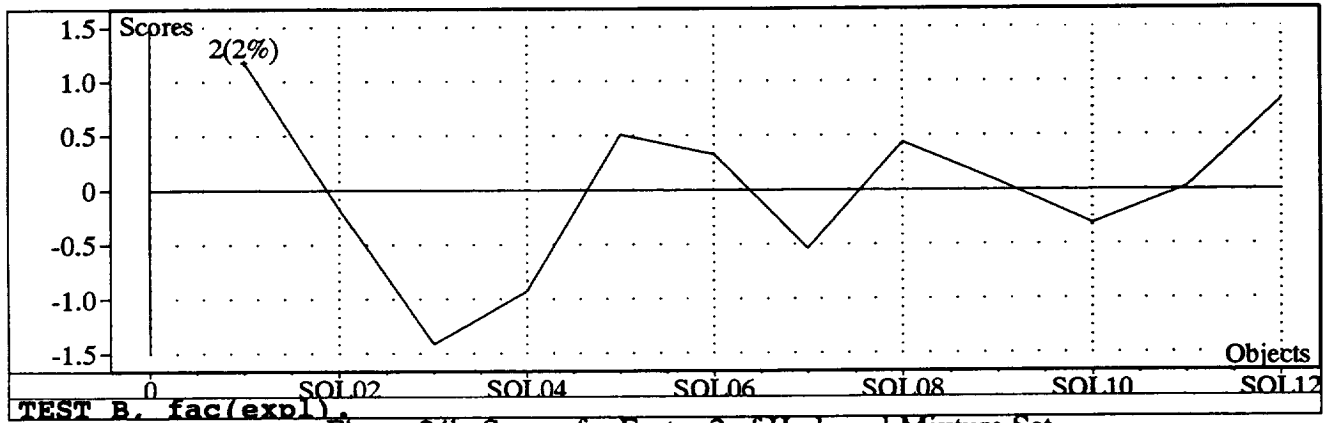


Figure 24b. Scores for Factor 2 of Hydroxyl Mixture Set

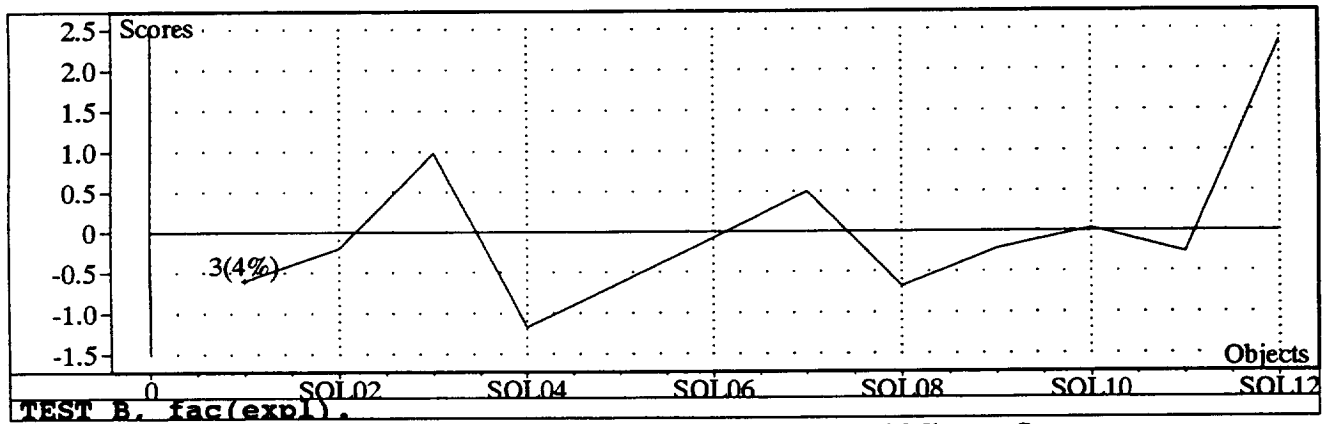


Figure 24c. Scores for Factor 3 of Hydroxyl Mixture Set

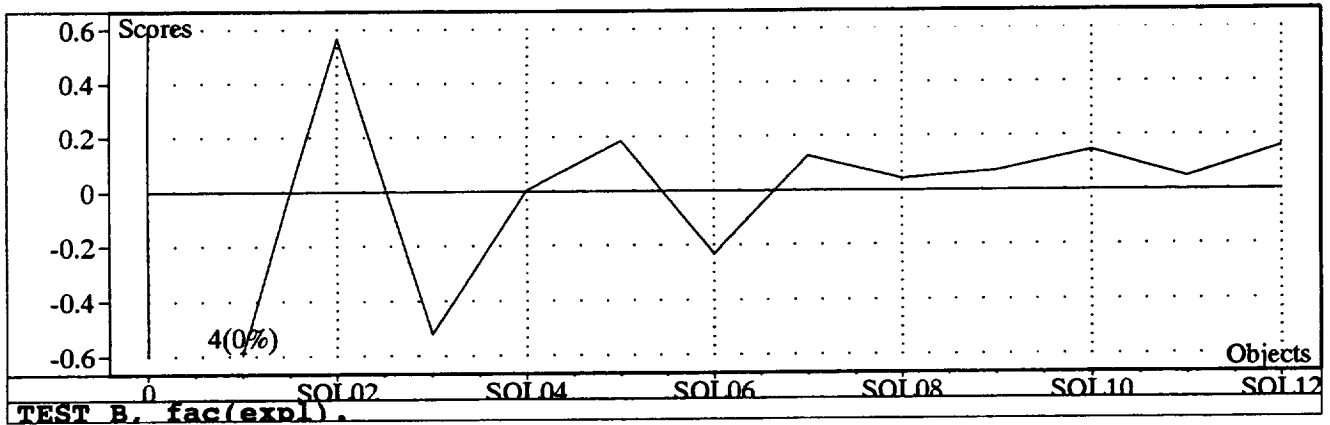


Figure 24d. Scores for Factor 4 of Hydroxyl Mixture Set

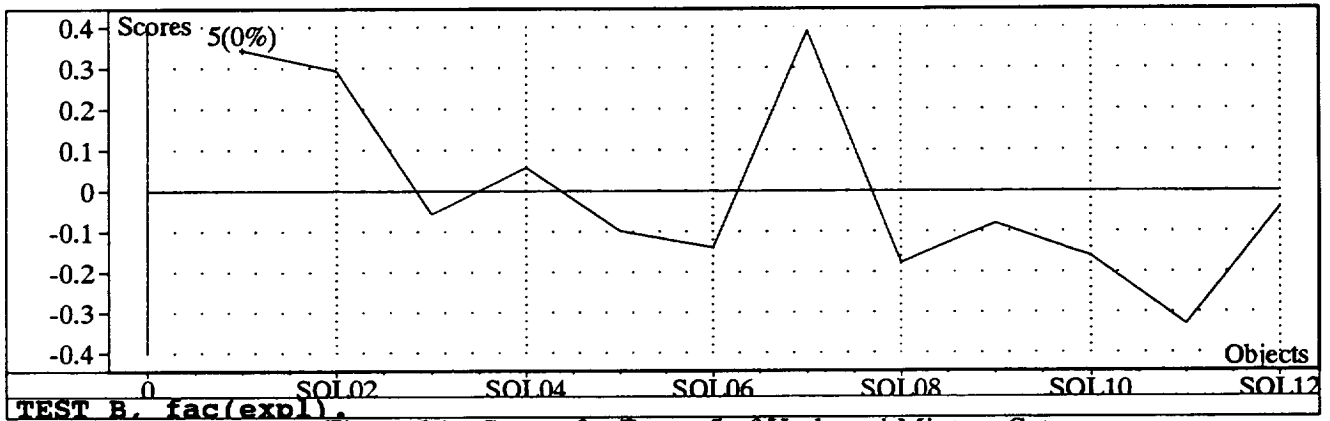


Figure 24e. Scores for Factor 5 of Hydroxyl Mixture Set

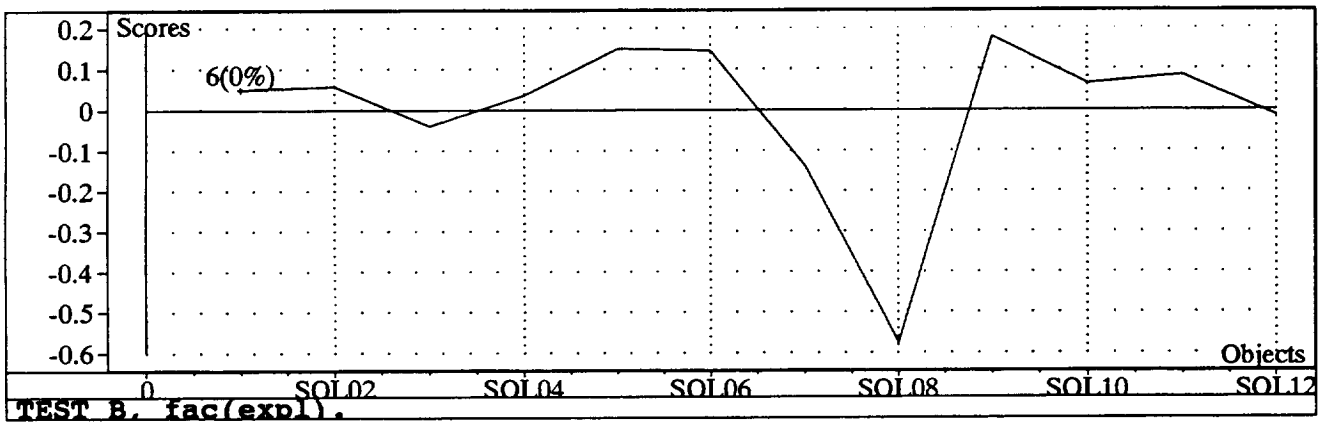


Figure 24f. Scores for Factor 6 of Hydroxyl Mixture Set

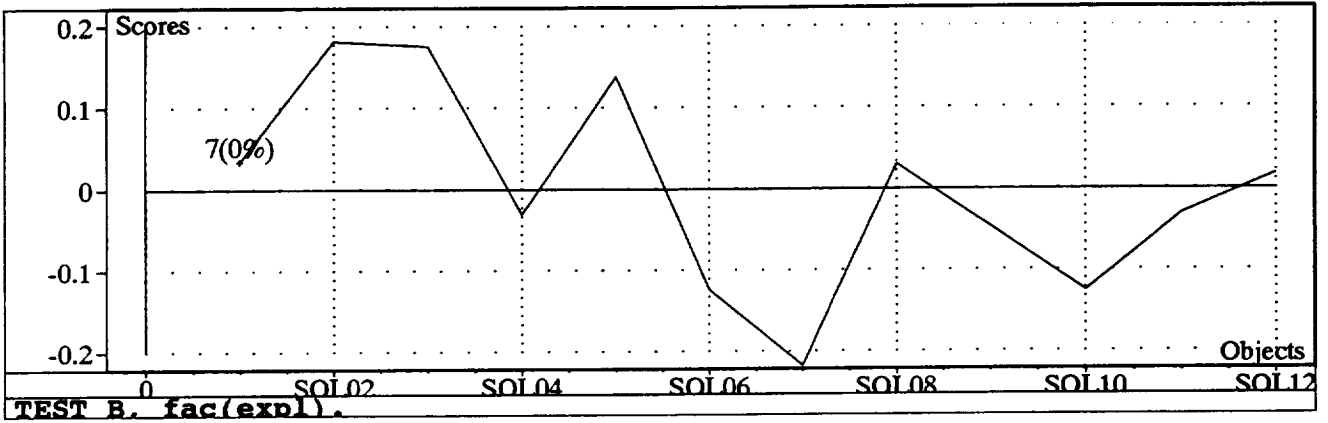


Figure 24g. Scores for Factor 7 of Hydroxyl Mixture Set

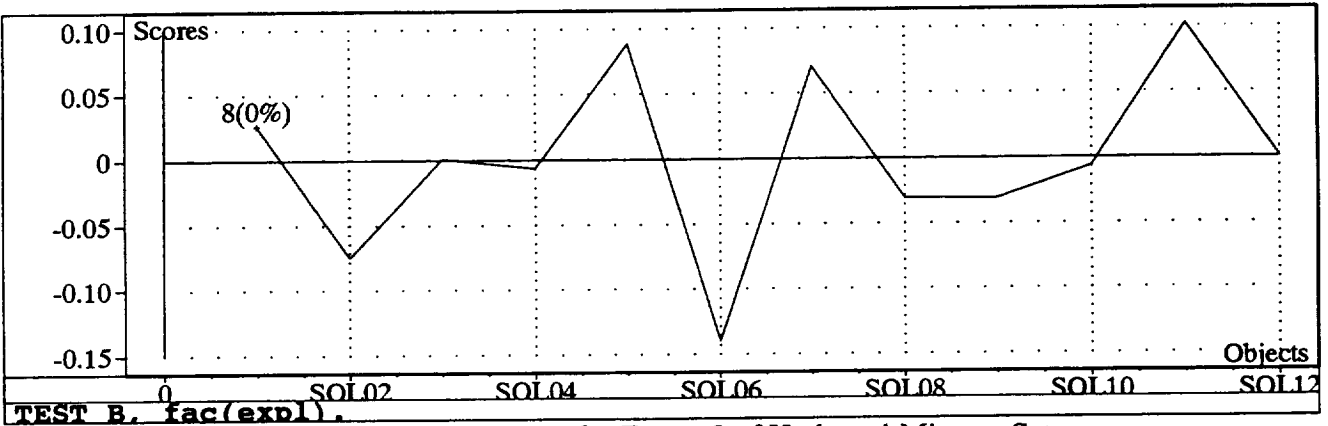


Figure 24h. Scores for Factor 8 of Hydroxyl Mixture Set

